Effect of Tilt Actuator Manipulation on Suspended Boom Sprayer Roll

A Thesis Submitted to the
College of Graduate Studies and Research
in Partial Fulfillment of the Requirements
for the Degree of Master of Science
in the Department of Mechanical Engineering,
University of Saskatchewan,
Saskatoon, Saskatchewan.

By:
Brad G. Hicks

Permission to Use

In presenting this thesis in partial fulfillment of the requirements for a Postgraduate degree from the University of Saskatchewan, I agree that the Libraries of this University may make it freely available for inspection. I further agree that permission for copying this thesis in any manner, in whole or in part, for scholarly purposes, may be granted by the professors who supervised my thesis work, or in their absence, by Head of the Department or Dean of the College in which my thesis work was done. It is understood that any copying, publication or use of this thesis or parts thereof for financial gain shall not be allowed without my written permission. It is also understood that due recognition shall be given to me and the University of Saskatchewan in any scholarly use which may be made of any material in my thesis.

Requests for permission to copy or to make other use of the material in this thesis, in whole or in part, should be addressed to:

Head of the Department of Mechanical Engineering
University of Saskatchewan
Engineering Building
57 Campus Drive
Saskatoon, Saskatchewan, S7N 5A9
Canada

Abstract

Agricultural sprayers are used to apply chemical treatments (pesticides and fertilizer) to crops. A sprayer distributes the chemical by employing many nozzles spaced evenly along a boom structure oriented perpendicular to the direction of travel to cover large areas with each machine pass. To maximize spray efficacy, the nozzles must be held a specific distance from the target to be sprayed. With diversification of crop types grown in Western Canada, foliar application of chemical treatments at multiple points during the plants' life cycles are now required. This multi-growth-stage application process requires a machine with a large range of vertical adjustment; thus permitting the nozzles to be maintained the correct distance from the target (crop) as it grows. Suspended boom sprayers provide the range of adjustment required.

The suspended boom structure consists of three controlled sections which are positioned via use of hydraulic actuators. To reduce the effect of terrain inputs through the carrying frame on the boom's orientation, most suspended boom sprayers incorporate a passive suspension system to limit coupling between the carrying frame and boom. By doing this however, a negative effect is created. During typical operation, the operator will use the actuator to reorient one section thereby maintaining the desired distance from the boom to the target; the opposing section will deviate from its desired position due to coupling of the boom sections through the passive suspension system. The quantification of this problem was the basis for this research.

A computer simulation model of the boom structure, passive suspension system, hydraulic actuator, and on/off type directional valve was created. Comparisons to experimental data showed the model was applicable for predicting trends in boom performance related to manipulation of actuator velocity profiles. Standardized changes in the actuated section's orientation were used to establish the existing performance baseline and quantify the problem. Alternative commercially available directional valves (proportional and pulse width modulated) were then simulated and used in conjunction with the boom model to determine if boom performance improvements may be realized by defining the actuator's acceleration rate during orientation changes.

The proportional valve was able to limit the acceleration and deceleration of the actuated section to reduce the coupling effect and improve the non-actuated section's performance. However, the performance of the actuated section degraded more significantly in all trials regardless of input profile. The performance degradation resulted as slower acceleration and deceleration of the actuator required an increased amount of time for the desired orientation of the actuated section to be reached. It was also concluded that performance of the dynamic orientation of the boom structure was equivalent for orientation changes driven wither by pulse width modulation of an on/off valve or a true proportional valve. The boom structure's large inertia and low natural frequency acted as a suitable filter for the flow and pressure pulsations introduced by pulse width modulation.

Acknowledgements

I would like to gratefully acknowledge my supervisors, Dr. R. T. Burton and Dr. T. G. Crowe, for their support, encouragement and guidance throughout the course of this research. The assistance of Dr. A. T. Dolovich, who gave generously of his time and knowledge, was also very much appreciated. I would also like to thank Mr. D. V. Bitner for his advice and laboratory support. As I was a part-time student, all who aided me rearranged their schedules liberally to accommodate mine.

I would like to acknowledge the financial assistance provided by both Norac Systems International and CNH Canada Limited in the form of tuition.

To my parents, a heartfelt thank-you for their never-ending encouragement.

Dedication

I would like to dedicate this thesis to my wife Angela. It would not have been possible without her tremendous support and sacrifices. For her love I am eternally grateful.

Table of Contents

List of Figures

List of Tables

Nomenclature

a	Identifier of port connection through three-position four-way valve.
$\boldsymbol{a}$	A generalized directional acceleration (m/s^2).
$\mathbf{a}_B$	Acceleration of point B (m/s^2).
$\mathbf{a}_C$	Acceleration of point C (m/s^2).
a_x	Magnitude of acceleration of the actuator rod (x_C-direction) (m/s^2).
a_{Bx}	Magnitude of acceleration of point B (x-direction) (m/s^2).
a_{By}	Magnitude of acceleration of point B (y-direction) (m/s^2).
$\mathbf{a}_Q$	Acceleration of point Q_{CL} (m/s^2).
a_{Qx}	Magnitude of acceleration of point Q_{CL} (x-direction) (m/s^2).
a_{Qy}	Magnitude of acceleration of point Q_{CL} (y-direction) (m/s^2).
$\mathbf{a}_O$	Acceleration of a generalized point O (m/s^2).
$\mathbf{a}_P$	Acceleration of a generalized point P (m/s^2).
$\mathbf{a}_R$	Acceleration of point R (m/s^2).
a_{Rx}	Magnitude of acceleration of point R (x-direction) (m/s^2).
a_{Ry}	Magnitude of acceleration of point R (y-direction) (m/s^2).
A	Point identifying the attachment location of actuator to center section.
A_o	Cross-sectional area of an orifice (m^2).
A_1	Area of the actuator piston (m^2).
A_2	Area of the actuator piston less the area of the rod (m^2).
b	Identifier of port connection through three-position four-way valve.
b	Length from point B to a point created by bisecting a vector from point A to point E with a line perpendicular to the vector and through point B (m).
b_1	Length of the line perpendicular to a vector from point C to point N1 and through point M1 (m).
B	Point identifying the attachment location (point of rotation) between the right and center sections.

B_x	Reaction force in the x-direction applied by the right boom section's tilt point of rotation (N).
B_y	Reaction force in the y-direction applied by the right boom section's tilt point of rotation (N).
C	Point identifying the attachment location of boom structure to carrying frame; also the boom roll point of rotation.
C_d	A constant (at large Reynolds numbers) for fluid flow through an orifice called the discharge coefficient.
C_x	Reaction force in the x-direction applied by the chassis attachment point of rotation (N).
C_y	Reaction force in the y-direction applied by the chassis attachment point of rotation (N).
d_1	Length from point A to a point created by bisecting a vector from point A to point E with a line perpendicular to the vector and through point B (m).
d_2	Length from point E to a point created by bisecting a vector from point A to point E with a line perpendicular to the vector and through point B (m).
d_3	Length from point C to a point created by bisecting a vector from point C to point N1 with a line perpendicular to the vector and through point M1 (m).
d_4	Length from point N1 to a point created by bisecting a vector from point C to point N1 with a line perpendicular to the vector and through point M1 (m).
E	Point identifying the attachment location of actuator to right section.
$\boldsymbol{F}$	A generalized force vector acting on a body (N).
FBD	Free body diagram.
$F_{E/A}$	Force applied by the tilt actuator (N).
ΣF_{Cx}	Summation of all forces in the x-direction acting on the actuator rod (N).

F_f	Force of friction which acts between the moving components of the actuator (N).
ΣF_{Qx}	Summation of all forces in the x-direction acting on the combined left and center sections (N).
ΣF_{Qy}	Summation of all forces in the y-direction acting on the combined left and center sections (N).
ΣF_{Rx}	Summation of all forces in the x-direction acting on the right section (N).
ΣF_{Ry}	Summation of all forces in the y-direction acting on the right section (N).
F_S	Force applied by each strut (N).
F_{S1}	Force applied by strut number 1 (N).
F_{S2}	Force applied by strut number 2 (N).
F_{S3}	Force applied by strut number 3 (N).
F_{S4}	Force applied by strut number 4 (N).
F_1	Force applied on the non-rod side of the piston by the pressurized fluid (N).
F_2	Force applied on the rod side of the piston by the pressurized fluid (N).
G	Point identifying the center boom section center of gravity.
$G(s)$	On/off valve transfer function.
$H(s)_{Large}$	Proportional valve transfer function for large signal changes (50% base signal ±40%).
$H(s)_{Small}$	Proportional valve transfer function for small signal changes (50% base signal ±10%).
h	Hour.
Hz	Hertz.
Δh_{SP}	Deviation of the outer tip from the desired distance to target (m).
I_Q	Mass moment of inertia of the combined left and center sections about the z-axis ($kg \cdot m^2$).

I_R	Mass moment of inertia of the right section about the z-axis ($kg \cdot m^2$).
k	Passive suspension system elements spring rate (N/m).
K	On/off valve transfer function gain (m/V).
kg	Kilogram.
km	Kilometer.
kph	Kilometers per hour (km/h).
ℓ	Length of the passive suspension system spring elements (m) at a point in time, t.
ℓ_O	Free length of the passive suspension system spring elements (m).
ℓ_1	Length of the spring on strut number 1 (m) at a point in time, t.
ℓ_2	Length of the spring on strut number 2 (m) at a point in time, t.
ℓ_3	Length of the spring on strut number 3 (m) at a point in time, t.
ℓ_4	Length of the spring on strut number 4 (m) at a point in time, t.
L	Point identifying the left boom section center of gravity.
L_C	Length from point C to the outermost spray tip on the left section (m).
L_R	Length from point B to the outermost spray tip on the right section (m).
LS	An additive series of terms that did not involve either $F_{E/A}$ or $\ddot{x}_C$ on the left side of the equation generated during simultaneous solution.
LS_F	An additive series of terms that all involved $F_{E/A}$ on the left side of the equation generated during simultaneous solution.
LS_x	An additive series of terms that all involved $\ddot{x}_C$ on the left side of the equation generated during simultaneous solution.
m	Meter.
m	Mass of a generalized body (kg).
m_C	Mass of the actuator (kg).
m_Q	Mass of the combined left and center sections (kg).

m_R	Mass of the right boom section (kg).
m_{SLOPE}	Desired slope of the actuator velocity profile to create sigmoidal shaped profile in actuator position (m/s^2).
ΣM_Q	Summation of all moments about the combined left and center sections' center of gravity (point Q_{CL}) (N·m).
ΣM_R	Summation of all moments about the right section's center of gravity (point R) (N·m).
MSD	Maximum spool displacement (m).
M1	Passive suspension system element attachment point to boom structure; strut number 1.
M2	Passive suspension system element attachment point to boom structure; strut number 2.
M3	Passive suspension system element attachment point to boom structure; strut number 3.
M4	Passive suspension system element attachment point to boom structure; strut number 4.
n_1	Needle valve used to isolate non-rod end of actuator from valve during bulk modulus experimentation.
n_2	Needle valve used to isolate rod end of actuator from valve during bulk modulus experimentation.
n_3	Needle valve used to release compressibility flow from non-rod end of actuator during bulk modulus experimentation.
n_4	Needle valve used to release compressibility flow from rod end of actuator during bulk modulus experimentation.
N	Newton.
N1	Passive suspension system element attachment point to carrying frame; strut number 1.
N2	Passive suspension system element attachment point to carrying frame; strut number 2.
N3	Passive suspension system element attachment point to carrying frame; strut number 3.

N4	Passive suspension system element attachment point to carrying frame; strut number 4.
P	Identifier of supply pressure port connection to three-position four-way valve.
ΔP	Pressure drop across an orifice (Pa).
Pa	Pascal.
P_{ATM}	Atmospheric pressure (Pa).
P_{EX}	System pressure before venting to atmosphere during bulk modulus experiment (Pa).
P_S	System supply pressure (Pa).
P_T	Pressure in the return line to the reservoir (Pa).
PWM	Pulse width modulation.
P_1	Fluid pressure in the non-rod end of the actuator (Pa).
P_2	Fluid pressure in the rod end of the actuator (Pa).
Q	Fluid flow through an orifice (m^3/s).
Q_{CL}	Point identifying the combined center and left boom sections' center of gravity.
ΣQ_{IN}	Summation of all flows entering a generalized control volume (m^3/s).
ΣQ_{OUT}	Summation of all flows exiting a generalized control volume (m^3/s).
Q_1	Flow entering the actuator non-rod end control volume from the valve (m^3/s).
Q_2	Flow exiting the actuator rod end control volume to the valve (m^3/s).
$r_{B/A}$	Magnitude of a vector between points A and B (m).
$\mathbf{r}_{B/C}$	Vector from point C to point B (m).
$\mathbf{r}_{B/R}$	Vector from point R to point B (m).
$r_{B/R}$	Magnitude of a vector between points R and B (m).
$r_{C/N1}$	Magnitude of a vector between points N1 and C (m).
$r_{C/N2}$	Magnitude of a vector between points N2 and C (m).
$r_{C/N3}$	Magnitude of a vector between points N3 and C (m).

$r_{C/N4}$	Magnitude of a vector between points N4 and C (m).
$r_{E/A}$	Magnitude of a vector between points A and E (m).
$r_{E/B}$	Magnitude of a vector between points B and E (m).
$r_{M1/C}$	Magnitude of a vector between points C and M1 (m).
$r_{M2/C}$	Magnitude of a vector between points C and M2 (m).
$r_{M3/C}$	Magnitude of a vector between points C and M3 (m).
$r_{M4/C}$	Magnitude of a vector between points C and M4 (m).
$\mathbf{r}_{P/O}$	Vector from a generalized point O to a generalized point P (m).
$r_{Q/A}$	Magnitude of a vector between points A and Q_{CL} (m).
$r_{Q/B}$	Magnitude of a vector between points B and Q_{CL} (m).
$r_{Q/C}$	Magnitude of a vector between points C and Q_{CL} (m).
$\mathbf{r}_{Q/C}$	Vector from point C to point Q_{CL} (m).
$r_{Q/M1}$	Magnitude of a vector between points M1 and Q_{CL} (m).
$r_{Q/M2}$	Magnitude of a vector between points M2 and Q_{CL} (m).
$r_{Q/M3}$	Magnitude of a vector between points M3 and Q_{CL} (m).
$r_{Q/M4}$	Magnitude of a vector between points M4 and Q_{CL} (m).
$r_{R/E}$	Magnitude of a vector between points E and R (m).
R	Point identifying the right boom section center of gravity.
RS	An additive series of terms that did not involve either $F_{E/A}$ or $\ddot{x}_C$ on the right side of the equation generated during simultaneous solution.
RS_F	An additive series of terms that all involved $F_{E/A}$ on the right side of the equation generated during simultaneous solution.
RS_x	An additive series of terms that all involved $\ddot{x}_C$ on the right side of the equation generated during simultaneous solution.
rad	Radian.
s	Second.
SMR	Signal modulation ratio.
SPE	Boom section set-point error (m s).
t	Time (s).
t_f	Time at the end of each bulk-modulus experiment trial (s).

t_o	Time at the beginning of each bulk-modulus experiment trial (s).
T	Identifier of tank (reservoir) port connection from three-position four-way valve.
w	Area gradient of the valve orifice (m^2/m).
W_Q	Weight of the combined center and left sections (N).
W_R	Weight of the right section (N).
V_A	Generalized control volume (m^3).
V_{AO}	Generalized control volume at the beginning of an evaluation period (m^3).
V_E	Volume of fluid in the fully extended control volume of the actuator (m^3).
V_{GC}	Volume of fluid in the actuator control volume due to bulk modulus effect (m^3).
V_I	Input voltage to the proportional valve solenoid (V).
V_R	Volume of fluid in the fully retracted control volume of the actuator (m^3).
V_1	Actuator non-rod end control volume (m^3).
V_{1o}	Actuator non-rod end control volume at the beginning of the evaluation period (m^3).
V_2	Actuator rod end control volume (m^3).
V_{2o}	Actuator rod end control volume at the beginning of the evaluation period (m^3).
$\dot{x}_C$	Linear velocity of the actuator rod in the x-direction (m/s).
$\ddot{x}_C$	Linear acceleration of the actuator rod in the x-direction (m/s^2).
x_V	Position of the valve spool (m).
z	Vertical distance between the initial position of the outermost spray tip on the left section and point C (m).
$\boldsymbol{\alpha}$	Angular acceleration of a generalized rigid body (rad/s^2).
$\boldsymbol{\alpha}_C$	Angular acceleration of the combined left and center sections (rad/s^2).

α_Q Magnitude of angular acceleration of the combined left and center sections about the z-axis (rad/s^2).

$\boldsymbol{\alpha}_Q$ Angular acceleration of the combined left and center sections (rad/s^2).

α_R Magnitude of angular acceleration of the right section about the z-axis (rad/s^2).

$\boldsymbol{\alpha}_R$ Angular acceleration of the right section (rad/s^2).

β_E Effective bulk modulus of the hydraulic fluid (Pa).

β_S Damping coefficient for the for the passive suspension system shock elements (kg/s).

ϕ_{b1} Angle between the negative y-axis and a vector created by bisecting a vector from point C to point N1 with a line perpendicular to the vector and through point M1 (rad).

ϕ_{b2} Angle between the negative y-axis and a vector created by bisecting a vector from point C to point N2 with a line perpendicular to the vector and through point M2 (rad).

ϕ_{b3} Angle between the negative y-axis and a vector created by bisecting a vector from point C to point N3 with a line perpendicular to the vector and through point M3 (rad).

ϕ_{b4} Angle between the negative y-axis and a vector created by bisecting a vector from point C to point N4 with a line perpendicular to the vector and through point M4 (rad).

$\phi_{B/A}$ Initial angle between the y-axis and a vector between points A and B (rad).

$\phi_{B/C}$ Initial angle between horizontal and a vector between points C and B (rad).

$\phi_{B/R}$ Initial angle between the y-axis and a vector between points R and B (rad).

ϕ_{CTIP} Initial angle between horizontal and a vector between the outermost spray tip on the left section and point C (rad).

$\phi_{E/A}$ Initial angle between the y-axis and a vector between points A and E (rad).

$\phi_{E/B}$ Initial angle between the x-axis and a vector between points B and E (rad).

$\phi_{Q/A}$ Initial angle between the negative x-axis and a vector between points A and Q_{CL} (rad).

$\phi_{Q/B}$ Initial angle between the negative x-axis and a vector between points B and Q_{CL} (rad).

$\phi_{Q/C}$ Initial angle between the negative x-axis and a vector between points C and Q_{CL} (rad).

$\phi_{Q/M1}$ Initial angle between the negative x-axis and a vector between points M1 and Q_{CL} (rad).

$\phi_{Q/M2}$ Initial angle between the negative x-axis and a vector between points M2 and Q_{CL} (rad).

$\phi_{Q/M3}$ Initial angle between the negative x-axis and a vector between points M3 and Q_{CL} (rad).

$\phi_{Q/M4}$ Initial angle between the negative x-axis and a vector between points M4 and Q_{CL} (rad).

$\phi_{N1/C}$ Initial angle between the y-axis and a vector between points C and N1 (rad).

$\phi_{N2/C}$ Initial angle between the y-axis and a vector between points C and N2 (rad).

$\phi_{N3/C}$ Initial angle between the x-axis and a vector between points C and N3 (rad).

$\phi_{N4/C}$ Initial angle between the x-axis and a vector between points C and N4 (rad).

$\phi_{R/E}$ Initial angle between the y-axis and a vector between points E and R (rad),

η_1 Angle between a vector connecting points B and A and a vector between points E and A (rad).

η_2	Angle between a vector created by points E and B, and the line created by bisecting a vector from point A to point E with a line perpendicular to that vector and through point B (rad).
η_3	Angle between a vector created by points B and A, and the line created by bisecting a vector from point A to point E with a line perpendicular to that vector and through point B (rad).
$\lambda_{M1/C}$	Initial angle between the y-axis and a vector between points C and M1 (rad).
$\lambda_{M2/C}$	Initial angle between the y-axis and a vector between points C and M2 (rad).
$\lambda_{M3/C}$	Initial angle between the x-axis and a vector between points C and M3 (rad).
$\lambda_{M4/C}$	Initial angle between the x-axis and a vector between points C and M4 (rad).
θ_C	Change in orientation of the vector between points A and E due to a change in the rotational position of the combined left and center sections (rad).
$\theta_{E/A}$	Change in orientation of the vector between points A and E due to a change in the length of the tilt actuator (rad).
θ_R	Angular change in orientation of the right section from the initial starting point (rad).
θ_{S1}	Angle of orientation of strut number 1 with respect to the negative y-axis (rad).
θ_{S2}	Angle of orientation of strut number 2 with respect to the negative y-axis (rad).
θ_{S3}	Angle of orientation of strut number 3 with respect to the negative y-axis (rad).
θ_{S4}	Angle of orientation of strut number 4 with respect to the negative y-axis (rad).

θ_W	Angular change in orientation of the right section due to length changes of the actuator (rad).
ρ	Density of hydraulic fluid (kg/m^3).
τ	On/off valve transfer function time constant (s).
$\tau_{B/A}$	Initial angle between the x-axis and a vector between points B and A (rad).
$\tau_{B/C}$	Initial angle between the y-axis and a vector between points B and C (rad).
τ_{N1}	Angle between a vector from point C to point N1 and a vector from point N1 to point M1 (rad).
τ_{N2}	Angle between a vector from point C to point N2 and a vector from point N2 to point M2 (rad).
τ_{N3}	Angle between a vector from point C to point N3 and a vector from point N3 to point M3 (rad).
τ_{N4}	Angle between a vector from point C to point N4 and a vector from point N4 to point M4 (rad).
ω	Angular velocity of a generalized rigid body (rad/s).
ω_C	Angular velocity of the combined left and center sections (rad/s).
ω_{NL}	Natural frequency for proportional valve transfer function; large signal changes (rad/s).
ω_{NS}	Natural frequency for proportional valve transfer function; small signal changes (rad/s).
ω_Q	Angular velocity of the combined left and center sections (rad/s).
ω_R	Angular velocity of the right section (rad/s).
ω_1	First cut-off frequency for proportional valve transfer function; small signal changes (rad/s).
ω_2	Second cut-off frequency for proportional valve transfer function; small signal changes (rad/s).
ζ_L	Damping ratio for proportional valve transfer function; large signal changes.

ζ_s	Damping ratio for proportional valve transfer function; small signal changes.

Chapter 1

Introduction and Thesis Research Goals

In this chapter, suspended boom sprayers and their expanding use in modern farming operations are introduced. A problem associated with independent control of a boom section is presented along with the objectives of this research, which were to quantify and potentially minimize this limitation.

1.1 Agricultural Application Machines (Suspended Boom Sprayers)

The business of farming in Western Canada has undergone tremendous change over the past 20-years. During the 1990's, the average Canadian farm size increased 17 percent, while the number of farms decreased 15 percent (Census of Agriculture, 2001). With more area to cover, bigger, faster, and more technologically advanced equipment is required. Contracting custom operators to ease seasonal workload and limit capital expenditure has also become more prominent. These operators use the latest equipment to perform efficiently and effectively to avoid liability for any resultant crop loss.

In order for farmers of today to remain prosperous, they must either increase crop yields or decrease input costs. To attain optimal yields, chemical treatments (whether pesticides or fertilizers) are used to provide the crop with a competitive advantage. Accurate and uniform application of only the required amount of treatment over the field eliminates secondary applications, thereby reducing input costs. Agricultural application machines are used to topically apply chemicals; to do so they employ liquid spray nozzles which rely on being the proper distance from the target to produce even coverage. Many nozzles are spaced evenly along a *boom* situated laterally to the direction of travel to cover large areas with each machine pass. Historically, wheels were spaced at intervals along the boom to maintain the nozzles at the proper distance from the target. Wheeled boom sprayers have two associated problems:

i. an inability to apply pre-harvest foliar treatments (desiccation) due to height range adjustment limitations, and

ii. damage the wheels cause when passing through the crop.

Due to these issues the market has tended towards *suspended boom sprayers* (Figure 1.1). This type of application machine has a boom that is suspended from a carrying chassis at the center to avoid the aforementioned pitfalls. Control of the boom distance from the target is one of the main issues with suspended boom sprayers; it has been shown that deviations in the distance between the nozzle and the target can cause extreme variations in application uniformity (from zero to 10-times that desired) (Ramon et al., 1997).

(photo courtesy CNH Canada Ltd.)

Figure 1.1: Suspended Boom Sprayer

The sprayer's frequency of use has increased over the past twenty years. To improve soil tilth, farming practice has moved towards reduced tillage; chemicals must then be used to control weeds. A broader variety of crop types are also being grown; many require topical chemical application throughout their growth cycle either for disease control or pre-harvest desiccation. To meet the additional requirements, agricultural sprayers are now commercially available in widths up to 40 m and boast application speeds of over 30 kph.

Due to the tremendous widths of these machines, small movements of the carrying frame are amplified to create large positional deviations at the boom ends. This rotational movement about an axis along the driving direction is defined as *roll*. The effect of boom roll on application uniformity is shown in Figure 1.2; insufficient distance from the target causes reduced coverage whereas excessive distance creates uneven overlap and promotes wind drift. Research has shown that the effect of roll can lead to deviations of spray deposits from 0% to 760% of desired application rates (Langenakens et al., 1999). Commercially available agricultural sprayers typically are designed using a passive suspension system to minimize the coupling between the carrying frame and the boom structure. This type of suspension is strictly reactive and uses springs to maintain some system stiffness and damping mechanisms to reduce the magnitude of oscillation.

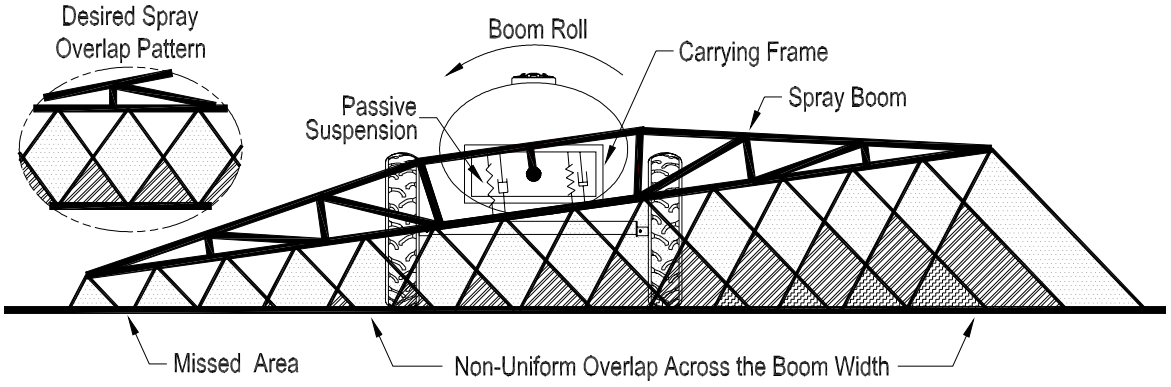

Figure 1.2: Effect of Boom Roll on Spray Efficacy

1.2 Passive Suspension Systems

There are almost as many passive suspension system designs as there are commercial manufacturers due to different geographical areas and operating conditions. Because of the broad variety of designs, a test standard has been developed to aid in design and optimization of sprayer boom suspensions (Jeon et al., 2004). Others have developed a hydraulically driven test bench, which simulated field motions allowing direct measurement of dynamic spray distribution across the width of the boom (Herbst and Wolf, 2000). More recent work developed a computer simulation model of a 39-m sprayer boom suspension system. The performance of the system exposed to many simulated field conditions was evaluated and the suspension system was optimized for effects of carrying frame motion on boom stability (Anthonis et al., 2004).

In certain hilly field conditions, it is undesirable to have the boom as an integral part of the carrying frame. By creating another piece of framework between the carrying frame and the passive suspension frame, a hydraulic actuator can be used to change the boom's orientation. This actuator is typically called the roll-bias actuator; its control over the average distance from the boom to the target is illustrated in Figures 1.3a and 1.3b. Recent work has investigated active control of the roll-bias actuator to optimize orientation of the boom in hilly conditions (Deprez et al., 2003).

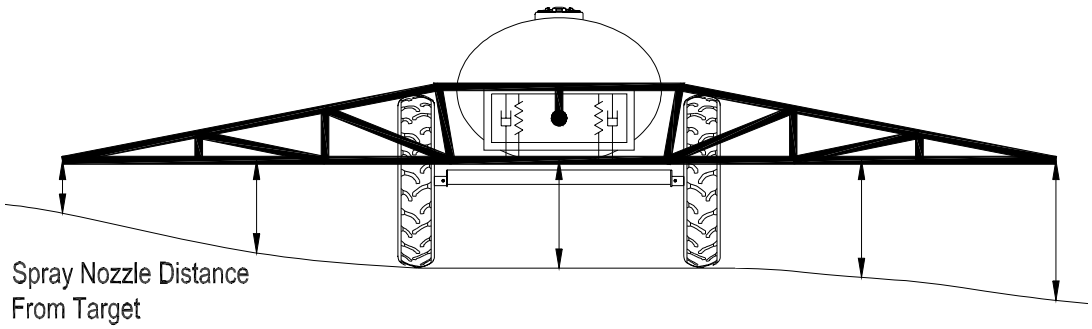

Figure 1.3a: Effect of Hilly Conditions on Spray Nozzle Distance from Target

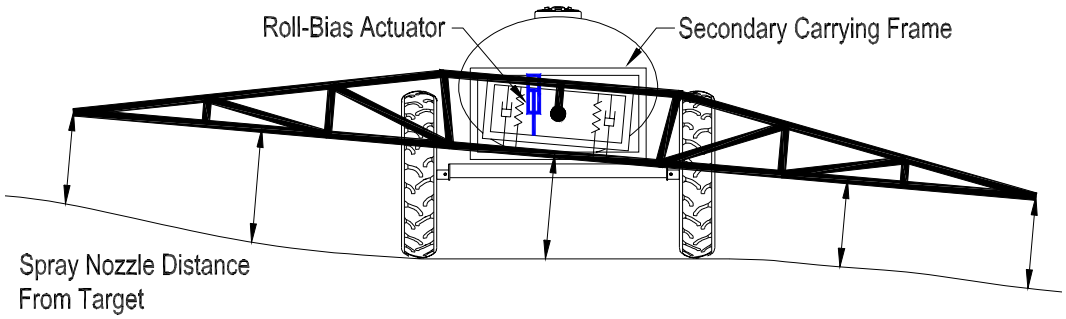

Figure 1.3b: Effect of Roll-Bias Actuator on Average Spray Nozzle Distance from Target

The research work in this field has treated boom motion in two categories:

i. rigid body motions, where the boom is considered as a single solid structure along its length, and

ii. flexible body motions, where the structural design and material composition of the boom allow deformation of the structure.

The modern sprayer boom is increasingly becoming much more complicated. Typical boom designs are comprised of three coupled sections; the center boom section which is a short length of boom usually the width of the carrying machine, and (as viewed from the rear of the machine) left and right boom sections which extend from both sides of the center section. Hydraulic actuators are employed to provide independent orientation of the left and right sections with respect to the center section (Figure 1.4). This feature allows the operator to achieve the optimum overall boom orientation.

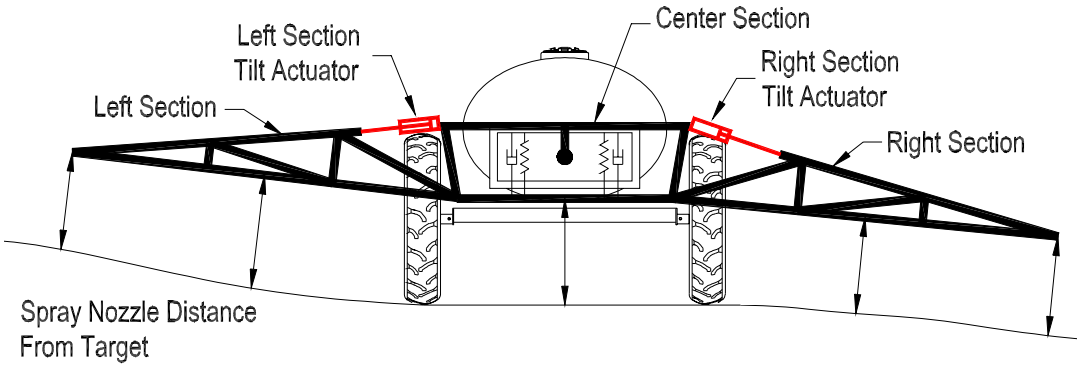

Figure 1.4: Effect of Wing-Tilt Actuators on Spray Nozzle Distance from Target

1.3 Effects of Tilt Actuator Motion

Consider a typical boom design consisting of three coupled sections and a passive suspension system as in Figure 1.4. The boom is a symmetric structure about the centerline of the machine, with the three sections' centers of gravity and points of rotation being the most important locations on the structure (Figure 1.5a). Due to this symmetry, in a static state the right and left sections counterbalance each other. To limit complexity it is desirable to focus on the effects of one tilt actuator only. The boom system is then simplified into two rigid bodies; the combined left and center sections and the right section (Figure 1.5b). The effect of using the tilt actuator to rotate the right section is shown in Figure 1.5c. Evaluating what is occurring during this change facilitates visualization of the effect on the combined left and center boom sections. To rotate the right section to an alternative position (a counter-clockwise rotation in this scenario), the force applied to it by the tilt actuator is increased. This increased actuator force creates a force imbalance on both structures. As the actuator is a two force member, the force it applies to the right section also gets applied to the center section. This force rotates the combined left and center sections clockwise (Figure 1.5d). When the desired position for the right section is reached, the force applied by the actuator is reduced in an attempt to bring the boom structure back to static balance. However, a static state is not immediately possible as the rotations have resulted in asymmetric positions of the sections' centers of gravities about the boom structure centerline. The weights of both sections will cause the structure to oscillate until the passive suspension system can damp out the oscillations and return the system to a static balance point. This static balance point will not match the original as the change in length of the tilt actuator has rotated the right section's center of gravity closer to the central pivot point. The new geometry on the right side requires the combined left and center sections to be oriented differently from their original static balance position.

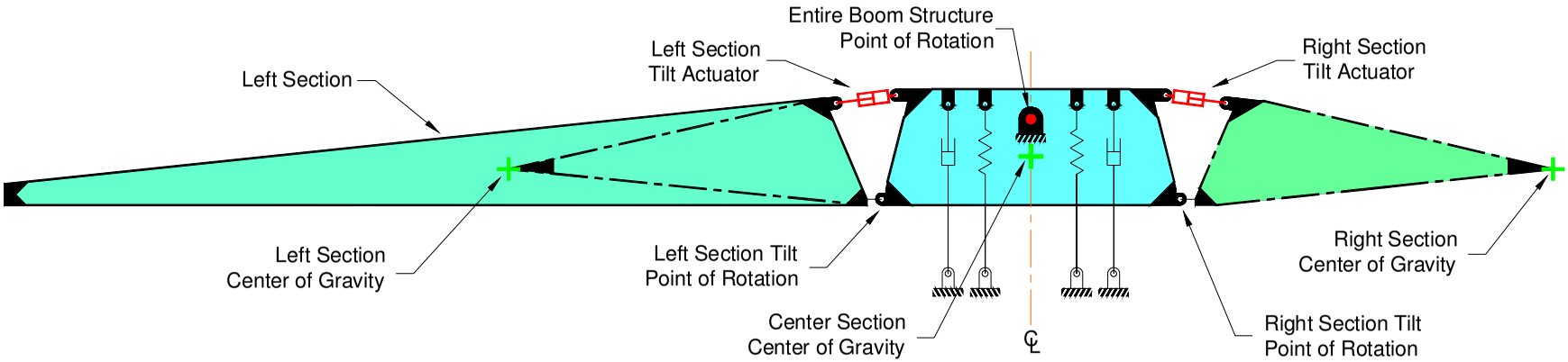

Figure 1.5a: Centers of Gravity and Points of Rotation of Symmetric Boom Structure (Note: Only part of the right section is shown; the actual shape is identical to the left section)

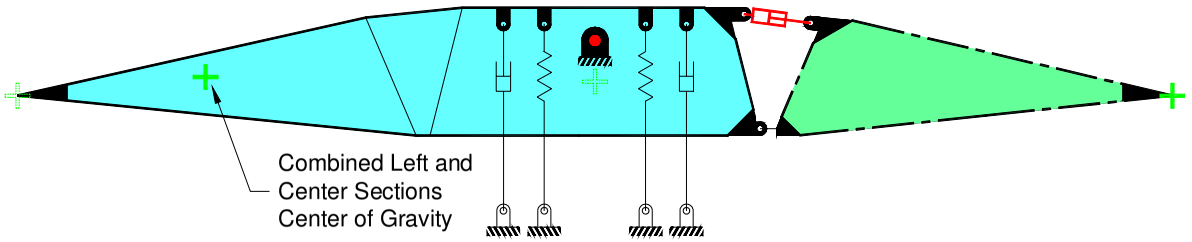

Figure 1.5b: Simplified Boom System Centers of Gravity (Note: The left and center sections have been combined to form a single rigid body)

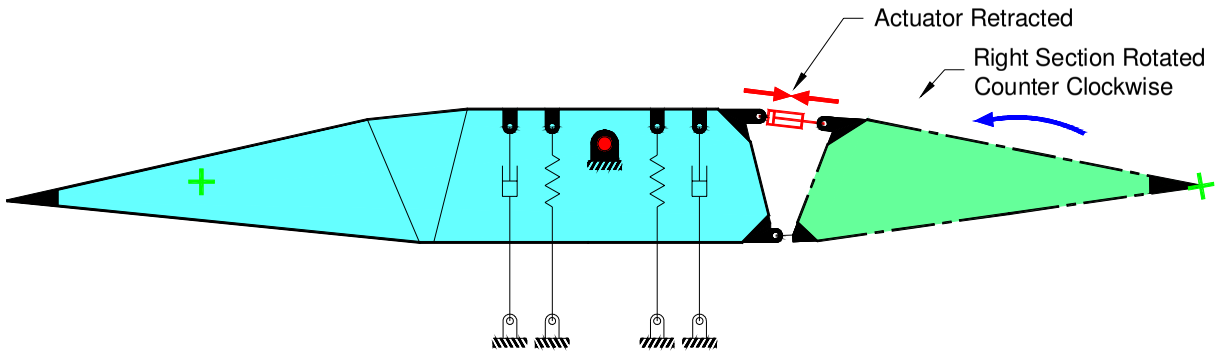

Figure 1.5c: Rotation of Right Section by Tilt Actuator

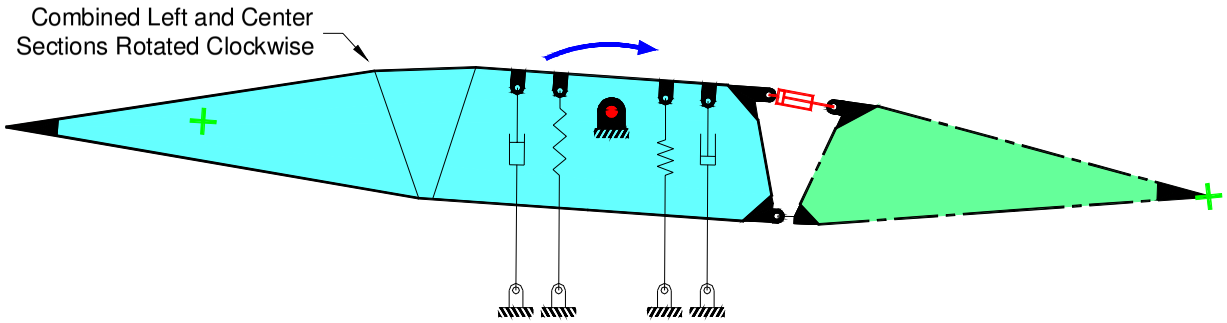

Figure 1.5d: Rotation of Combined Left and Center Sections Caused by Rotating Right Section

Similar logic can be applied when the right section is to be lowered. The force imbalance results in a counter clockwise rotation of the combined left and center sections. Again the asymmetry caused by the rotations of each section results in system oscillation and a different overall static balance point.

The dynamic motion of the boom sections is in fact more complicated than this explanation. This is due to the passive suspension elements and the boom sections' inertias. However, the crux of the problem remains that an attempt to correct the orientation of one section results in an 'orientation' error across the entire structure. In this context, orientation error is defined as a deviation of the desired distance from the boom to the target. By controlling the forces applied by the actuator this problem may be reduced/eliminated.

Only three forces act on the right section at any given time:

i. its weight acting through its center of gravity,
ii. the force provided by the tilt actuator, and
iii. a reaction force applied by the center section through its attachment point to the right section.

Using Newton's second law of motion, the force applied by the actuator is defined as a function of the right section's acceleration. The acceleration of the right section is controlled by changing the velocity of the actuator, which in turn is defined by the flow rate of hydraulic fluid provided. Therefore, by metering the amount of fluid supplied to the actuator through the use of hydraulic valves, the actuator acceleration can be controlled. Hence, it is conceivable that the overall system oscillation may be reduced.

1.4 Typical Hydraulic System

Valves control hydraulic fluid flow from a source (hydraulic pump) to a sink (actuator) (Figure 1.6). The valves have different positions to allow hydraulic fluid to flow in different paths. When the valve is closed, no fluid flows and the actuator is held in a fixed state; when the valve is fully opened, the flow

is maximized and the actuator moves accordingly. Typically, three-position valves are employed to allow an actuator to be extended, retracted, and held stationary (neutral).

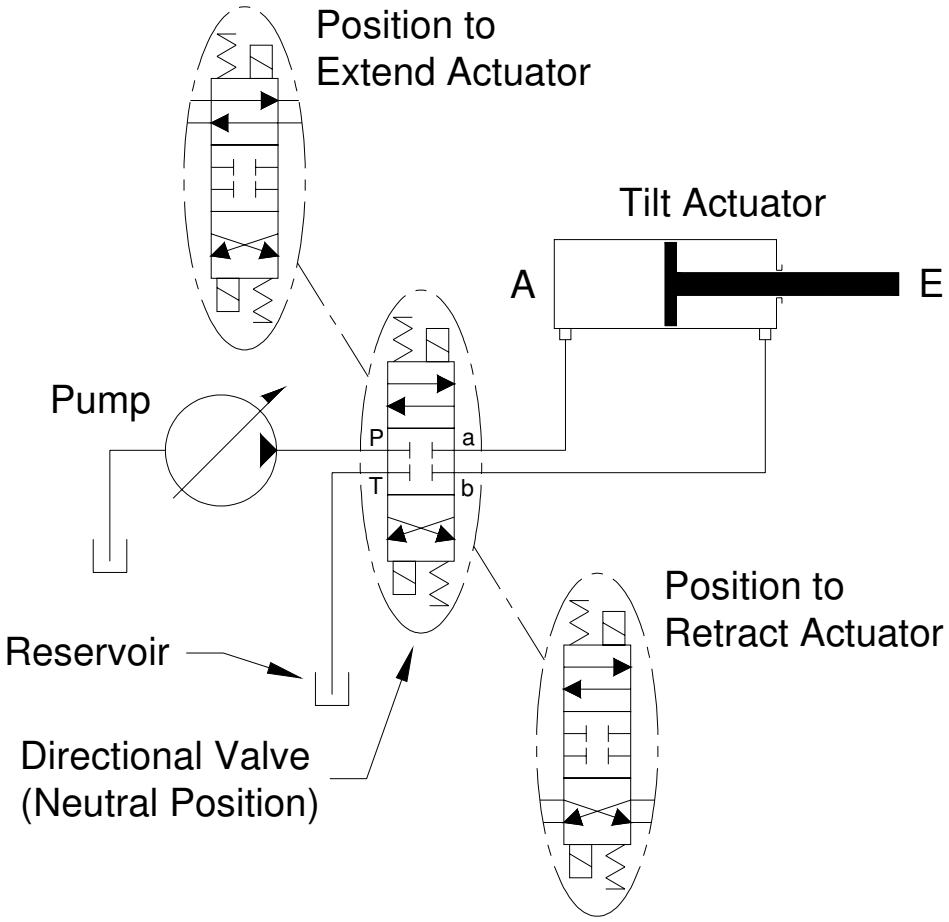

Figure 1.6: Typical Tilt Actuator Hydraulic Circuit

On/Off electro-hydraulic spool valves are used in the majority of commercially available sprayers as they can be activated remotely from the cab, continue to function with degraded fluid, and are cost effective. They use mechanical motion to control start, stop, and direction of flow.

The main components of an electro-hydraulic spool valve are the housing, spool, centering springs, and electrical solenoids. The housing directs both supply and return flow from the source through to the actuator and back to the reservoir. The spool controls the flow porting through the housing, the

centering springs ensure that the spool has a neutral position regardless of electrical energy supply, and the electrical solenoids move the spool to define the desired flow path (Figure 1.7). When the spool is moved in one direction the flow is routed to one side of the actuator (extended, for example) and the right section is tilted clockwise, while if it is moved in the opposite direction (retracted) the right section is tilted counter clockwise.

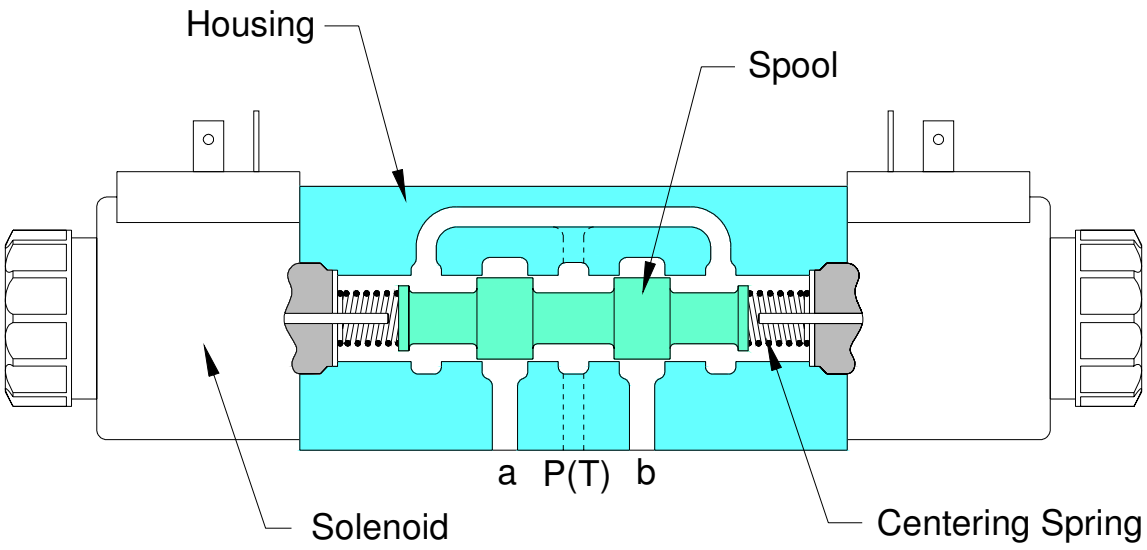

Figure 1.7: Electro-hydraulic Spool Valve

The amount of flow through the valve is derived from Bernoulli's equation (neglecting the effects of gravity and assuming turbulent flow) (Merritt, 1967) [1]:

$$Q = C_d * A_o * \sqrt{\frac{2}{\rho} * (\Delta P)}\,, \qquad [1.1]$$

where:

Q is the fluid flow through the orifice [m^3/s],

C_d is a constant (at large Reynolds numbers) called the discharge coefficient,

A_o is the cross-sectional area of the orifice [m^2],

ρ is the density of the hydraulic fluid [kg/m^3], and

ΔP is the pressure drop across the orifice [Pa].

[1] An asterisk (*) was used to clarify lengthy equations introduced in later chapters, thus it was adopted throughout for consistency.

Flow metering can be achieved by changing the orifice area, which in turn is a function of spool position and the pressure drop across the valve.

On/off valves have only two operating positions and therefore define only two flow rates – on and off. Because typically operated on/off valves cannot control actuator velocity, many sprayer manufacturers add a fixed orifice to the circuit. The orifice creates an additional pressure drop in the circuit that effectively limits the flow rate through the system more than the valve alone; therefore, the maximum velocity of the actuator is reduced. By reducing the maximum velocity, the momentum of the boom system is also reduced and the coupling effect between boom sections can be limited. The downsides of orifice use are the increased time required for boom orientation corrections, obstacle avoidance, and increased hydraulic energy losses.

In summary, a passive suspension system is typically employed on agricultural suspended boom sprayers to limit the effects of carrying-frame motion on boom orientation. Tilt actuators are used by the operator to optimally orient each wing section to match the terrain and maintain the desired distance from boom to target. These changes to one section induce an oscillating error across the machine width due to the suspension system. Use of a fixed orifice reduces this effect but also limits the functionality of the machine.

1.5 Research Objectives

To the author's knowledge, no academic research has been performed to quantify and reduce the oscillations caused by operator defined boom orientation changes. Therefore, the objectives of this research were:

1. to develop a computer simulation model of a 27-m Flexi-coil™ sprayer boom, passive suspension system, and tilt actuator,
2. to quantify the negative effects that independent tilt actuator control of one section has on the roll of the boom using an on/off valve, and

3. to evaluate whether these negative effects can be minimized by controlling tilt actuator acceleration rate with alternative commercially available valves.

The remainder of this thesis is structured into five chapters. Chapter 2 will focus on the development and validation of the boom simulation model using the tilt actuator as the system input. Chapter 3 further develops the model to relate the tilt actuator back to the valve which is the true source of system input. Chapter 4 details the experimental work completed to define necessary system parameters. A baseline for typical system performance is established in Chapter 5, along with a discussion of the benefits of two alternative valve types. Chapter 6 summarizes the conclusions of the work with a look forward to the possibilities for future work.

Chapter 2

Suspended Boom Structure - Simulation Model Development and Validation

Using kinetic, kinematic, and trigonometric relations, the necessary equations are developed in this chapter to create a dynamic computer simulation model of the boom and suspension system of a suspended boom sprayer. A comparison to experimental data is presented to validate the equations employed.

2.1 Benefits of Computer Simulation

Field evaluation of prototype concepts was historically undertaken to fully understand the impact of design changes on the operational performance of agricultural equipment. This methodology is undesirable because:

i. prototype manufacture of multiple concepts is costly,
ii. the desired field conditions are spread over a wide geographical area, and
iii. input variables are difficult to reproduce repeatedly for trial-to-trial comparisons.

Computer simulation provides an alternative that allows a large number of conditions to be evaluated quickly and consistently without the need for prototypes. The development of the equations for a two-dimensional dynamic model of a suspended boom sprayer to be implemented using a software simulation environment (Mathworks, 2001) is presented in this chapter.

2.2 Suspended Boom Sprayer Geometry

The sprayer chosen for evaluation was a Flexicoil 67XL™ trailing model with a 27-m boom (CNH Canada Ltd., 2003) and no additional suspension elements between the carrying frame and the tires. The boom is divided into two 12-m left and right sections and a 3-m center section. The points of interest include only the centers of gravity of each section, all points of rotation, and the location of the passive suspension system elements (struts); the struts include both springs and a viscous damping mechanism. To study the system, a 'skeleton' was created to connect these points of geometry (Figure 2.1). The two-dimensional movements of these points with respect to the carrying frame were the focus of this research.

For this study, the effect of only the right section's tilt actuator is to be evaluated; the center and left sections may then be considered as a single rigid body with a combined center of gravity, point Q_{CL}. The right section is attached to the center section and allowed to rotate with respect to it about point B. This rotation is controlled by the tilt actuator attached between points A and E. The center section is attached to and allowed to rotate about the carrying frame via point C. The passive suspension system elements (struts) are attached between points M1 and N1, M2 and N2, M3 and N3, and M4 and N4. Points designated with 'M' are attached to the boom structure while points designated with 'N' are attached to the carrying frame.

The global coordinate system is oriented with an x-axis directed 45-degrees counter-clockwise from horizontal; the y-axis is defined 45-degrees clockwise from horizontal. Positive rotations are defined using the right-hand rule through these two axes (clockwise); the positive z-axis is then defined in the machine direction of travel. This unique coordinate system was defined so that all rotations would occur within a 90-degree frame of reference. During dynamic simulation, this avoids any sign switching that may occur when using

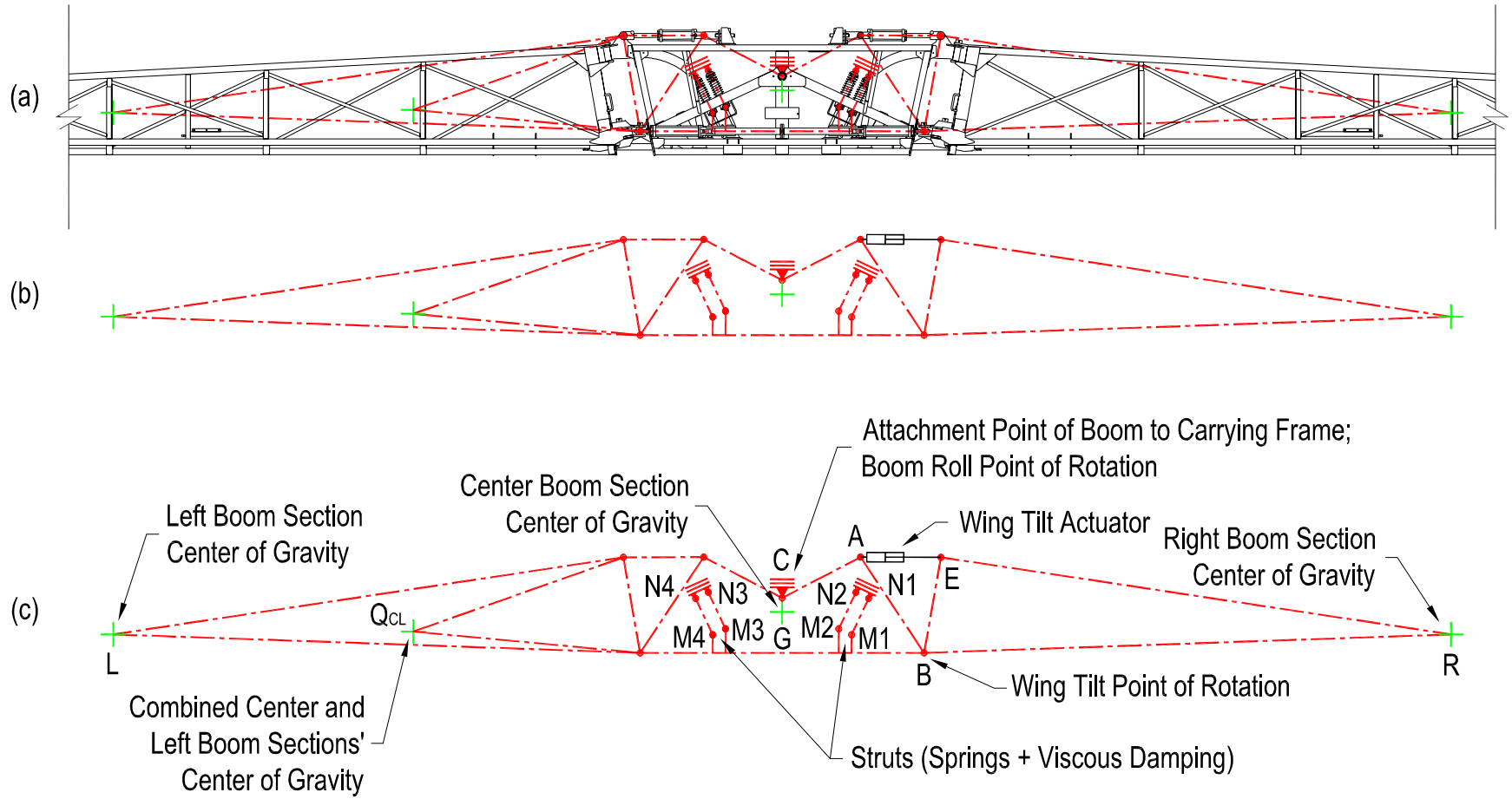

Figure 2.1: (a) Overlay of Skeleton to Important Points of Suspended Boom Sprayer
(b) Skeleton Geometry
(c) Definition of Important Points of Skeleton Geometry

trigonometric functions. Sign switching adds unnecessary complexity within the mathematical framework of the equations.

Development of the model requires definition of a series of kinetic, kinematic, and trigonometric equations. To develop the necessary kinetic equations, the structure must be divided into two free body diagrams (FBDs); the right section and the combined left and center section.

2.3 Kinetics of Boom Structure

Kinetics is the branch of mechanics which studies the effects of forces on the motion of a body. Newton's second law of motion states *a body acted upon by an unbalanced force, **F,** experiences an acceleration, **a,** that has the same direction as the force and a magnitude that is directly proportional to the force*. Mathematically, the equation of motion is given by:

$$\Sigma \boldsymbol{F} = m * \boldsymbol{a}, \qquad [2.1]$$

where:

$\Sigma \boldsymbol{F}$ is the vector summation of all forces acting on the body (N),

m is the mass of the body (kg), and

$\boldsymbol{a}$ is the acceleration (m/s^2).

2.3.1 Right Section Free Body Diagram

Using the equation of motion to evaluate the right section FBD (Figure 2.2) for forces acting in the x-direction yields:

$$\sum F_{Rx} = m_R * a_{Rx}, \qquad [2.2]$$

where:

ΣF_{Rx} is the summation of all forces in the x-direction acting on the right section (N),

m_R is the mass of the right section (kg), and

a_{Rx} is the acceleration of point R in the x-direction (m/s^2).

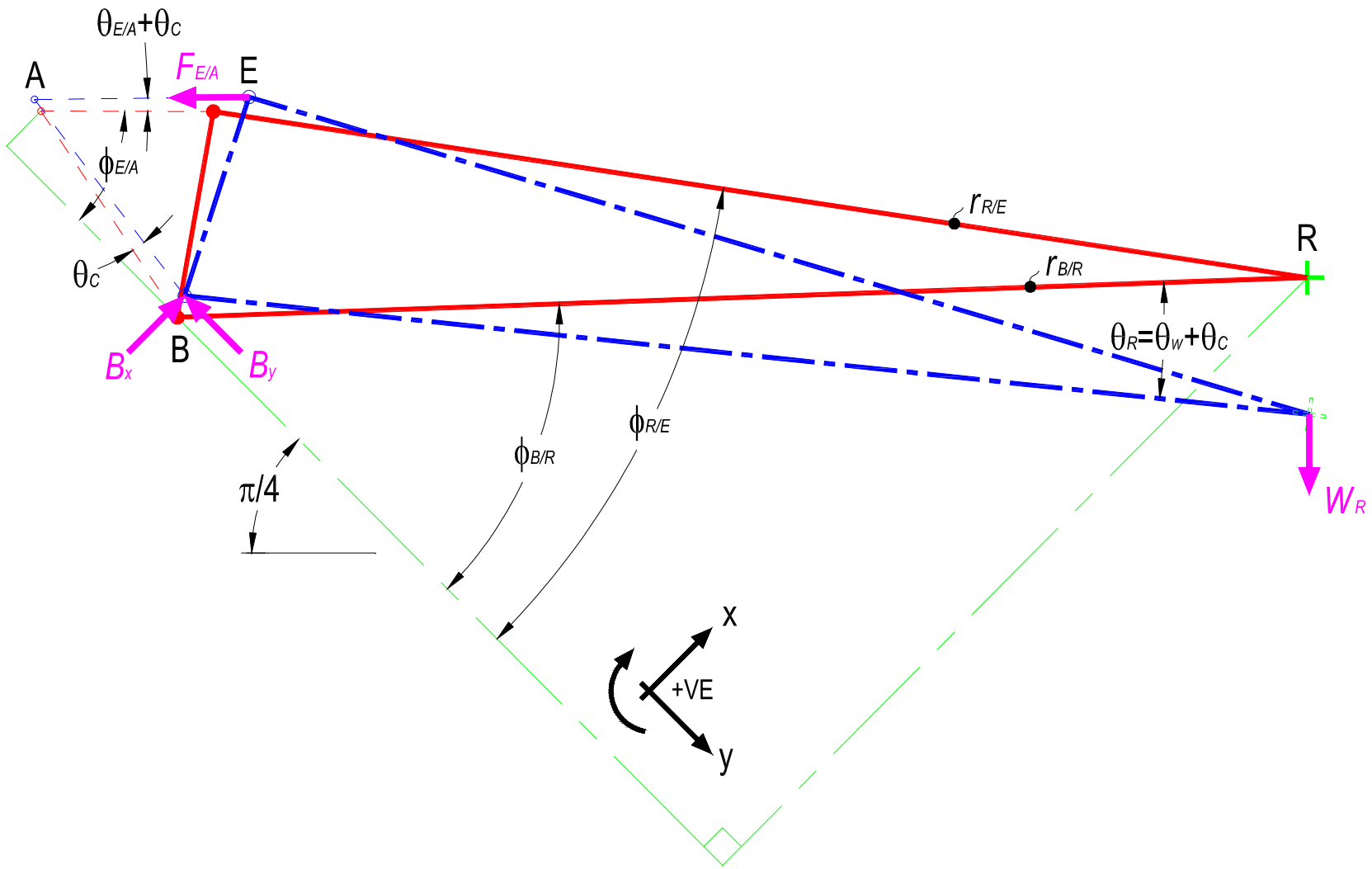

Figure 2.2: Right Section Starting Geometry (Solid Red Line) and Free Body Diagram (Dashed Blue Line)

Expanding equation 2.2 for individual forces acting in the x-direction yields:

$$B_x - W_R * \sin\left(\pi/4\right) - F_{E/A} * \sin\left(\phi_{E/A} - \theta_{E/A} - \theta_C\right) = m_R * a_{Rx}, \quad [2.3$$

where:

B_x is the reaction force in the x-direction applied by the tilt point of rotation (N),

W_R is the weight of the right section (N),

$F_{E/A}$ is the force applied by the tilt actuator (N),

$\phi_{E/A}$ is the initial angle between the y-axis and a vector between points A and E (rad),

$\theta_{E/A}$ is the change in orientation of the vector between points A and E due to a change in the length of the tilt actuator (rad), and

θ_C is the change in orientation of the vector between points A and E due to a change in the rotational position of the combined left and center sections (rad).

Solving this equation for B_x gives:

$$B_x = W_R * \sin\left(\pi/4\right) + F_{E/A} * \sin\left(\phi_{E/A} - \theta_{E/A} - \theta_C\right) + m_R * a_{Rx}. \quad [2.4]$$

A similar equation is defined for forces acting in the y-direction:

$$\sum F_{Ry} = m_R * a_{Ry}, \quad [2.5]$$

where:

ΣF_{Ry} is the summation of all forces in the y-direction acting on the right section (N), and

a_{Ry} is the acceleration of point R in the y-direction (m/s^2).

Evaluating equation 2.5 for individual forces acting in the y-direction yields:

$$-B_y + W_R * \cos\left(\pi/4\right) - F_{E/A} * \cos\left(\phi_{E/A} - \theta_{E/A} - \theta_C\right) = m_R * a_{Ry}, \quad [2.6]$$

where:

B_y is the reaction force in the y-direction applied by the tilt point of rotation (N).

Solving equation 2.6 for B_y yields:

$$B_y = W_R * \cos\left(\pi/4\right) - F_{E/A} * \cos(\phi_{E/A} - \theta_{E/A} - \theta_C) - m_R * a_{Ry}. \quad [2.7]$$

A third general equation of two-dimensional motion for a rigid body can be written as the summation of moments about an axis perpendicular to the x-y plane through the center of gravity:

$$\sum M_R = I_R * \alpha_R, \quad [2.8]$$

where:

ΣM_R is the summation of all moments about the right section's center of gravity (point R) (N·m),

I_R is the mass moment of inertia of the right section about an axis perpendicular to the x-y plane through the center of gravity (kg·m^2), and

α_R is the magnitude of angular acceleration of the right section about an axis perpendicular to the x-y plane (rad/s^2).

Expanding equation 2.8 for individual moments gives:

$$\begin{aligned} &B_x * r_{B/R} * \cos(\phi_{B/R} - \theta_R) + B_y * r_{B/R} * \sin(\phi_{B/R} - \theta_R) - \\ &F_{E/A} * r_{R/E} * \cos(\phi_{R/E} - \theta_R) * \sin(\phi_{E/A} - \theta_{E/A} - \theta_C) + \\ &F_{E/A} * r_{R/E} * \sin(\phi_{R/E} - \theta_R) * \cos(\phi_{E/A} - \theta_{E/A} - \theta_C) = I_R * \alpha_R \end{aligned}, \quad [2.9]$$

where:

$r_{B/R}$ is the magnitude of a vector between points R and B (m),

$\phi_{B/R}$ is the initial angle between the y-axis and a vector between points R and B (rad),

$r_{R/E}$ is the magnitude of a vector between points E and R (m),

$\phi_{R/E}$ is the initial angle between the y-axis and a vector between points E and R (rad), and

θ_R is the angular change in orientation of the right section from the initial starting point (rad).

Solving equation 2.9 for $F_{E/A}$ yields [2]:

$$F_{E/A} = \frac{\left(-B_x * r_{B/R} * \cos(\phi_{B/R} - \theta_R) - B_y * r_{B/R} * \sin(\phi_{B/R} - \theta_R) + I_R * \alpha_R\right)}{\left(\begin{array}{l} r_{R/E} * \sin(\phi_{R/E} - \theta_R) * \cos(\phi_{E/A} - \theta_{E/A} - \theta_C) - \\ r_{R/E} * \cos(\phi_{R/E} - \theta_R) * \sin(\phi_{E/A} - \theta_{E/A} - \theta_C) \end{array}\right)}. \quad [2.10]$$

The angular change in orientation of the right section (θ_R) is defined as:

$$\theta_R = \theta_W + \theta_C, \quad [2.11]$$

where:

θ_W is the angular change in orientation of the right section due to length changes of the actuator (rad).

Breaking the angular change into a summation of its components was done to allow use of the trigonometric identities developed in section 2.5.

2.3.2 Combined Left and Center Sections Free Body Diagram

Performing a similar evaluation on the combined left and center sections FBD (Figures 2.3a and 2.3b) for forces acting in the x-direction gives:

$$\sum F_{Qx} = m_Q * a_{Qx}, \quad [2.12]$$

where:

ΣF_{Qx} is the summation of all forces in the x-direction acting on the combined left and center sections (N),

m_Q is the mass of the combined left and center sections (kg), and

a_{Qx} is the acceleration of point Q_{CL} in the x-direction (m/s^2).

Expanding ΣF_{Qx} yields:

$$\begin{array}{l} -B_x + C_x - W_Q * \sin\left(\pi/4\right) + F_{E/A} * \sin(\phi_{E/A} - \theta_{E/A} - \theta_C) - \\ F_{S1} * \sin(\theta_{S1}) - F_{S2} * \sin(\theta_{S2}) - F_{S3} * \sin(\theta_{S3}) - F_{S4} * \sin(\theta_{S4}) = m_Q * a_{Qx} \end{array}, \quad [2.13]$$

[2] The form of the equation is not to be confused with a matrix. This particular form was adopted to accommodate lengthy equations.

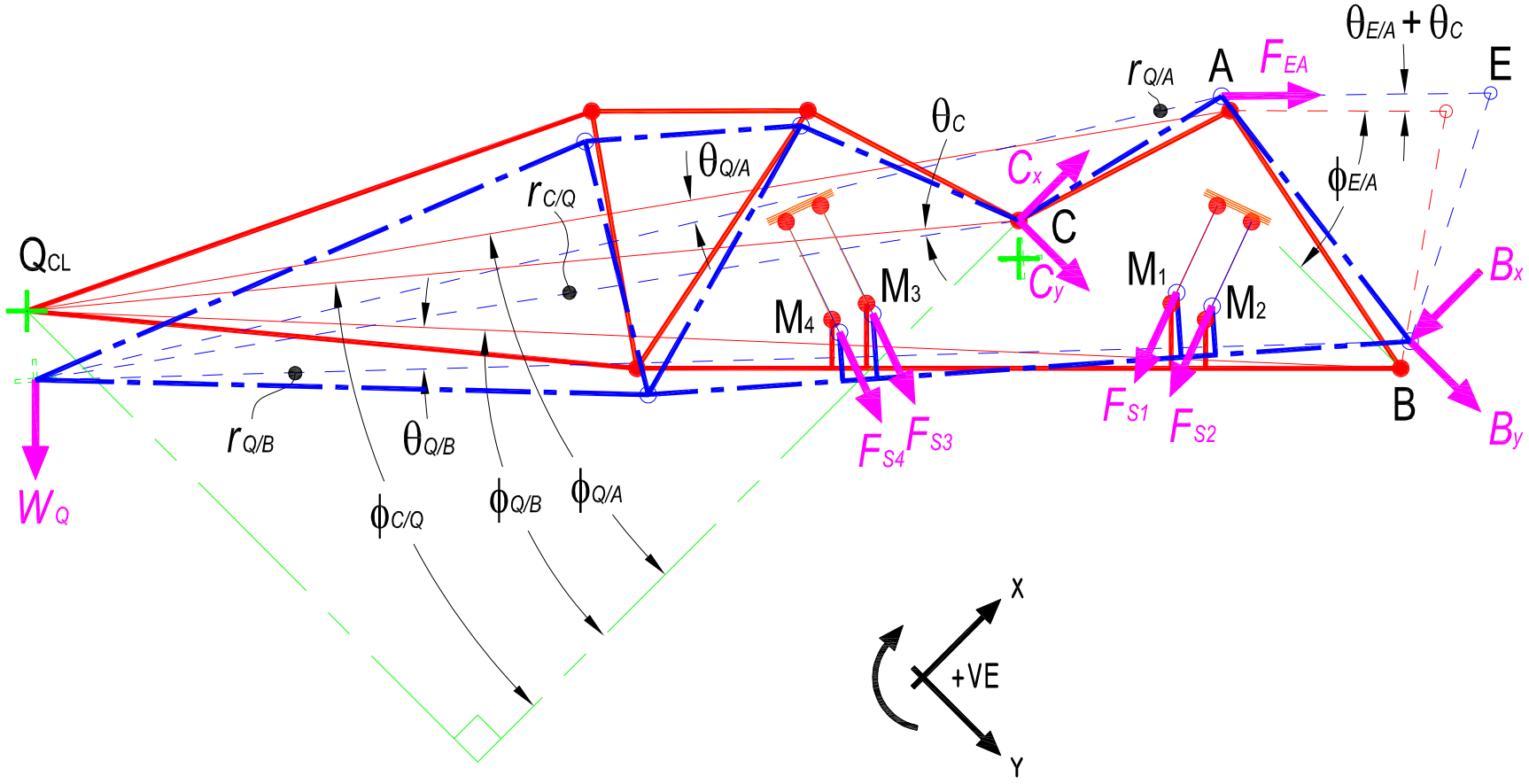

Figure 2.3a: Combined Left and Center Sections Starting Geometry (Solid Red Line) and FBD (Dashed Blue Line) – Definitions of Locations for Points A, B, and C with respect to Q_{CL}

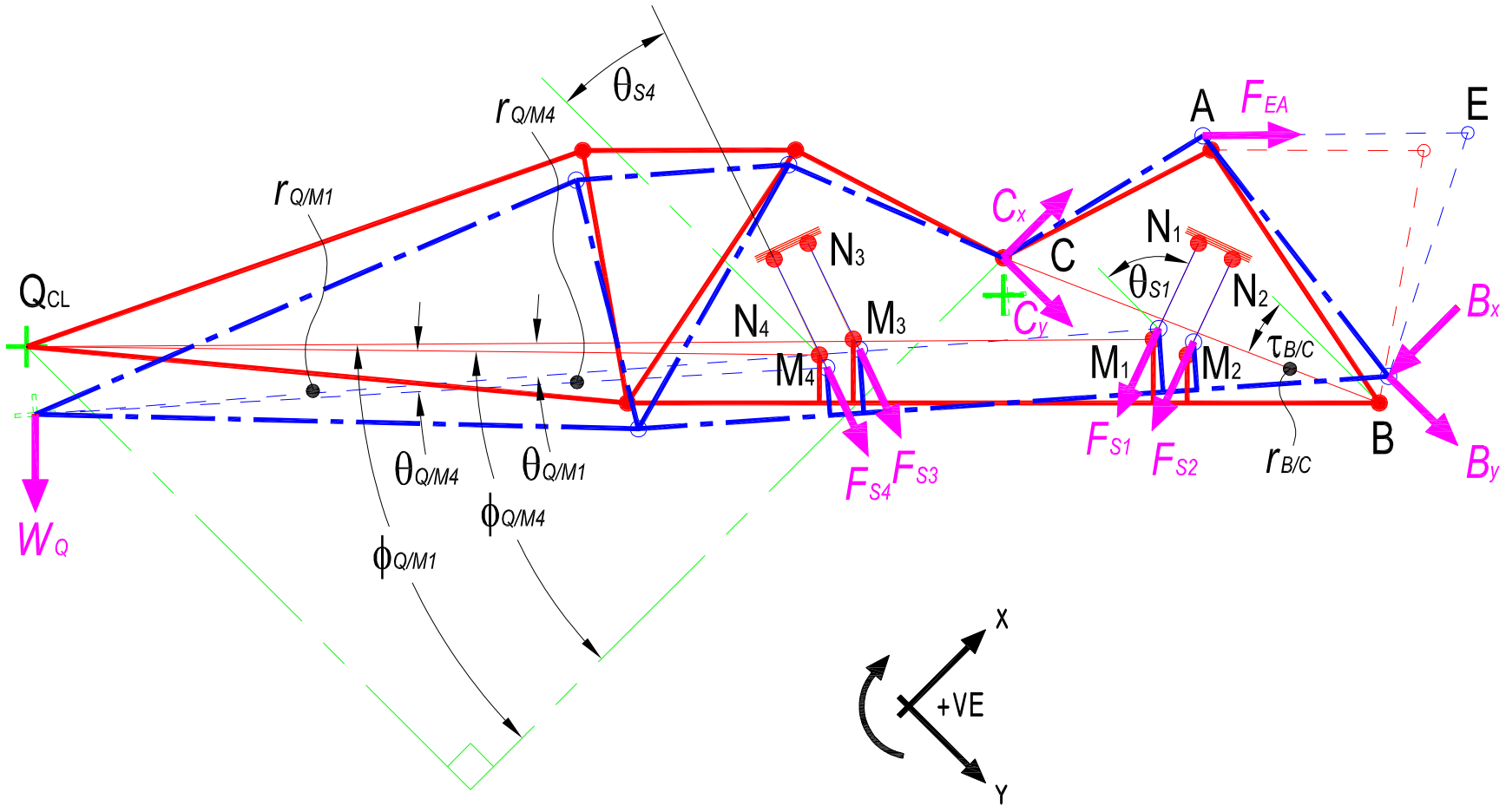

Figure 2.3b: Combined Left and Center Sections Starting Geometry (Solid Red Line) and FBD (Dashed Blue Line) – Definitions of Locations for Points M1 and M4 with respect to Q_{CL} (Points M2 and M3 are Similar) and Point B with Respect to C

where:

C_x is the reaction force in the x-direction applied by the chassis attachment point of rotation (N),

W_Q is the weight of the combined left and center sections (N),

F_{S1} is the force applied by strut number 1 (N),

F_{S2} is the force applied by strut number 2 (N),

F_{S3} is the force applied by strut number 3 (N),

F_{S4} is the force applied by strut number 4 (N),

θ_{S1} is the angle of orientation of strut number 1 with respect to the y-axis (rad),

θ_{S2} is the angle of orientation of strut number 2 with respect to the y-axis (rad),

θ_{S3} is the angle of orientation of strut number 3 with respect to the y-axis (rad), and

θ_{S4} is the angle of orientation of strut number 4 with respect to the y-axis (rad).

Solving this equation for C_x gives:

$$C_x = B_x + W_Q * \sin\left(\pi/4\right) - F_{E/A} * \sin(\phi_{E/A} - \theta_{E/A} - \theta_C) + m_Q * a_{Qx} + F_{S1} * \sin(\theta_{S1}) + F_{S2} * \sin(\theta_{S2}) + F_{S3} * \sin(\theta_{S3}) + F_{S4} * \sin(\theta_{S4}) \quad [2.14]$$

Forces in the y-direction relate to acceleration through use of the equation:

$$\sum F_{Qy} = m_Q * a_{Qy} \quad [2.15]$$

where:

ΣF_{Qy} is the summation of all forces in the y-direction acting on the combined left and center sections (N), and

a_{Qy} is the acceleration of point Q_{CL} in the y-direction (m/s^2).

Substituting the individual forces into equation 2.15 yields:

$$B_y + C_y + W_Q * \cos\left(\pi/4\right) + F_{E/A} * \cos(\phi_{E/A} - \theta_{E/A} - \theta_C) + F_{S1} * \cos(\theta_{S1}) + F_{S2} * \cos(\theta_{S2}) + F_{S3} * \cos(\theta_{S3}) + F_{S4} * \cos(\theta_{S4}) = m_Q * a_{Qy} \quad [2.16]$$

which can be rewritten to solve for C_y:

$$C_y = -B_y - W_Q * \cos\left(\pi/4\right) - F_{E/A} * \cos\left(\phi_{E/A} - \theta_{E/A} - \theta_C\right) + m_Q * a_{Qy} - F_{S1} * \cos\left(\theta_{S1}\right) - F_{S2} * \cos\left(\theta_{S2}\right) - F_{S3} * \cos\left(\theta_{S3}\right) - F_{S4} * \cos\left(\theta_{S4}\right). \quad [2.17]$$

The third equation of motion, summation of moments about the center of gravity, is given by:

$$\sum M_Q = I_Q * \alpha_Q, \quad [2.18]$$

where:

ΣM_Q is the summation of all moments about the combined left and center sections' center of gravity (point Q_{CL}) (N·m),

I_Q is the mass moment of inertia of the combined left and center sections about an axis perpendicular to the x-y plane through the center of gravity (kg·m^2), and

α_Q is the angular acceleration of the combined left and center sections about an axis perpendicular to the x-y plane (rad/s^2).

Substituting all moments into equation 2.18 yields:

$$\begin{aligned}
&B_x * r_{Q/B} * \sin\left(\phi_{Q/B} + \theta_C\right) + B_y * r_{Q/B} * \cos\left(\phi_{Q/B} + \theta_C\right) - \\
&C_x * r_{Q/C} * \sin\left(\phi_{Q/C} + \theta_C\right) + C_y * r_{Q/C} * \cos\left(\phi_{Q/C} + \theta_C\right) - \\
&F_{E/A} * \sin\left(\phi_{E/A} - \theta_{E/A} - \theta_C\right) * r_{Q/A} * \sin\left(\phi_{Q/A} + \theta_C\right) + \\
&F_{E/A} * \cos\left(\phi_{E/A} - \theta_{E/A} - \theta_C\right) * r_{Q/A} * \cos\left(\phi_{Q/A} + \theta_C\right) + \\
&F_{S1} * \sin\left(\theta_{S1}\right) * r_{Q/M1} * \sin\left(\phi_{Q/M1} + \theta_C\right) + \\
&F_{S1} * \cos\left(\theta_{S1}\right) * r_{Q/M1} * \cos\left(\phi_{Q/M1} + \theta_C\right) + \\
&F_{S2} * \sin\left(\theta_{S2}\right) * r_{Q/M2} * \sin\left(\phi_{Q/M2} + \theta_C\right) + \\
&F_{S2} * \cos\left(\theta_{S2}\right) * r_{Q/M2} * \cos\left(\phi_{Q/M2} + \theta_C\right) + \\
&F_{S3} * \sin\left(\theta_{S3}\right) * r_{Q/M3} * \sin\left(\phi_{Q/M3} + \theta_C\right) + \\
&F_{S3} * \cos\left(\theta_{S3}\right) * r_{Q/M3} * \cos\left(\phi_{Q/M3} + \theta_C\right) + \\
&F_{S4} * \sin\left(\theta_{S4}\right) * r_{Q/M4} * \sin\left(\phi_{Q/M4} + \theta_C\right) + \\
&F_{S4} * \cos\left(\theta_{S4}\right) * r_{Q/M4} * \cos\left(\phi_{Q/M4} + \theta_C\right) \\
&= I_Q * \alpha_Q
\end{aligned} \quad , \quad [2.19]$$

where:

$r_{Q/B}$ is the magnitude of a vector between points B and Q_{CL} (m),

$\phi_{Q/B}$ is the initial angle between the negative x-axis and a vector between points B and Q_{CL} (rad),

$r_{Q/C}$ is the magnitude of a vector between points C and Q_{CL} (m),

$\phi_{Q/C}$ is the initial angle between the negative x-axis and a vector between points C and Q_{CL} (rad),

$r_{Q/A}$ is the magnitude of a vector between points A and Q_{CL} (m),

$\phi_{Q/A}$ is the initial angle between the negative x-axis and a vector between points A and Q_{CL} (rad),

$r_{Q/M1}$ is the magnitude of a vector between points M1 and Q_{CL} (m),

$\phi_{Q/M1}$ is the initial angle between the negative x-axis and a vector between points M1 and Q_{CL} (rad),

$r_{Q/M2}$ is the magnitude of a vector between points M2 and Q_{CL} (m),

$\phi_{Q/M2}$ is the initial angle between the negative x-axis and a vector between points M2 and Q_{CL} (rad),

$r_{Q/M3}$ is the magnitude of a vector between points M3 and Q_{CL} (m),

$\phi_{Q/M3}$ is the initial angle between the negative x-axis and a vector between points M3 and Q_{CL} (rad),

$r_{Q/M4}$ is the magnitude of a vector between points M4 and Q_{CL} (m), and

$\phi_{Q/M4}$ is the initial angle between the negative x-axis and a vector between points M4 and Q_{CL} (rad).

Solving equation 2.19 for α_Q yields:

$$\alpha_Q = \frac{1}{I_Q}\begin{pmatrix} B_x * r_{Q/B} * \sin(\phi_{Q/B} + \theta_C) + B_y * r_{Q/B} * \cos(\phi_{Q/B} + \theta_C) - \\ C_x * r_{Q/C} * \sin(\phi_{Q/C} + \theta_C) + C_y * r_{Q/C} * \cos(\phi_{Q/C} + \theta_C) - \\ F_{E/A} * \sin(\phi_{E/A} - \theta_{E/A} - \theta_C) * r_{Q/A} * \sin(\phi_{Q/A} + \theta_C) + \\ F_{E/A} * \cos(\phi_{E/A} - \theta_{E/A} - \theta_C) * r_{Q/A} * \cos(\phi_{Q/A} + \theta_C) + \\ F_{S1} * \sin(\theta_{S1}) * r_{Q/M1} * \sin(\phi_{Q/M1} + \theta_C) + \\ F_{S1} * \cos(\theta_{S1}) * r_{Q/M1} * \cos(\phi_{Q/M1} + \theta_C) + \\ F_{S2} * \sin(\theta_{S2}) * r_{Q/M2} * \sin(\phi_{Q/M2} + \theta_C) + \\ F_{S2} * \cos(\theta_{S2}) * r_{Q/M2} * \cos(\phi_{Q/M2} + \theta_C) + \\ F_{S3} * \sin(\theta_{S3}) * r_{Q/M3} * \sin(\phi_{Q/M3} + \theta_C) + \\ F_{S3} * \cos(\theta_{S3}) * r_{Q/M3} * \cos(\phi_{Q/M3} + \theta_C) + \\ F_{S4} * \sin(\theta_{S4}) * r_{Q/M4} * \sin(\phi_{Q/M4} + \theta_C) + \\ F_{S4} * \cos(\theta_{S4}) * r_{Q/M4} * \cos(\phi_{Q/M4} + \theta_C) \end{pmatrix}. \quad [2.20]$$

Six two-dimensional kinetic equations of motion for this system are defined by equations 2.4, 2.7, 2.10, 2.14, 2.17, and 2.20. Due to the number of unknown variables in this system, numerous other equations need to be developed using the laws of kinematics.

2.4 Kinematic Equations

As opposed to kinetics, kinematics does not consider the mass of a body or the forces acting on it when evaluating motion. Linear acceleration of any point (P) on a rigid body may be defined with respect to any other point (O) on the rigid body if the angular acceleration and angular velocity of the body are known (Hibbeler, 1992). This formula is given by:

$$\mathbf{a}_P = \mathbf{a}_O + \boldsymbol{\alpha} \times \mathbf{r}_{P/O} - \omega^2 * \mathbf{r}_{P/O}, \quad [2.21]$$

where:

$\mathbf{a}_P$ is the acceleration of point P (m/s^2),

$\mathbf{a}_O$ is the acceleration of point O (m/s^2),

$\boldsymbol{\alpha}$ is the angular acceleration of the rigid body (rad/s^2),

$\mathbf{r}_{P/O}$ is a vector from point O to point P (m), and

ω is the angular velocity of the rigid body (rad/s).

The symbol × signifies the cross product of two vectors; this process accounts for both magnitude and direction (Hibbeler, 1992).

Equation 2.21 can be written for point B with respect to the right section's center of gravity (point R) as:

$$\mathbf{a}_B = \mathbf{a}_R + \boldsymbol{\alpha}_R \times \mathbf{r}_{B/R} - \omega_R^{\,2} * \mathbf{r}_{B/R}, \qquad [2.22]$$

where:

$\mathbf{a}_B$ is the acceleration of point B (m/s^2),

$\mathbf{a}_R$ is the acceleration of point R (m/s^2),

$\boldsymbol{\alpha}_R$ is the angular acceleration of the right section (rad/s^2),

$\mathbf{r}_{B/R}$ is a vector from point R to point B (m), and

ω_R is the angular velocity of the right section (rad/s).

By separating the vectors into magnitudes and directions, equation 2.22 can be rewritten as:

$$a_{Bx} * \hat{i} + a_{By} * \hat{j} = \begin{pmatrix} a_{Rx} * \hat{i} + a_{Ry} * \hat{j} + \\ \alpha_R * \hat{k} \times \begin{pmatrix} -r_{B/R} * \sin(\phi_{B/R} - \theta_R) * \hat{i} - \\ r_{B/R} * \cos(\phi_{B/R} - \theta_R) * \hat{j} \end{pmatrix} - \\ \omega_R^{\,2} * \left(-r_{B/R} * \sin(\phi_{B/R} - \theta_R) * \hat{i} - r_{B/R} * \cos(\phi_{B/R} - \theta_R) * \hat{j}\right) \end{pmatrix}, \qquad [2.23]$$

where:

a_{Bx} is the acceleration of point B in the x-direction (m/s^2), and

a_{By} is the acceleration of point B in the y-direction (m/s^2).

After calculating the cross product, the x and y components of this equation yield two separate independent equations. These are:

$$a_{Bx} = a_{Rx} + \alpha_R * r_{B/R} * \cos(\phi_{B/R} - \theta_R) + \omega_R^{\,2} * r_{B/R} * \sin(\phi_{B/R} - \theta_R), \text{ and} \qquad [2.24]$$

$$a_{By} = a_{Ry} - \alpha_R * r_{B/R} * \sin(\phi_{B/R} - \theta_R) + \omega_R^{\,2} * r_{B/R} * \cos(\phi_{B/R} - \theta_R). \qquad [2.25]$$

Solving equation 2.24 for a_{Rx} gives:

$$a_{Rx} = a_{Bx} - \alpha_R * r_{B/R} * \cos(\phi_{B/R} - \theta_R) - \omega_R{}^2 * r_{B/R} * \sin(\phi_{B/R} - \theta_R). \quad [2.26]$$

Similarly, equation 2.25 can be rewritten as:

$$a_{Ry} = a_{By} + \alpha_R * r_{B/R} * \sin(\phi_{B/R} - \theta_R) - \omega_R{}^2 * r_{B/R} * \cos(\phi_{B/R} - \theta_R). \quad [2.27]$$

Referencing the combined left and center sections, a similar equation can be written for points B and C:

$$\mathbf{a}_B = \mathbf{a}_C + \boldsymbol{\alpha}_C \times \mathbf{r}_{B/C} - \omega_C{}^2 * \mathbf{r}_{B/C}, \quad [2.28]$$

where:

$\mathbf{a}_C$ is the directional linear acceleration of point C (m/s^2),

$\boldsymbol{\alpha}_C$ is the directional angular acceleration of the combined left and center sections (rad/s^2),

$\mathbf{r}_{B/C}$ is a vector from point B to point C (m), and

ω_C is the angular velocity of the combined left and center sections (rad/s).

Point C has no relative motion with respect to the carrying frame, therefore $\mathbf{a}_C$ is zero. Substituting the vectors' magnitudes and directions, calculating the cross product, and separating the x and y components yields:

$$a_{Bx} = -\alpha_C * r_{B/C} * \cos(\tau_{B/C} - \theta_C) - \omega_C{}^2 * r_{B/C} * \sin(\tau_{B/C} - \theta_C), \text{ and} \quad [2.29]$$

$$a_{By} = \alpha_C * r_{B/C} * \sin(\tau_{B/C} - \theta_C) - \omega_C{}^2 * r_{B/C} * \cos(\tau_{B/C} - \theta_C), \quad [2.30]$$

where:

$\tau_{B/C}$ is the initial angle between the y-axis and a vector between points B and C (rad).

The linear acceleration for points C and Q_{CL} is given by:

$$\mathbf{a}_Q = \mathbf{a}_C + \boldsymbol{\alpha}_C \times \mathbf{r}_{Q/C} - \omega_C{}^2 * \mathbf{r}_{Q/C}, \quad [2.31]$$

where:

$\mathbf{a}_Q$ is the acceleration of point Q_{CL} (m/s^2), and

$\mathbf{r}_{Q/C}$ is a vector from point C to point Q_{CL} (m).

Again, by substituting the vectors' magnitudes and directions, calculating the cross product, and separating the x and y components, two equations are produced:

$$a_{Qx} = \alpha_C \cdot r_{Q/C} \cdot \sin(\phi_{Q/C} + \theta_C) + \omega_C^{\,2} \cdot r_{Q/C} \cdot \cos(\phi_{Q/C} + \theta_C), \text{ and} \quad [2.32]$$

$$a_{Qy} = -\alpha_C \cdot r_{Q/C} \cdot \cos(\phi_{Q/C} + \theta_C) + \omega_C^{\,2} \cdot r_{Q/C} \cdot \sin(\phi_{Q/C} + \theta_C). \quad [2.33]$$

All points on a rigid body experience the same angular acceleration (Hibbeler, 1992), therefore:

$$\boldsymbol{\alpha}_C = \boldsymbol{\alpha}_Q. \quad [2.34]$$

Through integration, it can also be shown that (assuming boom sections are initially at rest):

$$\int \alpha_Q * dt = \int \frac{d\omega_Q}{dt} * dt = \omega_Q, \text{ and} \quad [2.35]$$

$$\int \omega_Q * dt = \int \frac{d\theta_Q}{dt} * dt = \theta_Q. \quad [2.36]$$

Therefore, from equations 2.35 and 2.36 it is also shown that:

$$\omega_C = \omega_Q, \text{ and} \quad [2.37]$$

$$\theta_C = \theta_Q. \quad [2.38]$$

Using equations 2.34 and 2.37, equation 2.29 can be rewritten as:

$$a_{Bx} = -\alpha_Q * r_{B/C} * \cos(\tau_{B/C} - \theta_C) - \omega_Q^{\,2} * r_{B/C} * \sin(\tau_{B/C} - \theta_C). \quad [2.39]$$

Similarly, equations 2.30, 2.32, and 2.33 can be rewritten as:

$$a_{By} = \alpha_Q * r_{B/C} * \sin(\tau_{B/C} - \theta_C) - \omega_Q^{\,2} * r_{B/C} * \cos(\tau_{B/C} - \theta_C), \quad [2.40]$$

$$a_{Qx} = \alpha_Q * r_{Q/C} * \sin(\phi_{Q/C} + \theta_C) + \omega_Q^{\,2} * r_{Q/C} * \cos(\phi_{Q/C} + \theta_C), \text{ and} \quad [2.41]$$

$$a_{Qy} = -\alpha_Q * r_{Q/C} * \cos(\phi_{Q/C} + \theta_C) + \omega_Q^{\,2} * r_{Q/C} * \sin(\phi_{Q/C} + \theta_C), \quad [2.42]$$

respectively.

2.5 Other Equations

The equations developed in the following section are required to allow simultaneous solution of the kinetic and kinematic equations developed previously.

2.5.1 Strut Forces

The struts used in the passive suspension system are each comprised of a shock absorber (viscous damping) and spring. The force applied by each strut (F_S) can be generalized as:

$$F_S = k \cdot (\ell_O - \ell) - \beta_S \cdot \frac{d\ell}{dt}, \quad [2.43]$$

where:

k is the spring rate (N/m),

ℓ_O is the free length of the spring (m),

ℓ is the length of the spring (m) at a point in time, t, and

β_S is the damping coefficient for the shock absorbers (kg/s).

The struts are common components at the four annotated positions on the machine, however due to different attachment points on the frame each has a unique length and rate of change at any point in time. The equations for each strut are given by:

$$F_{S1} = k \cdot (\ell_O - \ell_1) - \beta_S \cdot \frac{d\ell_1}{dt}, \quad [2.44]$$

$$F_{S2} = k \cdot (\ell_O - \ell_2) - \beta_S \cdot \frac{d\ell_2}{dt}, \quad [2.45]$$

$$F_{S3} = k \cdot (\ell_O - \ell_3) - \beta_S \cdot \frac{d\ell_3}{dt}, \text{ and} \quad [2.46]$$

$$F_{S4} = k \cdot (\ell_O - \ell_4) - \beta_S \cdot \frac{d\ell_4}{dt}, \quad [2.47]$$

where:

ℓ_1 is the length of the spring on strut number 1 (m) at a point in time, t,

ℓ_2 is the length of the spring on strut number 2 (m) at a point in time, t,

ℓ_3 is the length of the spring on strut number 3 (m) at a point in time, t, and
ℓ_4 is the length of the spring on strut number 4 (m) at a point in time, t.

The remaining equations required for the simulation model are derived through use of trigonometric equations.

2.5.2 Trigonometric Equations

Equations for the length of each strut's spring are developed using trigonometric identities. Referencing figure 2.4, it can be shown using trigonometric rules and the Pythagorean Theorem that:

$$d_3 = r_{M1/C} * \cos(\phi_{N1/C} - \lambda_{M1/C} + \theta_C), \quad [2.48]$$

$$b_1^2 = r_{M1/C}^2 - d_3^2, \quad [2.49]$$

$$d_4 = r_{C/N1} - d_3, \text{ and} \quad [2.50]$$

$$\ell_1^2 = d_4^2 + b_1^2, \quad [2.51]$$

where:

d_3 is the length from point C to a point created by bisecting a vector from point C to point N1 with a line perpendicular to the vector and through point M1 (m),
$r_{M1/C}$ is the scalar length of a vector to point C from M1 (m),
$\phi_{N1/C}$ is the angle between the y-axis and a vector between points C and N1 (rad),
$\lambda_{M1/C}$ is the initial angle between the y-axis and a vector between points C and M1 (rad),
b_1 is the length of the line perpendicular to a vector from point C to point N1 and and through point M1 (m),
$r_{C/N1}$ is the scalar length of a vector to point N1 from C (m), and
d_4 is the length from point N1 to a point created by bisecting a vector from point C to point N1 with a line perpendicular to the vector and through point M1 (m).

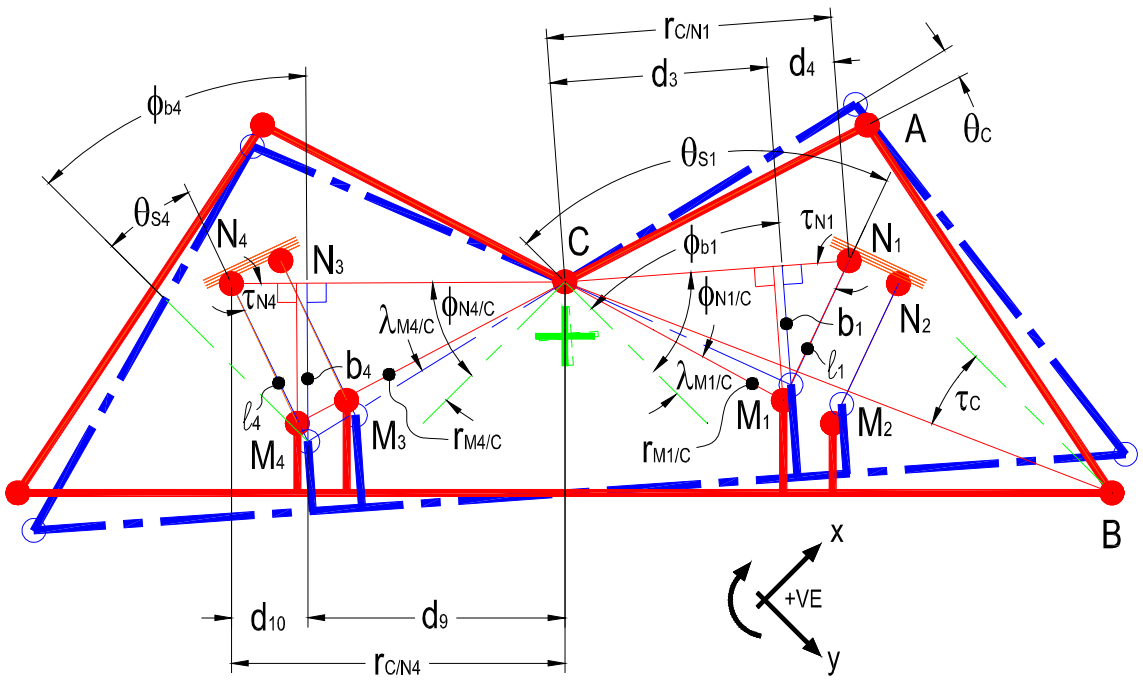

Figure 2.4: Passive Suspension System Starting Geometry (Solid Red Line) and Secondary Position (Dashed Blue Line)

Substituting equations 2.48, 2.49, and 2.50 into 2.51 and solving for ℓ_1 yields:

$$\ell_1 = \sqrt{\begin{matrix}(r_{C/N1} - (r_{M1/C} * \cos(\phi_{N1/C} - \lambda_{M1/C} + \theta_C)))^2 + \\ r_{M1/C}{}^2 - (r_{M1/C} * \cos(\phi_{N1/C} - \lambda_{M1/C} + \theta_C))^2\end{matrix}} . \qquad [2.52]$$

The derivative of this equation is also required for use in the damping portion of the strut force equations. Using the product and change rules (Stewart, 1999) to differentiate with respect to time gives:

$$\frac{d\ell_1}{dt} = \frac{1}{2 * \sqrt{\begin{matrix}(r_{C/N1} - (r_{M1/C} * \cos(\phi_{N1/C} - \lambda_{M1/C} + \theta_C)))^2 \\ + r_{M1/C}{}^2 - (r_{M1/C} * \cos(\phi_{N1/C} - \lambda_{M1/C} + \theta_C))^2\end{matrix}}} * \left[\begin{matrix}\left(\begin{matrix}2 * (r_{C/N1} - r_{M1/C} * \cos(\phi_{N1/C} - \lambda_{M1/C} + \theta_C)) * \\ r_{M1/C} * \sin(\phi_{N1/C} - \lambda_{M1/C} + \theta_C) * \frac{d\theta_C}{dt}\end{matrix}\right) + \\ \left(\begin{matrix}2 * r_{M1/C} * \cos(\phi_{N1/C} - \lambda_{M1/C} + \theta_C) * \\ r_{M1/C} * \sin(\phi_{N1/C} - \lambda_{M1/C} + \theta_C) * \frac{d\theta_C}{dt}\end{matrix}\right)\end{matrix}\right] . \quad [2.53]$$

Following the same logic, similar equations to 2.52 can be derived for the length of the other struts (ℓ_2, ℓ_3, and ℓ_4):

$$\ell_2 = \sqrt{\begin{matrix}(r_{C/N2} - (r_{M2/C} * \cos(\phi_{N2/C} - \lambda_{M2/C} + \theta_C)))^2 + \\ r_{M2/C}{}^2 - (r_{M2/C} * \cos(\phi_{N2/C} - \lambda_{M2/C} + \theta_C))^2\end{matrix}}, \quad [2.54]$$

$$\ell_3 = \sqrt{\begin{matrix}(r_{C/N3} - (r_{M3/C} * \cos(\phi_{N3/C} - \lambda_{M3/C} - \theta_C)))^2 + \\ r_{M3/C}{}^2 - (r_{M3/C} * \cos(\phi_{N3/C} - \lambda_{M3/C} - \theta_C))^2\end{matrix}}, \text{ and} \quad [2.55]$$

$$\ell_4 = \sqrt{\begin{matrix}(r_{C/N4} - (r_{M4/C} * \cos(\phi_{N4/C} - \lambda_{M4/C} - \theta_C)))^2 + \\ r_{M4/C}{}^2 - (r_{M4/C} * \cos(\phi_{N4/C} - \lambda_{M4/C} - \theta_C))^2\end{matrix}}, \quad [2.56]$$

where:

$r_{M2/C}$ is the scalar length of a vector to point C from M2 (m),

$\phi_{N2/C}$ is the angle between the y-axis and a vector between points C and N2 (rad),

$\lambda_{M2/C}$ is the initial angle between the y-axis and a vector between points C and M2 (rad),

$r_{C/N2}$ is the scalar length of a vector to point N2 from C (m),

$r_{M3/C}$ is the scalar length of a vector to point C from M3 (m),

$\phi_{N3/C}$ is the angle between the negative x-axis and a vector between points C and N3 (rad),

$\lambda_{M3/C}$ is the initial angle between the negative x-axis and a vector between points C and M3 (rad),

$r_{C/N3}$ is the scalar length of a vector to point N3 from C (m),

$r_{M4/C}$ is the scalar length of a vector to point C from M4 (m),

$\phi_{N4/C}$ is the angle between the negative x-axis and a vector between points C and N4 (rad),

$\lambda_{M4/C}$ is the initial angle between the negative x-axis and a vector between points C and M4 (rad), and

$r_{C/N4}$ is the scalar length of a vector to point N4 from C (m).

Differentiating equations 2.54, 2.55, and 2.56 yield:

$$\frac{d\ell_2}{dt} = \frac{1}{2*\sqrt{\begin{matrix}(r_{C/N2} - (r_{M2/C} * \cos(\phi_{N2/C} - \lambda_{M2/C} + \theta_C)))^2 + \\ r_{M2/C}{}^2 - (r_{M2/C} * \cos(\phi_{N2/C} - \lambda_{M2/C} + \theta_C))^2\end{matrix}}} * \left[\begin{matrix}\left(\begin{matrix}2*(r_{C/N2} - r_{M2/C} * \cos(\phi_{N2/C} - \lambda_{M2/C} + \theta_C))* \\ r_{M2/C} * \sin(\phi_{N2/C} - \lambda_{M2/C} + \theta_C) * \frac{d\theta_C}{dt}\end{matrix}\right) + \\ \left(\begin{matrix}2 * r_{M2/C} * \cos(\phi_{N2/C} - \lambda_{M2/C} + \theta_C)* \\ r_{M2/C} * \sin(\phi_{N2/C} - \lambda_{M2/C} + \theta_C) * \frac{d\theta_C}{dt}\end{matrix}\right)\end{matrix}\right], \quad [2.57]$$

$$\frac{d\ell_3}{dt} = \frac{1}{2*\sqrt{\begin{matrix}(r_{C/N3} - (r_{M3/C} * \cos(\phi_{N3/C} - \lambda_{M3/C} - \theta_C)))^2 \\ + r_{M3/C}{}^2 - (r_{M3/C} * \cos(\phi_{N3/C} - \lambda_{M3/C} - \theta_C))^2\end{matrix}}} * \left[\begin{matrix}\left(\begin{matrix}2*(r_{C/N3} - r_{M3/C} * \cos(\phi_{N3/C} - \lambda_{M3/C} - \theta_C))* \\ r_{M3/C} * \sin(\phi_{N3/C} - \lambda_{M3/C} - \theta_C) * \left(-\frac{d\theta_C}{dt}\right)\end{matrix}\right) + \\ \left(\begin{matrix}2 * r_{M3/C} * \cos(\phi_{N3/C} - \lambda_{M3/C} - \theta_C)* \\ r_{M3/C} * \sin(\phi_{N3/C} - \lambda_{M3/C} - \theta_C) * \left(-\frac{d\theta_C}{dt}\right)\end{matrix}\right)\end{matrix}\right], \quad [2.58]$$

and

$$\frac{d\ell_4}{dt} = \frac{1}{2 * \sqrt{\begin{matrix}(r_{C/N4} - (r_{M4/C} * \cos(\phi_{N4/C} - \lambda_{M4/C} - \theta_C)))^2 \\ + {r_{M4/C}}^2 - (r_{M4/C} * \cos(\phi_{N4/C} - \lambda_{M4/C} - \theta_C))^2\end{matrix}}} * \left[\begin{matrix}\left(\begin{matrix}2 * (r_{C/N4} - r_{M4/C} * \cos(\phi_{N4/C} - \lambda_{M4/C} - \theta_C)) * \\ r_{M4/C} * \sin(\phi_{N4/C} - \lambda_{M4/C} - \theta_C) * \left(-\frac{d\theta_C}{dt}\right)\end{matrix}\right) + \\ \left(\begin{matrix}2 * r_{M4/C} * \cos(\phi_{N4/C} - \lambda_{M4/C} - \theta_C) * \\ r_{M4/C} * \sin(\phi_{N4/C} - \lambda_{M4/C} - \theta_C) * \left(-\frac{d\theta_C}{dt}\right)\end{matrix}\right)\end{matrix}\right] . \quad [2.59]$$

As the three internal angles of a triangle must sum to π rad, from Figure 2.4 it can be shown that:

$$\tau_{N1} = \phi_{b1} + \pi/2 - \theta_{S1}, \quad [2.60]$$

where:

ϕ_{b1} is the angle between the negative y-axis and a vector created by bisecting a vector from point C to point N1 with a line perpendicular to the vector and through point M1 (rad), and

τ_{N1} is the angle between a vector from point C to point N1 and a vector from point N1 to point M1 (rad).

From trigonometric relations, the equation for θ_{S1} is then:

$$\cos\left(\phi_{b1} + \pi/2 - \theta_{S1}\right) = \frac{r_{N1/C} - r_{M1/C} * \cos(\phi_{N1/C} - \lambda_{M1/C} + \theta_C)}{\ell_1}. \quad [2.61]$$

Similarly,

$$\cos\left(\phi_{b2} + \pi/2 - \theta_{S2}\right) = \frac{r_{N2/C} - r_{M2/C} * \cos(\phi_{N2/C} - \lambda_{M2/C} + \theta_C)}{\ell_2}, \quad [2.62]$$

$$\cos\left(\phi_{b3} + \pi/2 - \theta_{S3}\right) = \frac{r_{N3/C} - r_{M3/C} * \cos(\phi_{N3/C} - \lambda_{M3/C} - \theta_C)}{\ell_3}, \quad [2.63]$$

and

$$\cos\left(\phi_{b4} + \pi/2 - \theta_{S4}\right) = \frac{r_{N4/C} - r_{M4/C} * \cos\left(\phi_{N4/C} - \lambda_{M4/C} - \theta_C\right)}{\ell_4}, \quad [2.64]$$

where:

ϕ_{b2} is the angle between the x-axis and a vector created by bisecting a vector from point C to point N2 with a line perpendicular to the vector and through point M2 (rad),

τ_{N2} is the angle between a vector from point C to point N2 and a vector from point N2 to point M2 (rad),

ϕ_{b3} is the angle between the x-axis and a vector created by bisecting a vector from point C to point N3 with a line perpendicular to the vector and through point M3 (rad),

τ_{N3} is the angle between a vector from point C to point N3 and a vector from point N3 to point M3 (rad),

ϕ_{b4} is the angle between the x-axis and a vector created by bisecting a vector from point C to point N4 with a line perpendicular to the vector and through point M4 (rad), and

τ_{N4} is the angle between a vector from point C to point N4 and a vector from point N4 to point M4 (rad).

The final two equations required are generated by examining geometry changes created by a change in length of the tilt actuator. Referencing Figure 2.5, it can be shown that:

$$\cos(\eta_1) = \frac{d_1}{r_{B/A}}, \quad [2.65]$$

$$\eta_1 = \phi_{B/A} + \phi_{E/A} - \theta_{E/A}, \quad [2.66]$$

$$\eta_3 = \pi/2 - \eta_1, \quad [2.67]$$

$$\eta_2 = \tau_{B/A} - \eta_3 - \phi_{E/B} + \theta_W, \quad [2.68]$$

$$\sin(\eta_2) = \frac{d_2}{r_{E/B}}, \quad [2.69]$$

$$r_{E/A} = d_1 + d_2, \quad [2.70]$$

$$r_{B/A}{}^2 = d_1{}^2 + b^2, \quad [2.71]$$

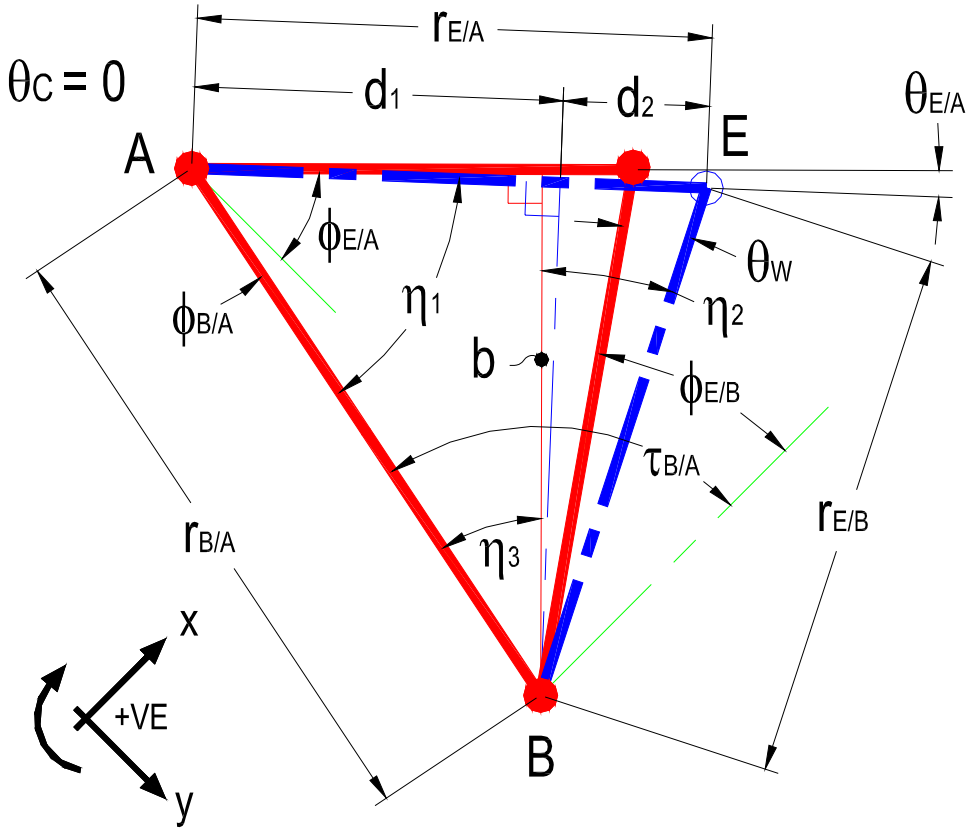

Figure 2.5: Wing Tilt Actuator Length Change Effect on Geometry; Starting Geometry (Solid Red Line) and Secondary Position (Dashed Blue Line)

and

$$r_{E/B}{}^2 = d_2{}^2 + b^2, \quad [2.72]$$

where:

η_1 is the angle between a vector connecting points B and A and a vector between points E and A (rad),

d_1 is the length from point A to a point created by bisecting a vector from point A to point E with a line perpendicular to the vector and through point B (m),

$r_{B/A}$ is the scalar length of a vector to point A from B (m),

$\phi_{B/A}$ is the angle between the y-axis and a vector between points A and B (rad),

η_3 is the angle between a vector created by points B and A, and the line created by bisecting a vector from point A to point E with a line perpendicular to that vector and through point B (rad),
η_2 is the angle between a vector created by points E and B, and the line created by bisecting a vector from point A to point E with a line perpendicular to that vector and through point B (rad),
$\tau_{B/A}$ is the angle between the x-axis and a vector between points A and B (rad),
$\phi_{E/B}$ is the angle between the x-axis and a vector between points B and E (rad),
d_2 is the length from point E to a point created by bisecting a vector from point A to point E with a line perpendicular to the vector and through point B (m),
$r_{E/B}$ is the scalar length of a vector to point B from E (m),
$r_{E/A}$ is the scalar length of a vector to point A from E (m), and
b is the length from point B to a point created by bisecting a vector from point A to point E with a line perpendicular to the vector and through point B (m).

Substituting equations 2.66, 2.70, 2.71, and 2.72 into 2.65 gives:

$$\theta_{E/A} = \phi_{B/A} + \phi_{E/A} - \cos^{-1}\left(\frac{r_{B/A}{}^2 - r_{E/B}{}^2 + r_{E/A}{}^2}{2 * r_{B/A} * r_{E/A}}\right). \qquad [2.73]$$

Substituting equations 2.66, 2.67, 2.68, 2.70, 2.71, and 2.72 into 2.69 yields:

$$\theta_W = -\tau_{B/A} + \pi/2 - \phi_{B/A} - \phi_{E/A} + \theta_{E/A} + \phi_{E/B} + \sin^{-1}\left(\frac{r_{E/B}{}^2 - r_{B/A}{}^2 + r_{E/A}{}^2}{2 * r_{E/A} * r_{E/B}}\right). \qquad [2.74]$$

The second derivatives with respect to time of equations 2.73 and 2.74 were required for simulation purposes; this detail is provided in Appendix A.

To solve the series of equations listed in this chapter, many initial values and constants were required. Assembly models of the boom developed by CNH Canada Ltd. in three-dimensional computer-aided drafting software (Parametric

Technology Corporation, 2001) were used to obtain masses, mass moment of inertias, and all centers of gravity. All of these values are defined in Appendix B.

Using the equations developed in this chapter, a dynamic simulation model was created in a software simulation environment (Mathworks, 2001). The type of numerical analysis performed by this software during dynamic simulation requires explicit solution of many of the variable equations derived in this chapter. By numerically solving many of the equations in series (Wolfram Research, 2000), the algebraic loops which in initial studies caused instability for the software were avoided. The final equation set used for simulation purposes are defined in Appendix C.

2.6 Model Validation

Experimental data from the sprayer in question were accumulated at the onset of this research. Because the machine in its instrumented form was not available for experimental testing after the model was fully developed, only limited information was collected from the actual system. In addition, the boom configuration used in the simulation studies was not exactly as that used in the experimental tests; therefore, only trends from the two systems could be compared.

To validate the model, the experimental natural frequency, amplitude of first oscillation, and duration of oscillation were compared to the simulation results. In an experiment (laboratory environment with concrete floor) at the CNH Saskatoon facility during January 2004, the natural frequency information was obtained by manually rotating the boom structure about the center point, C. The boom was then released and the orientation of the boom recorded using ultrasonic distance sensors attached at the outer ends of the left and right sections. The distance measurements were then converted to an angular orientation using trigonometric relations.

The natural frequency predicted by the model was 0.3 Hz as compared to the measured value of 0.2 Hz. The model was deemed acceptable due to the extremely low frequencies; any frequency effects from the hydraulic system would occur at a value much larger than this and would be effectively filtered by the boom system.

Other system effects present in the experimental system and not accounted for in the model were:

i. the deflection of the machine's tires,
ii. torsion of the frame members connecting the carrying frame to the chassis, and
iii. flexure of members of the boom structure.

As the model did not include these effects and incorporated only motion of the boom structure with respect to the carrying frame, a direct comparison to the experimental data was difficult. The intent of this research was to provide directional information using comparisons between only simulation results and not to experimental data. For this reason the strut damping coefficient in the simulations was altered from the manufacturer's information to bring the amplitude of the first oscillation more in line with the experimental data (Figure 2.6). The emphasis was placed on the magnitude of first oscillation as this creates the maximum deviation of the boom from intended orientation, while the discrepancy in natural frequency is dealt with by only comparing simulation results (trend type study).

The strut manufacturer provided a non-linear rating for the damping coefficient of 2200 kg/s when the strut was changing length at a rate of 0.05 m/s to 1200 kg/s at 0.25 m/s (Monroe Automotive Equipment Company, 2001). Due to the low natural frequency of the boom structure, the rate of length change of the strut was always less than 0.05 m/s. For this reason a constant value for damping coefficient was assumed and a value of 10,000 kg/s employed in the model to bring the amplitude of first oscillation equivalent to experimental data.

The model was then considered acceptable for providing directional information on the effects of tilt actuator control.

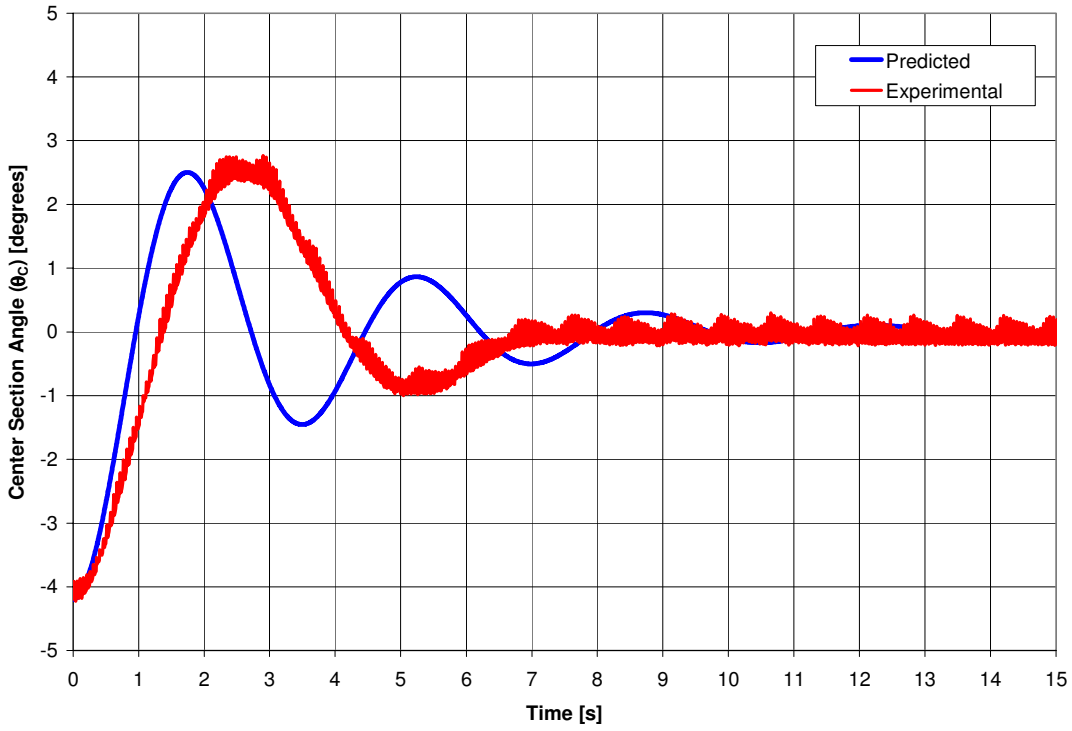

Figure 2.6: Predicted and Experimental Center Section Orientation (Note: Predicted Natural Frequency = 0.3 Hz and Experimental Natural Frequency = 0.2 Hz)

Chapter 3

Hydraulic Actuator and Spool Valves - Simulation Model Development

In this chapter the equations required to relate the force applied by the right section's tilt actuator to the input of the electro-hydraulic spool valve are developed. The concepts of proportional and pulse width modulation (PWM) spool valve technology are also introduced.

3.1 Hydraulic Actuator

A hydraulic actuator provides the means for fluid under pressure to perform work. In the boom system, an actuator is used to control the right section's angular orientation with respect to the center section. Actuators can be of double rod design (symmetric operation during extension/retraction) or single rod design (asymmetric operation). In the system studied, only a single rod actuator is considered as this is typical for suspended boom sprayers. The actuator's rod is connected to a piston which is allowed to move linearly within the body (Figure 3.1a). By maintaining a seal between the piston and body, two separate chambers are created. Control of the amount of fluid in each chamber allows different lengths of the actuator to be produced (Figure 3.1b). It is important to note that for the orientation changes examined in this research the actuator piston does not fully retract or extend to its extremities (called 'bottoming out'). This 'bottoming out' effect prevents the fluid in the actuator

from behaving as a spring (compressibility) and would result in a different dynamic response of the boom to that of actuator movement between the extents. As this scenario is not typical of normal field operation it was not considered.

In Chapter 2, equation 2.10 defined the force applied by the actuator ($F_{E/A}$). The relationship between $F_{E/A}$ and the fluid flow through the valve are now developed using kinetics and fluid flow fundamentals.

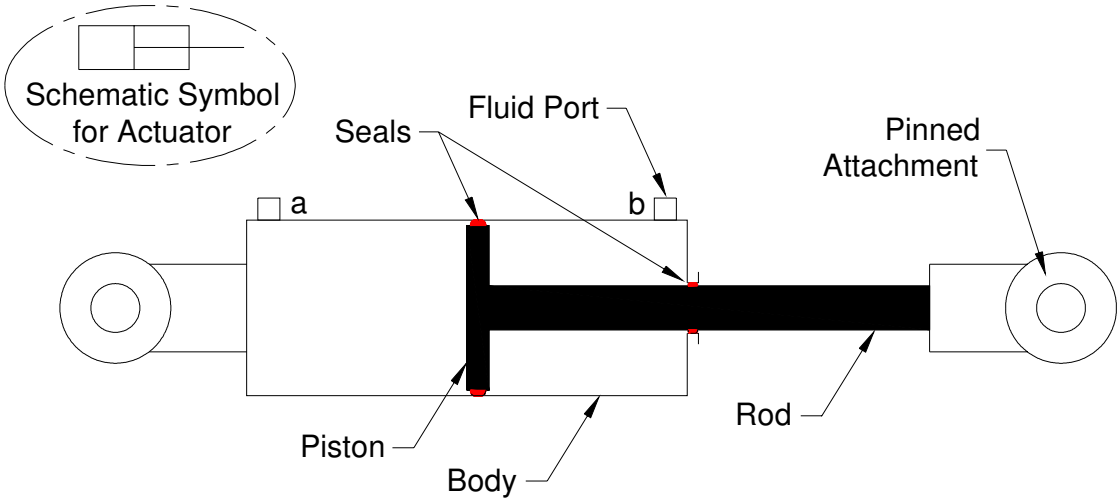

Figure 3.1a: Hydraulic Actuator Components and Schematic Symbol

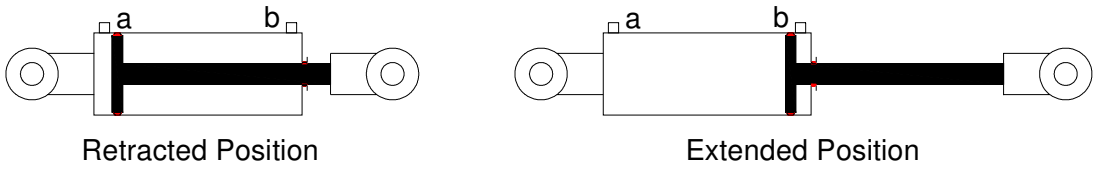

Figure 3.1b: Hydraulic Actuator Position Extents (Operational Movements are Typically between these Limits)

3.2 Hydraulic Actuator Kinetics

The FBD of the tilt actuator rod is shown in Figure 3.2. A local coordinate system is used for this component as the force applied by the actuator is independent of orientation; the positive x_C-direction is defined along the axis of the actuator rod. The equation of motion relates all forces in the equation:

$$\sum F_{Cx} = m_C * a_x, \qquad [3.1]$$

where:

ΣF_{Cx} is the summation of all forces in the x_C-direction acting on the actuator rod (N),

m_C is the mass of the actuator (kg), and

a_x is the linear acceleration of the actuator rod in the x_C-direction (m/s^2), or written in another form the second derivative of position, $\ddot{x}_C$.

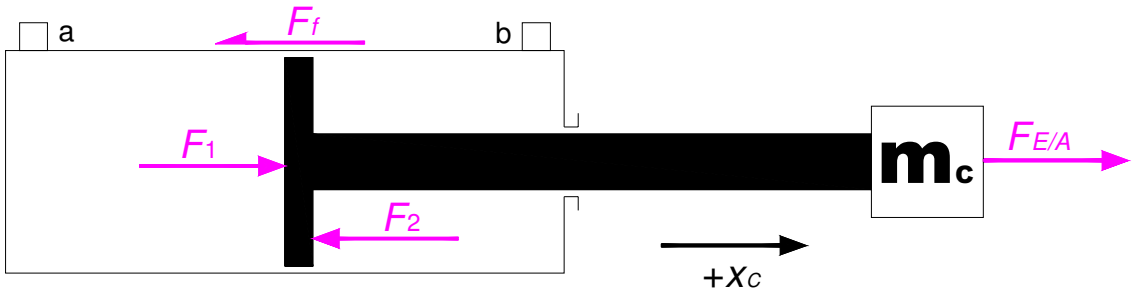

Figure 3.2: Tilt Actuator Free Body Diagram

Expanding this equation using the individual forces yields:

$$F_1 + F_{E/A} - F_2 - F_f = m_C * \ddot{x}_C, \qquad [3.2]$$

where:

F_1 is the force applied on the non-rod side of the piston by the pressurized fluid (N),

F_2 is the force applied on the rod side of the piston by the pressurized fluid (N), and

F_f is the force of friction which acts between the moving components (N).

Solving equation 3.2 for $F_{E/A}$ yields:

$$F_{E/A} = F_2 + F_f - F_1 + m_C * \ddot{x}_C. \qquad [3.3]$$

Fluid under pressure provides a force which is proportional to the acting area, therefore:

$F_1 = P_1 * A_1$, and [3.4]

$F_2 = P_2 * A_2$, [3.5]

where:

P_1 is the fluid pressure in the non-rod end of the actuator (Pa),

A_1 is the area of the piston (m^2),

P_2 is the fluid pressure in the rod end of the actuator (Pa), and

A_2 is the area of the piston less the area of the rod (m^2).

Friction is defined as *a force which resists the tendency of and relative motion between two bodies*. In the case of the actuator, the friction force will be a non-linear function that can be broken into two portions – a static portion, or *stiction*, and a dynamic portion comprised of coulomb and viscous friction. Stiction is caused by surface roughness and prevents two bodies from moving with respect to each other until a force threshold is met. Once this threshold is exceeded, the amount of force to continue movement is decreased. The force required to maintain movement is called coulomb friction and is independent of velocity. Viscous friction is due to the fluid's resistance to shear. As the relative velocity increases, the viscous friction force resisting change tends to increase linearly (Figure 3.3). There is a non-linear transition region from stiction to viscous and coulomb friction defined as the Stribeck effect (Olsson et al., 1998). Values of the parameters described above for the actuator used in this particular system were experimentally obtained; the procedure and results are discussed in Chapter 4.

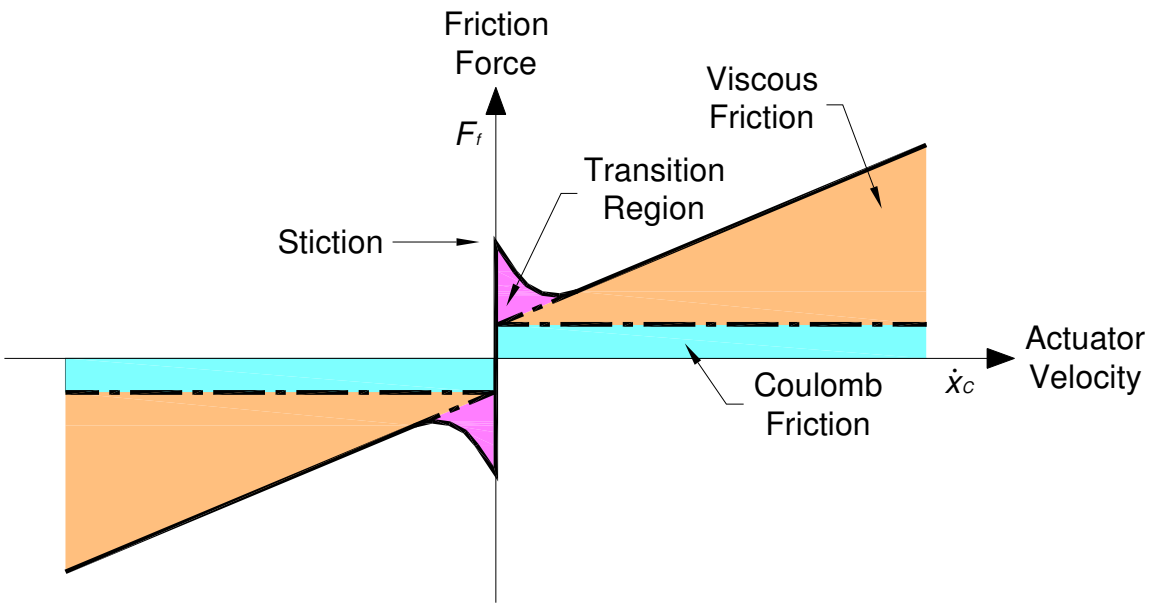

Figure 3.3: Theoretical Actuator Friction Force versus Velocity

Equations 3.3 and 3.4 define the actuator forces as a function of fluid pressure. Fluid fundamentals are used to relate these pressures back to the intended input in this research – the valve. Assumptions about fluid flow are made to simplify the resulting equations with little impact on the results. The hydraulic reservoir and cooling system will maintain the fluid at a temperature within a few degrees Celsius under normal operating conditions; this makes it practical to assume a constant temperature for the fluid. With the assumption of constant temperature, density and viscosity are other fluid properties which may then be assumed constant.

3.3 Hydraulic Actuator – Fluid Fundamentals

Two control volumes for the tilt actuator are defined; non-rod end and rod end (Figure 3.4). Due to short lengths of connection lines between the actuator and the valve, pressure losses through them are assumed negligible. The line volumes may then be lumped with the respective actuator volumes. The continuity equation can be used for both ends of the actuator (Merritt, 1967):

$$\sum Q_{IN} - \sum Q_{OUT} = \frac{dV_A}{dt} + \frac{V_{AO}}{\beta_E} * \frac{dP}{dt}, \qquad [3.6]$$

where:

ΣQ_{IN} is the summation of all flows entering the control volume (m^3/s),

ΣQ_{OUT} is the summation of all flows exiting the control volume (m^3/s),

V_A is the control volume (m^3),

V_{AO} is the control volume at the beginning of the evaluation period (m^3),

β_E is the bulk modulus of the fluid (Pa), and

P is the pressure in the control volume (Pa).

The first term on the right side of equation 3.6 is the flow consumed by the change in position of the rod; that is, a change in the control volume. The second term accounts for volume changes due to the compressibility of the fluid. The bulk modulus defines the compressibility, or stiffness, of the fluid. Air entrainment in the fluid and the 'flex' of other system components (hydraulic lines) will affect the bulk modulus. For these reasons, the *effective bulk modulus* for the system will be much lower than that provided by the manufacturer and must be experimentally obtained. The procedure to measure this parameter and the experimental results for effective bulk modulus are presented in Chapter 4.

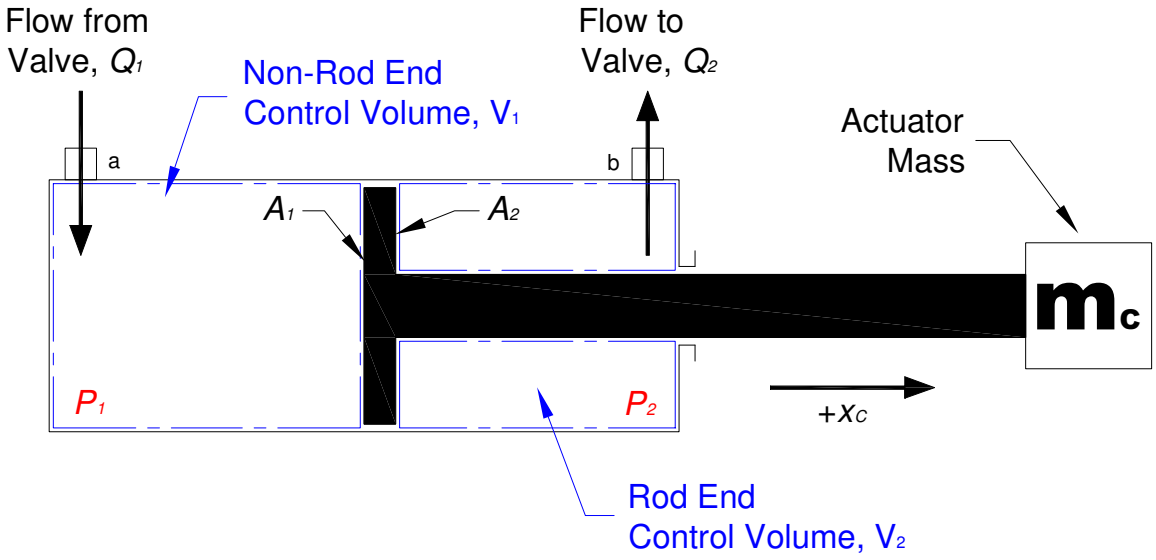

Figure 3.4: Tilt Actuator Properties

Assuming there is no leakage past the piston seals, evaluating equation 3.6 for the non-rod end of the actuator yields (Merritt, 1967):

$$Q_1 = \frac{dV_1}{dt} + \frac{V_{1o}}{\beta_E} * \frac{dP_1}{dt}, \qquad [3.7]$$

where:

Q_1 is the flow entering the control volume from the valve (m^3/s),

V_1 is the non-rod end control volume (m^3), and

V_{1o} is the non-rod end control volume at the beginning of the evaluation period (m^3).

The change in the control volume is related to the velocity of the rod and may be written as:

$$\frac{dV_1}{dt} = A_1 * \dot{x}_C, \qquad [3.8]$$

where:

$\dot{x}_C$ is the velocity of the rod (m/s).

If the system is assumed to be initially at rest (static pressures in both the rod and non-rod ends of the actuator at t=0), substituting equation 3.8 into 3.7 and solving for P_1 yields:

$$P_1 = \frac{\beta_E}{V_{1o}} \int (Q_1 - A_1 * \dot{x}_C) * dt. \qquad [3.9]$$

Similarly for the rod end control volume, assuming no leakage past the rod seals:

$$P_2 = \frac{\beta_E}{V_{2o}} \int (A_2 * \dot{x}_C - Q_2) * dt, \qquad [3.10]$$

where:

Q_2 is the flow exiting the rod end control volume to the valve (m^3/s),

V_2 is the rod end control volume (m^3), and

V_{2o} is the rod end control volume at the beginning of the evaluation period (m^3).

The final required equations define the flow through the valve as a function of the spool position.

3.4 Valve Flow

Electro-hydraulic solenoid valves use mechanical motion to direct flow. Solenoids drive the spool one direction or the other to define the flow path through the valve. As shown in Figure 3.5, flow through a 3-position 4-way valve can be defined as flow through two matched sharp-edged orifices. As presented in Chapter 1, turbulent flow through each orifice is assumed and then defined by Bernoulli's equation to be:

$$Q = C_d * A_O * \sqrt{\frac{2}{\rho} * (\Delta P)}. \qquad [1.1]$$

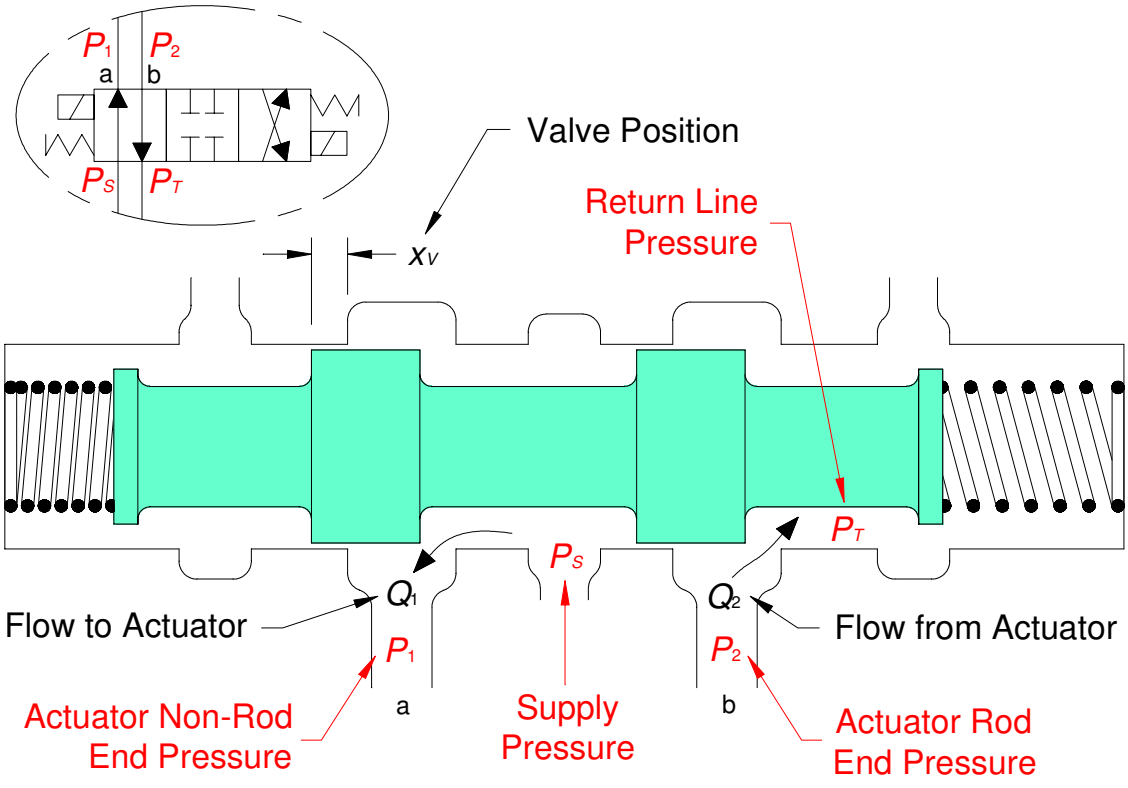

Figure 3.5: Flow through a Three-Position Four-Way Electro-Hydraulic Spool Valve

For high Reynolds numbers (which is the case in this study), a constant value for the discharge coefficient (C_d) is usually assumed throughout the industry (Merritt, 1967). The value for discharge coefficient will vary with Reynolds number, however the slope of a Reynolds number versus discharge coefficient plot is almost nil for Reynolds numbers greater than 1000. For this reason, a value of 0.60 was chosen.

For simplification purposes it is useful to assume that the valves to be investigated are manufactured perfectly; no radial clearance between the spool and housing and minimally overlapped, thus eliminating any leakage paths. Although nearly impossible to achieve, new manufacturing practices are able to closely meet these ideals.

The body of the valve directs flow to a rectangular orifice that is covered by the spool. As the spool shifts, the area of the orifice is then defined as:

$$A_o = x_V * w, \qquad [3.11]$$

where:

x_V is the position of the spool (m), and

w is the area gradient of the orifice (m^2/m).

The area gradient of the orifice relates the area uncovered by the spool with respect to the change in its position. For a rectangular orifice this value is a constant. Because all valves evaluated in this study employ the same housing, the area gradient derived from the valve manufacturer's literature and used throughout this research was 0.0017 m^2/m. The process used to determine this value is discussed in Chapter 4.

For derivation purposes, only one position of the spool will be discussed. When the spool is in the position to extend the actuator, the nomenclature is as shown below. When the spool is in the position to retract the actuator, the rod end is exposed to the supply pressure and the non-rod end is exposed to the return line pressure. The format of the equations discussed remains the same,

with supply and return pressures being substituted for one another. The sign of the change in pressure term will determine flow direction.

Using equations 1.1 and 3.11 the flow from the pump through the valve to the actuator is then defined as:

$$Q_1 = C_d * x_V * w * \sqrt{\frac{2}{\rho} * (P_S - P_1)}, \qquad [3.12]$$

where:

P_S is the pressure supplied by the pump (Pa).

The sprayer being evaluated in this research is a pull-type machine. The source of hydraulic power is provided by a tractor whose hydraulic pump is sized to meet the demands of multiple applications (air seeding, tillage, etc…). The combined hydraulic flow demands of a suspended boom sprayer (chemical supply pump and boom orientation actuators) are typically much less than the tractor is capable of providing. Hydraulic power is transferred to the towed implement via remotely operated valves. When the towed implement is connected, the supply valve on the tractor is opened and the pump attempts to supply the flow rate demanded. If a pressure-compensated variable-displacement pump is employed, the pump will start to 'deadhead' (reduce flow output) if the load pressure exceeds a preset value. If a fixed displacement pump is used the pump will deliver any excess flow over a relief valve if the load pressure exceeds the preset value of the relief valve. By defining the maximum flow requirements of the sprayer as always less than the tractor can provide, the pump operates at either the deadhead or relief valve pressure setting. Hence, the supply pressure can then be considered constant. For the system evaluated in this research a value of 17.2 MPa was used (based on data obtained at the CNH Saskatoon facility).

A similar equation to 3.12 can be written for flow from the actuator through the valve and returning to the reservoir:

$$Q_2 = C_d * x_V * w * \sqrt{\frac{2}{\rho} * (P_2 - P_T)}, \qquad [3.13]$$

where:

P_T is the pressure in the return line to the reservoir (Pa).

As flow returns to the system reservoir it passes through a series of lines and connectors and is also filtered to remove contaminants. This process requires energy, therefore a pressure loss occurs. The pressure loss will vary depending on the line lengths, connectors used, and level of filtration performed. For this research a constant value of 0.3 MPa was used (based on data obtained at the CNH Saskatoon facility).

Equations 3.4, 3.5, 3.9, 3.10, 3.12, and 3.13 can then be substituted into equation 3.3 to relate valve position back to the force applied to the boom system by the tilt actuator. The final step is to define the relationship between the electrical input to the valve and its position.

3.5 Valve Position

Using information available from the manufacturer, a transfer function relating valve response time to electrical input was derived. The transfer function was then used to input the spool position for simulation purposes.

3.5.1 On/Off Valve Transfer Function

The on/off valve used in this research was a Bosch/Rexroth model 4WE 6 E6X/SG24N9K4/V (Bosch Rexroth AG, 2002). The time for the spool to move, or switch, from the neutral position to the open, or 'on', position is stated as 20 to 45 ms; when shifting the spool closed, 10 to 25 ms is required. As these ranges overlap, a constant value of 24 ms was used to develop the transfer function.

For this study, a first-order system was assumed to describe the dynamics of the spool and solenoid system. Knowing the time required for full displacement of the spool (24 ms as referenced above), and that it typically takes four times the value of the time constant to achieve full displacement (Phillips et al., 1996), a value of 0.006 s was assumed for the on/off valve time constant. The general form of a first-order transfer function (Phillips et al., 1996) is given by:

$$G(s) = \frac{K}{\tau * s + 1}, \qquad [3.14]$$

where:

K is the system gain (m/V), and

τ is the system time constant (s).

The extent of spool travel in each direction was 0.003 m, which equated to the normalized system gain (the solenoids employed were 12 V). The transfer function for the on/off valve thus became:

$$G(s) = \frac{0.003/12}{0.006 * s + 1}. \qquad [3.15]$$

It should be noted that from the literature (Merritt, 1967), it has been shown that the spool behaves as a second-order system. However, it was not readily possible to extract any parameters which could be implemented in the model to represent the on/off valve as such. A first-order system was believed to be sufficient for approximation of the opening and closing effects for the on/off valve. The actual form of the transfer function (first or second order) was a moot point as the natural frequency of the boom system and actuator were much lower than that for the solenoid spool system; hence, any error introduced by this approximation would have little effect on the overall simulation outcome.

Throughout this research the input (voltage) was assumed to be ideal (i.e. true step functions). Any effects on the electrical signal due to the solenoids were assumed to be negligible.

In this study, two 'alternative' commercially available valve types were investigated to determine their effects on system operation; these are now considered.

3.5.2 Proportional Valve Transfer Function

An alternative type of spool valve is a 'proportional' valve. This valve type is similar to an on/off valve except the position of the spool can be controlled between the closed and open limits by varying the amount of input voltage supplied to the solenoid. By controlling the location of the spool, the flow rate through the valve and hence the actuator velocity can be modulated. With this technique, the actuator velocity can be confined to an infinite number of values between the valve's operational limits. The disadvantages associated with proportional valve technology are the requirement of additional electronics to control the input to the solenoid, susceptibility to fluid contamination, and higher initial and maintenance costs.

The proportional valve considered in this research was a Bosch/Rexroth model 4WRAB6E12-1X/G12N9DK26MR (Rexroth Hydraulics Division, 1998). A graph of the frequency responses for both large signal changes (50% signal ± 40%) and small signal changes (50% signal ±10%) was provided by the manufacturer. The transfer functions for both types of changes were extracted from these data; the process is defined in Chapter 4. For large signal changes the normalized transfer function was found to be a standard second-order form:

$$H(s)_{Large} = \frac{\omega_{NL}^{\,2} \big/ V_l}{s^2 + 2 * \zeta_L * \omega_{NL} + \omega_{NL}^{\,2}}, \qquad [3.16]$$

where:

ω_{NL} is the natural frequency for large signal changes (rad/s),
V_I is the input voltage to the solenoid (V), and
ζ_L is the damping ratio for large signal changes.

For small signal changes the normalized transfer function takes on a more complicated form found to be represented reasonably by:

$$H(s)_{Small} = \frac{\left(\frac{1}{\omega_1} * s + 1\right) * \omega_{NS}^{\,4} \Big/ V_I}{\left(\frac{1}{\omega_2} * s + 1\right)\left(s^2 + 2 * \zeta_S * \omega_{NS} + \omega_{NS}^{\,2}\right)\left(s^2 + 2 * \zeta_S * \omega_{NS} + \omega_{NS}^{\,2}\right)}, \quad [3.17]$$

where:
ω_1 is the first cut-off frequency (rad/s),
ω_2 is the second cut-off frequency (rad/s),
ω_{NS} is the natural frequency for small signal changes (rad/s), and
ζ_S is the damping ratio for small signal changes.

Both the large-signal-change and small-signal-change transfer functions will be integrated with the boom model in Chapter 5 to evaluate the complete simulated transient response of the valve, tilt actuator, and boom.

3.5.3 Pulse Width Modulated Valve

A third electro-hydraulic spool valve attempts to gain the operational advantages of both on/off and proportional valves (flow modulation with simplified electronics requirements and lower initial and maintenance costs). By rapidly turning a valve on and off, the average flow through the valve will be a ratio of 'on' time versus 'off' time. The ratio is defined as the signal modulation ratio (SMR) and is the input pulse width divided by the period of the drive frequency. This technique is called pulse width modulation (PWM) and provides different flow rates by varying the SMR with an on/off valve; examples of different SMRs are presented in Figures 3.6a and 3.6b.

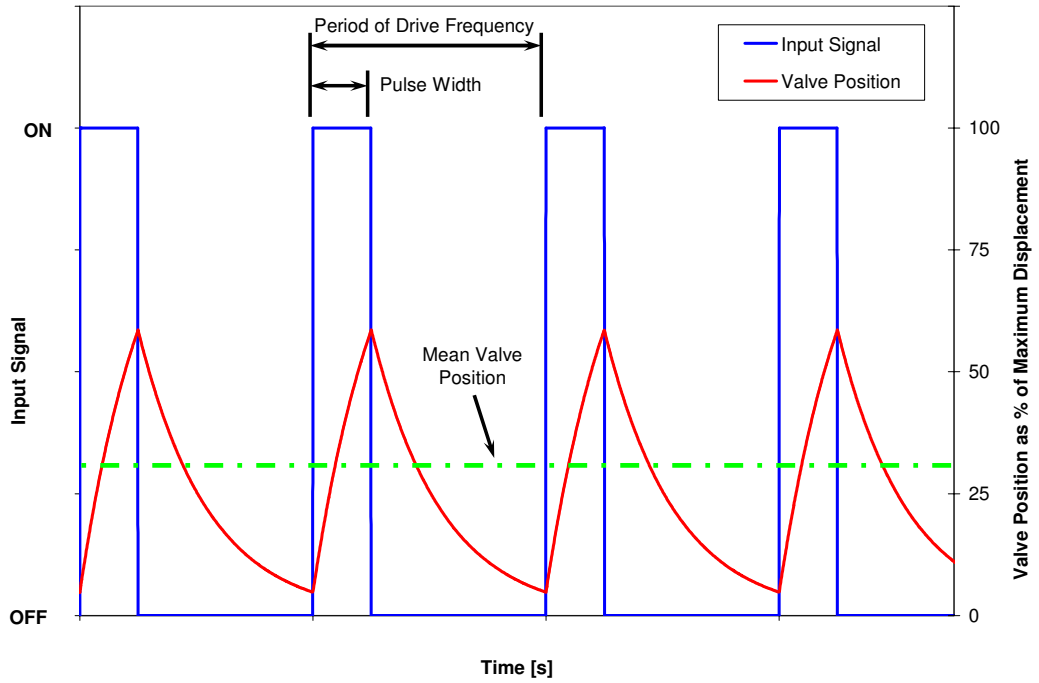

Figure 3.6a: Effect of Driving an On/Off Valve with a PWM Input (SMR of 0.25)

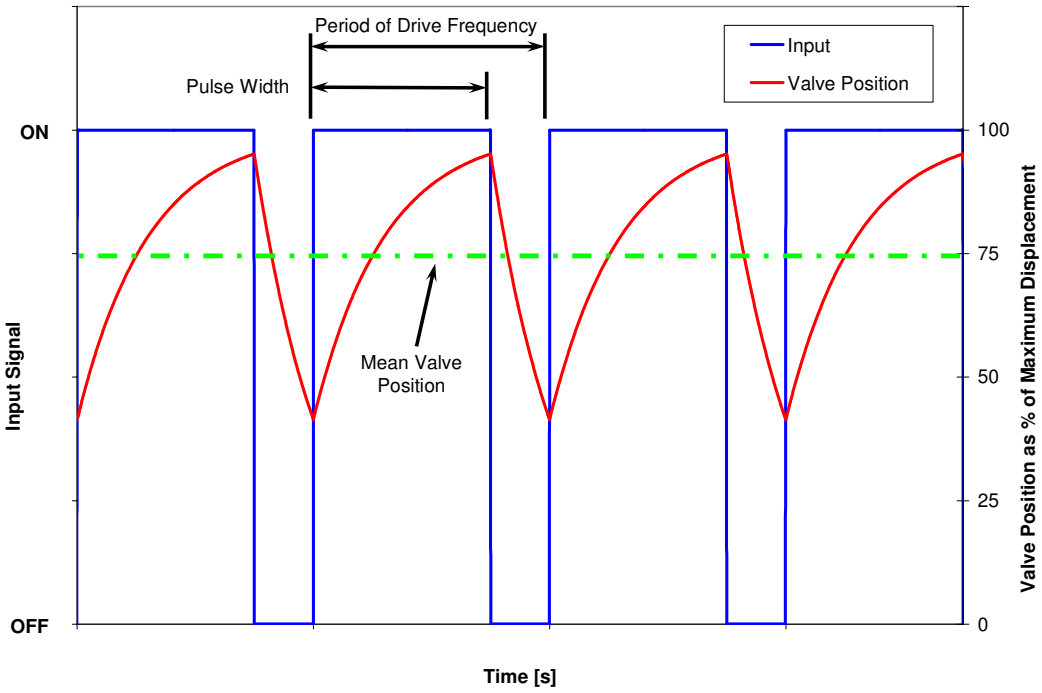

Figure 3.6b: Effect of Driving an On/Off Valve with a PWM Input (SMR of 0.75)

Due to the periodic valve spool position created through use of the PWM technique, pulsations in flow through the valve are generated. These pulsations create undesired perturbations in flow and pressure, of which the magnitude is dependent on the load being manipulated. In this research the tilt actuator is driving a large inertial load with low natural frequency that acts as filter to remove these effects.

As the on/off valve studied in this research had a relatively 'slow' response time, the cyclical positions of the spool due to the PWM input were always somewhere between the 'on' and 'off' positions. The response of a 'faster' on/off valve would allow the spool to reach both positional extents during each pulse. This would create greater disturbances in flow and pressure due to the larger changes in spool position every cycle. Although this regime is considered typical for many PWM applications, the on/off valve model developed in section 3.5.1 was used to maintain consistency with the valves used in this study.

The equations necessary to solve for the effect of valve position on the orientation of the suspended boom sprayer under investigation have all been presented. A complete dynamic simulation model was developed in a computer software package (Mathworks, 2001) and is considered in Chapter 5. Complete details of the boom and hydraulic model are presented in Appendix C.

Chapter 4

System Parameters Obtained from Experimental and Manufacturer's Data

The fluid bulk modulus and actuator friction profile are both highly system-dependent parameters. In this chapter the experimental methods used to determine both are presented. Also, the process used to obtain the proportional valve transfer functions from the manufacturer's data is discussed.

4.1 System Effective Bulk Modulus

The bulk modulus is a measure of the compressibility of a fluid. When considered in conjunction with the overall hydraulic system, the value will incorporate component effects (i.e. hydraulic hose flex) along with being dependent on system issues (i.e. air entrainment). To ensure the simulation model adequately reflected these effects, it was necessary to experimentally obtain this value. The method used in this study was introduced by Hindman (2004) which facilitated the estimation of the fluid bulk modulus. The following information outlines the necessary background information for the estimation.

By extending or retracting the actuator rod to its fully retracted or extended positions, a known control volume is created (volume of the actuator and its connecting line) (Figure 4.1). Assuming negligible leakage and without the addition of flow, the actuator maintains its position, and thus, there is no change in the control volume; the continuity equation (3.6) presented in Chapter 3 may then be reduced to:

$$-\sum Q_{OUT} = \frac{V_{AO}}{\beta_E} * \frac{dP}{dt}. \qquad [4.1]$$

By integrating both sides of equation 4.1 with respect to time, it is shown that:

$$\int_{t_o}^{t_f} -\sum Q_{OUT} * dt = \frac{V_{AO}}{\beta_E} \int_{t_o}^{t_f} \frac{dP}{dt} * dt, \qquad [4.2]$$

where:

t_o is the time at the beginning of the experiment (s), and

t_f is the time at the end of the experiment (s).

By venting the control volume to atmospheric pressure during the experiment, equation 4.2 can be rewritten as:

$$\int_{t_o}^{t_f} -\sum Q_{OUT} * dt = \frac{V_{AO}}{\beta_E} * (P_{ATM} - P_{EX}), \qquad [4.3]$$

where:

P_{ATM} is atmospheric pressure (Pa), and

P_{EX} is the system experimental pressure before venting to atmosphere (Pa).

Neglecting leakage, the only flow exiting the control volume is due to compressibility of the fluid and 'flex' of the system components. Also, P_{ATM} is negligible in comparison to the pressures to be used in this experiment. Therefore, equation 4.3 can be rewritten in the form:

$$\beta_E = \frac{V_{AO}}{V_{GC}} * P_{EX}, \qquad [4.4]$$

where:

V_{GC} is the volume of fluid in the actuator control volume due to bulk modulus effect collected during the experimental trial (m^3).

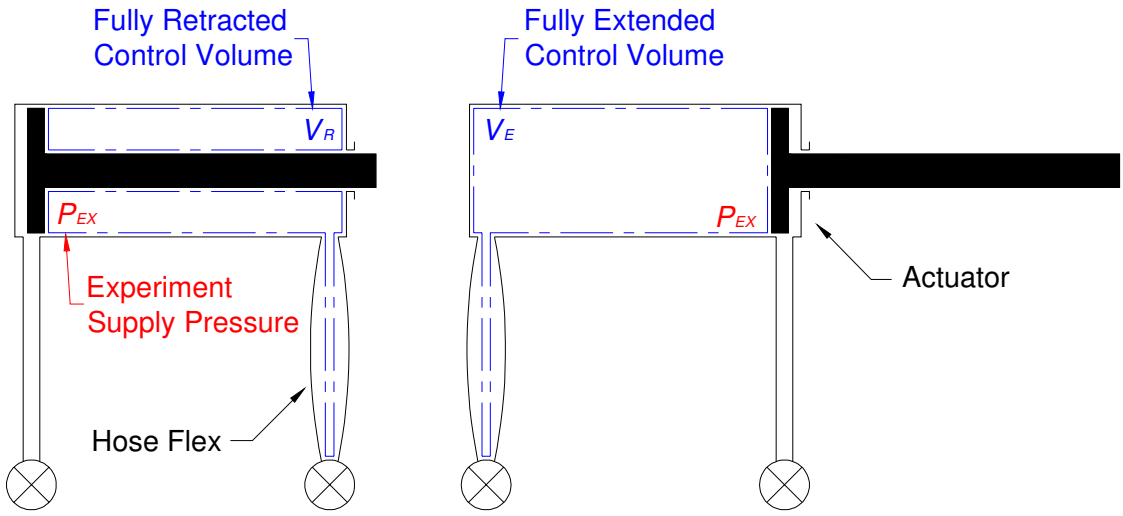

(a) Actuator Fully Retracted (b) Actuator Fully Extended

Figure 4.1: Actuator Experimental Control Volumes

For the fully retracted actuator condition, equation 4.4 yields:

$$\beta_E = \frac{V_R}{V_{GC}} * P_{EX}, \qquad [4.5]$$

where:

V_R is the volume of fluid in the fully retracted control volume (m^3).

Similarly, for the fully extended condition:

$$\beta_E = \frac{V_E}{V_{GC}} * P_{EX}, \qquad [4.6]$$

where:

V_E is the volume of fluid in the fully extended control volume (m^3).

As both the experimental pressure and compressed fluid volume can be measured, equations 4.5 and 4.6 allow the effective bulk modulus for this system to be calculated.

The experimental set-up is shown in Figure 4.2. The actuator and hoses used on the sprayer were set-up in the University of Saskatchewan Fluid Power lab (December 2004) with pressure transducers attached in-line on both the rod and non-rod ends. The actuator was moved all the way to one positional extent using the directional valve. Two zero-leakage needle valves (n_1 and n_2) were then used to isolate the actuator and hold the system pressure in the control volume; the pressure in the control volume was recorded via the transducers. Next, the required needle valve (n_3 or n_4) was opened to vent the desired side of the actuator to atmosphere over a 0.00013 m diameter control orifice. The compressibility flow was collected and measured in a graduated cylinder giving V_{GC}. Four trials were completed; two with the actuator fully retracted and two with it fully extended. Due to the small volumes collected during experimentation, control orifices were used to ensure droplet formation and allow all of the test volume to be collected (increase test accuracy). Also, it should be noted that fluid temperature varied from 46.7 °C to 54.9 °C over the duration of the testing. The results of all experiments are shown in Table 4.1.

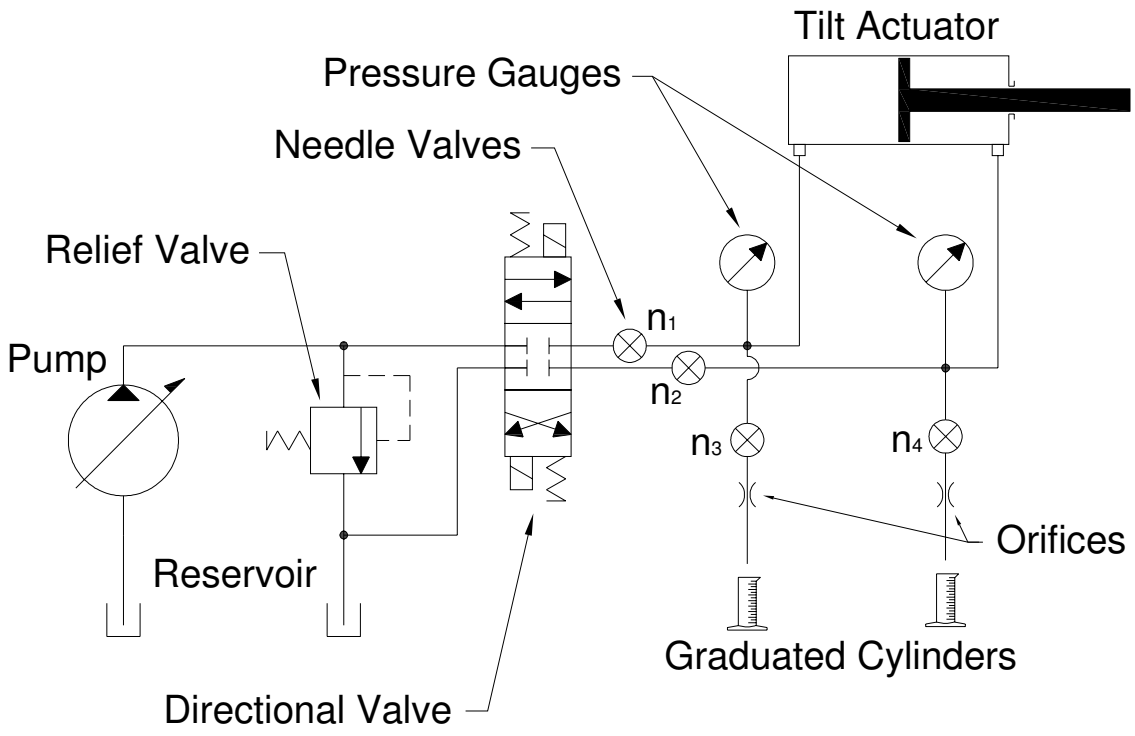

Figure 4.2: Effective Bulk Modulus Experimental Set-up

Table 4.1: Experimental Results of Effective Bulk Modulus

Trial #	Cylinder Position	Fluid Control Volume [m^3]	Experimental Pressure, P_{EX} [MPa]	Compressed Fluid Volume, V_{GC} [m^3 X 10^{-3}]	Effective Bulk Modulus, β_E [MPa]
1	Extended	0.00101	7	0.0054	1295
2	Retracted	0.00082	7	0.0046	1227
3	Extended	0.00101	7	0.0054	1295
4	Retracted	0.00082	7	0.0046	1227
				Mean	1261
				Standard Deviation	39

From these results it was shown with a 95% confidence level that the effective bulk modulus of the system was within the range of 1183 to 1339 MPa

(±2 standard deviations of the mean). The simulation employed the mean value of 1261 MPa for bulk modulus.

4.2 Actuator Friction Profile

To develop the actuator friction force profile, an experimental system similar to that shown in Figure 4.2 was set-up to reproduce an experiment introduced by Chinniah (2004). The needle valves were removed and the directional valve replaced with a highly accurate servo-valve. From equation 3.2, for a constant velocity and no external load on the actuator:

$$P_1 * A_1 - P_2 * A_2 = F_f . \qquad [4.7]$$

Using the servo-valve, the actuator was driven at a series of different constant velocities. The velocities were selected primarily by operating the actuator as slow as possible, as fast as possible, and at a mid-point between (for both extension and retraction of the actuator). The pressure differential to create each velocity was recorded via the pressure transducers. An example of one experimental trial is shown in Figure 4.3. Data points around the transition region from extension to retraction were discarded; an average value of each pressure was calculated from the remaining data points. From this same time period, the slope of the position data was calculated using a spreadsheet software package (Microsoft, 2001) to generate a 'best fit' linear equation and yield actuator velocity. As the actuator areas were known, equation 4.7 then permitted calculation of the friction force for each experimental velocity.

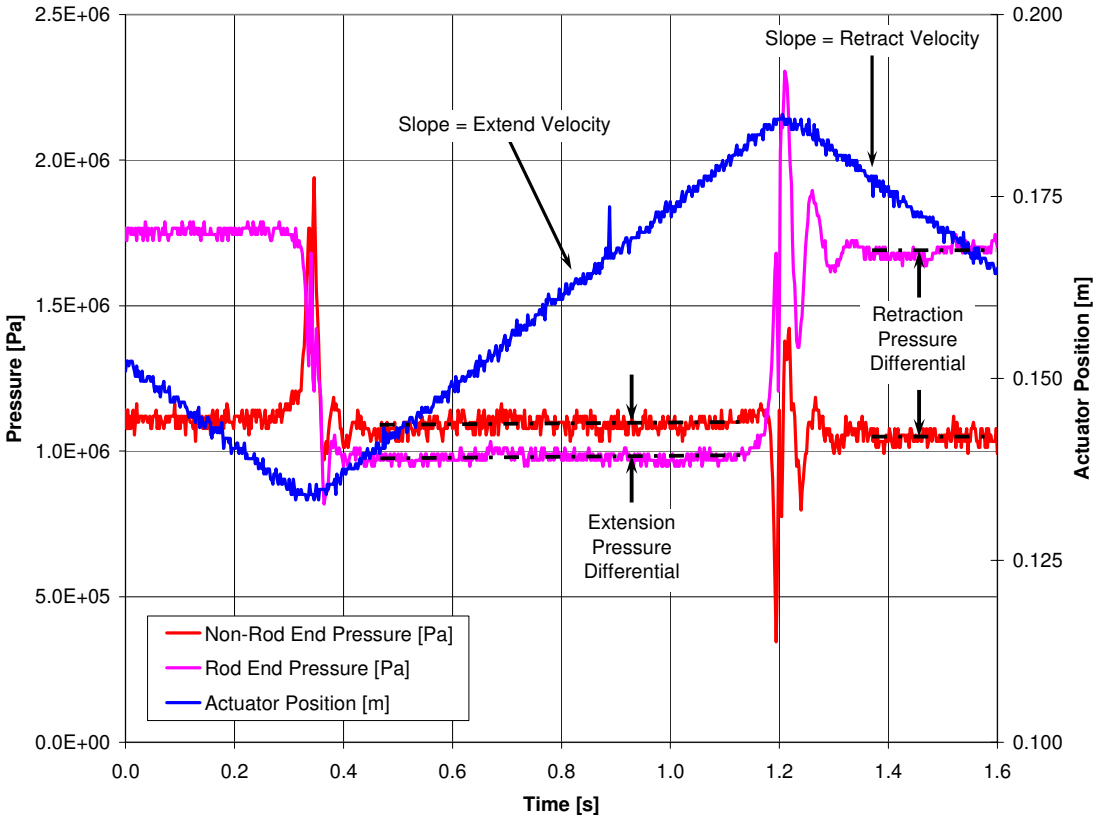

Figure 4.3: Example of Actuator Friction Force Experimental Data

The experiment was repeated multiple times to create a good representation of the force profile throughout the expected range of actuator velocities (Figure 4.4). A spreadsheet software package (Microsoft, 2001) was used to independently generate 'best fit' linear equations for both positive and negative velocities. As the friction force of the actuator near zero velocity was small compared to the other forces involved with the boom system, the complex Stribeck transition regions along with the stiction values were simplified to a pair of constants. The constants were determined using the average of the slowest two velocities for each direction, and made effective from zero velocity to the point of intersection with the 'best fit' profiles. For extension, the value used was 485 N for actuator velocities from zero to 0.014 m/s; for retraction a value of -819 N was used from zero to –0.026 m/s. To avoid the non-linearity when the actuator velocity changes from positive to negative (extension to retraction) and

vice versa, a very rapid slope crossing through zero was employed. Using all of the aforementioned regions, the following equation was used to represent actuator friction force in the model:

$$F_f = \begin{cases} 21364 * \dot{x}_C + 187 & for\ \dot{x}_C > 0.014 \text{ m/s} \\ 485 & for\ 0.000001 \text{ m/s} \le \dot{x}_C \le 0.014 \text{ m/s} \\ \left(485 / 0.000001\right) * \dot{x}_C & for\ 0 \text{ m/s} < \dot{x}_C < 0.000001 \text{ m/s} \\ 0 & for\ \dot{x}_C = 0 \text{ m/s} \\ \left(819 / 0.000001\right) * \dot{x}_C & for\ 0 \text{ m/s} > \dot{x}_C > -0.000001 \text{ m/s} \\ -819 & for\ -0.000001 \text{ m/s} \ge \dot{x}_C \ge -0.026 \text{ m/s} \\ 30573 * \dot{x}_C - 15 & for\ -\dot{x}_C < -0.026 \text{ m/s} \end{cases} . \quad [4.8]$$

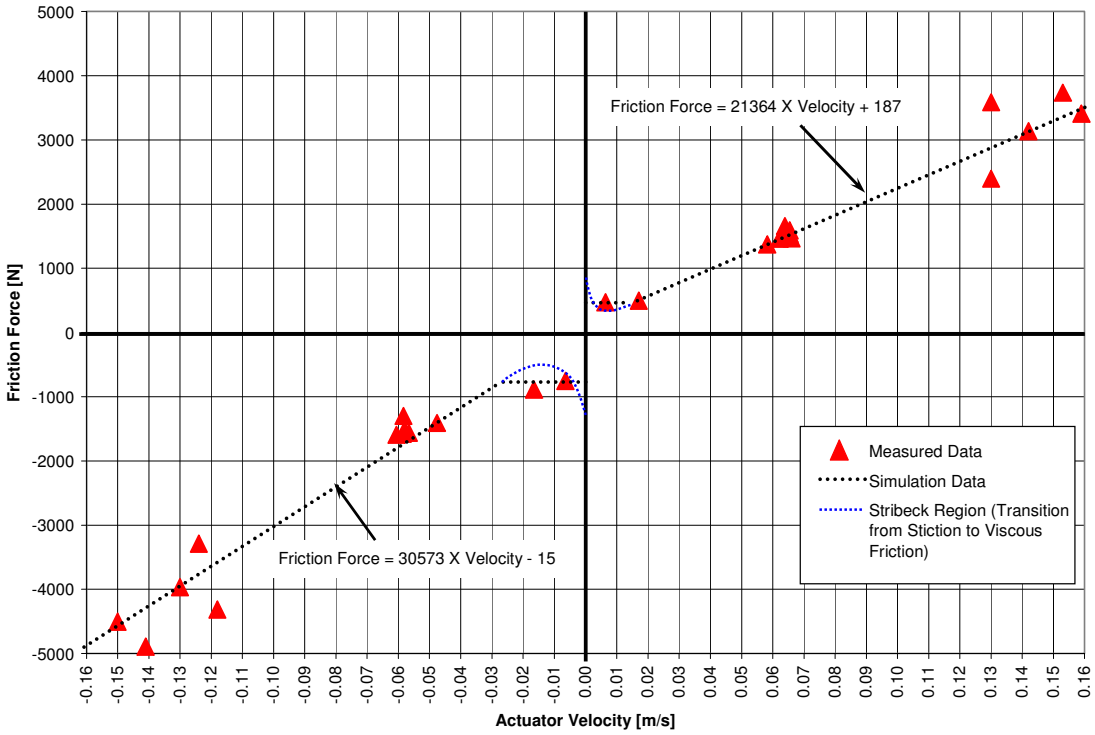

Figure 4.4: Actuator Friction Force Profile

4.3 Proportional Valve Transfer Functions

The transfer functions used to represent the proportional valve were presented in Chapter 3. Two separate transfer functions were used in the course of this research as the manufacturer distinguishes separate responses between large (approximately 50%±40% of maximum spool displacement) and small (approximately 50%±10%) spool displacements. To derive the transfer functions, the Bode plot of valve frequency response provided by the manufacturer was used. The theoretical asymptotes of first and second order transfer functions were overlaid on the Bode plot. By summing the asymptotes, a 'best fit' to the manufacturer's data was created (Figures 4.5 and 4.6). The transfer functions derived via this graphical technique provided excellent approximations.

The required parameters to define the transfer functions for large changes were determined to be:

ω_{NL} = 30 Hz (188 rad/s), and

ζ_L = 0.7.

For the small change transfer function, parameters were defined as:

ω_1 = 10 Hz (63 rad/s),

ω_2 = 18 Hz (113 rad/s),

ω_{NS} = 35 Hz (220 rad/s), and

ζ_S = 0.7.

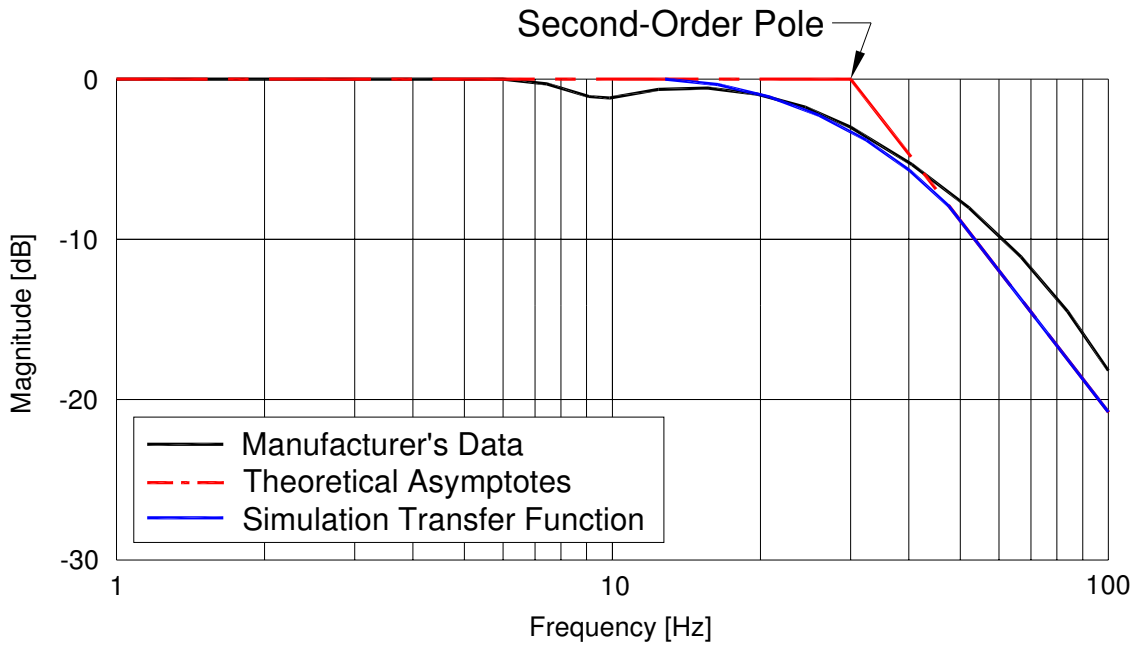

Figure 4.5: Frequency Response of Proportional Valve for Large Changes (50%±40% of Maximum Spool Displacement)

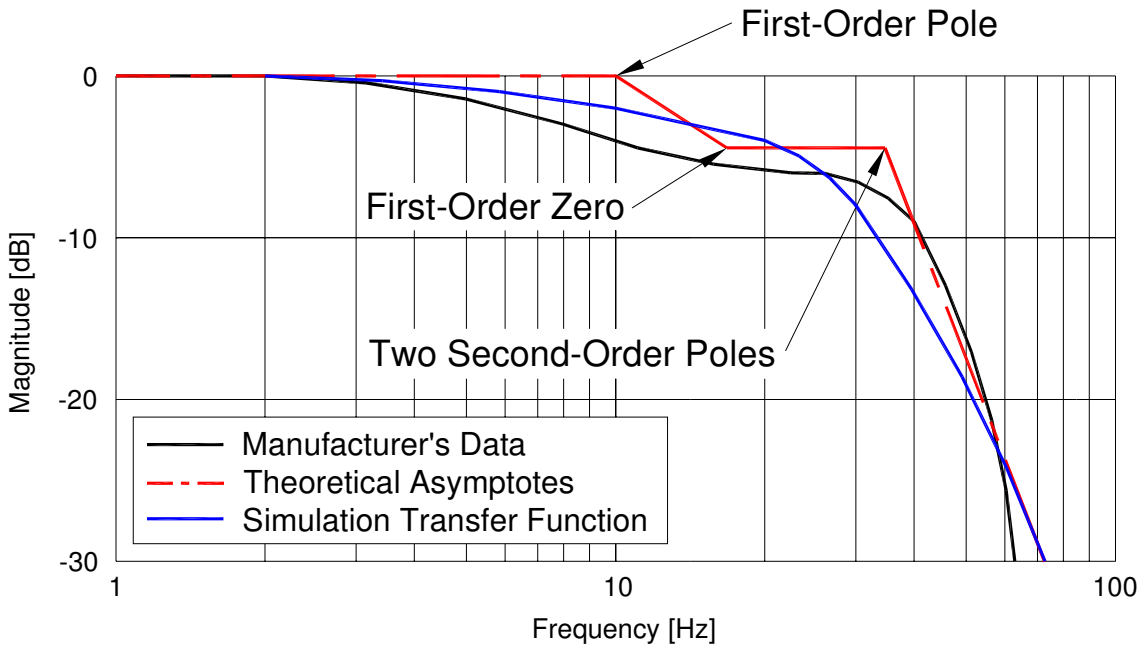

Figure 4.6: Frequency Response of Proportional Valve for Small Changes (50%±10% of Maximum Spool Displacement)

4.4 Valve Area Gradient

The area gradient of the valves used in this research was extracted from data provided by the manufacturer and from experimental results. Using the orifice equation (equation 1.1) and the equation for orifice area at a particular spool displacement (equation 3.11) consider the following equation for valve area gradient:

$$w = \frac{Q}{C_d * x_V * \sqrt{\frac{2}{\rho} * (\Delta P)}}. \qquad [4.9]$$

The manufacturer specifies maximum flow through the proportional valve of $0.5X10^{-3}$ m^3/s for a pressure drop across the valve of 21.0 MPa. Substituting these values into equation 4.9 and assuming a maximum spool displacement of 3 mm, *w*, the valve area gradient, was found to be 0.0012 m^2/m.

From some preliminary experimental results using a new on/off valve in the sprayer boom system, it was determined that a maximum actuator velocity of 0.1 m/s was possible when raising the right section (Figure 4.7). Knowing that:

$$Q_2 = A_2 * \dot{x}_C, \qquad [4.10]$$

a velocity of 0.1 m/s equates to a flow of $0.4X10^{-3}$ m^3/s. The average pressure during the change (ignoring the pressure spike) was found using a spreadsheet software package (Microsoft, 2001) to be 13.2 MPa; as the source pressure was measured to be constant at 17.2 MPa the pressure drop across the valve to produce this flow was 4.0 MPa. Substituting these values into equation 4.9, the area gradient was calculated to be 0.0022 m^2/m. An average value of 0.0017 m^2/m was used to represent both valves throughout the course of this research to maintain consistency when comparing the effects on the boom system between the different valve types.

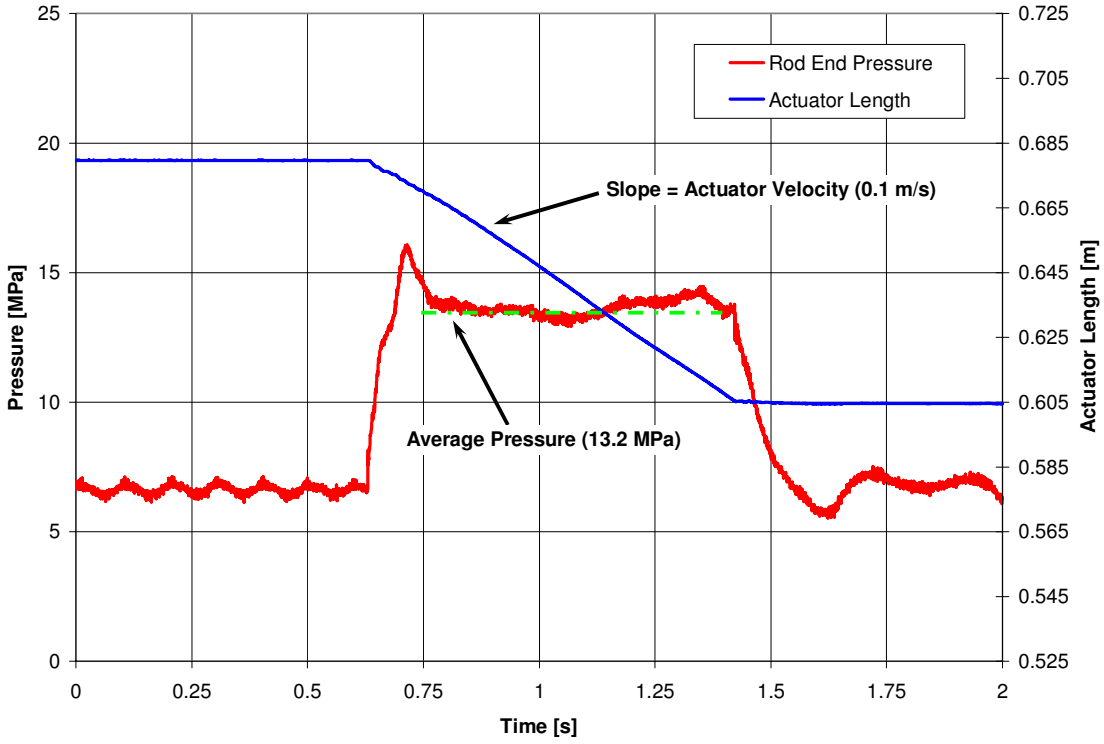

Figure 4.7: Actuator Velocity (Experimental) versus Time for an On/Off Valve

All necessary equations and parameters have been developed in Chapters 2, 3, and 4. The simulation model was now used to pursue the remaining objectives of this research.

Chapter 5

Simulation Results

Using the equations developed in Chapters 2 and 3, the effect of operating the right boom section's tilt actuator on the spray nozzle 'distance from the target' for a typical suspended boom system is quantified. Using these results, a proportional valve is introduced to investigate its ability to improve overall system performance. Finally, the effects of the perturbations in flow and pressure introduced into the boom system by use of a PWM driven on/off valve are investigated. All results presented in this Chapter are based on simulation trials.

5.1 Performance of a Typical System (On/Off Valve)

As discussed in Chapter 1, to maximize spray efficacy the nozzles used to apply chemical must be positioned at an optimum distance from the target to be sprayed. Therefore, when using a suspended boom sprayer, the operator must reorient each boom section as the terrain changes beneath to maintain the desired distance of the nozzles from the target. For the purposes of this research it was assumed that the original orientation of the entire boom was horizontal (Figure 5.1). Terrain changes beneath the right section would then require the operator to reorient the right section from this horizontal position while desiring that the left section stay in its original horizontal orientation.

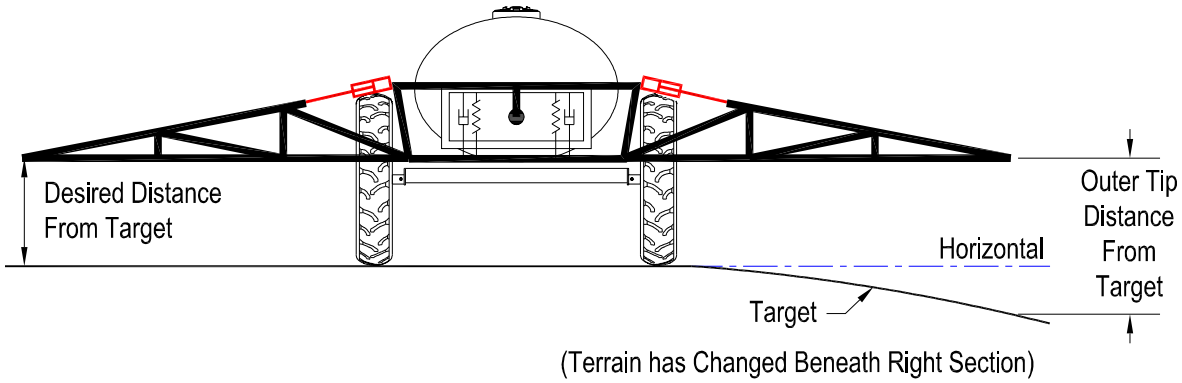

Figure 5.1: Suspended Sprayer Boom Orientation Definitions

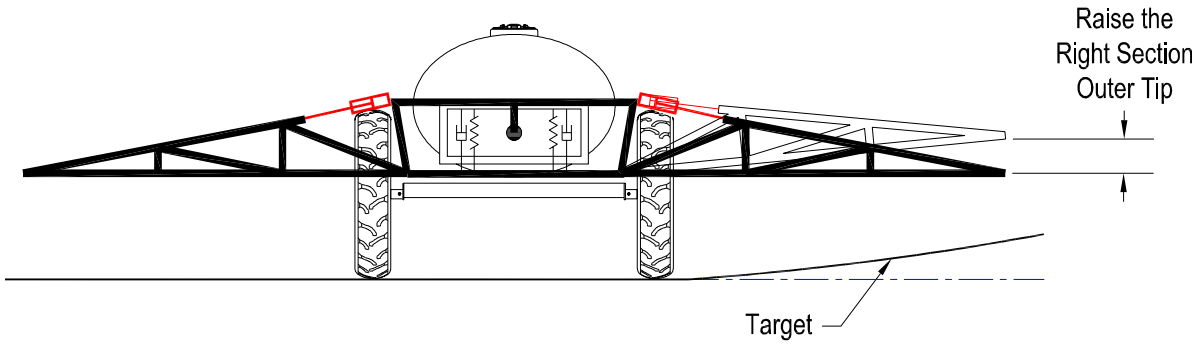

Figure 5.2: Suspended Sprayer Boom Orientation Change to Raise the Right Section's Outer Tip after Terrain Change

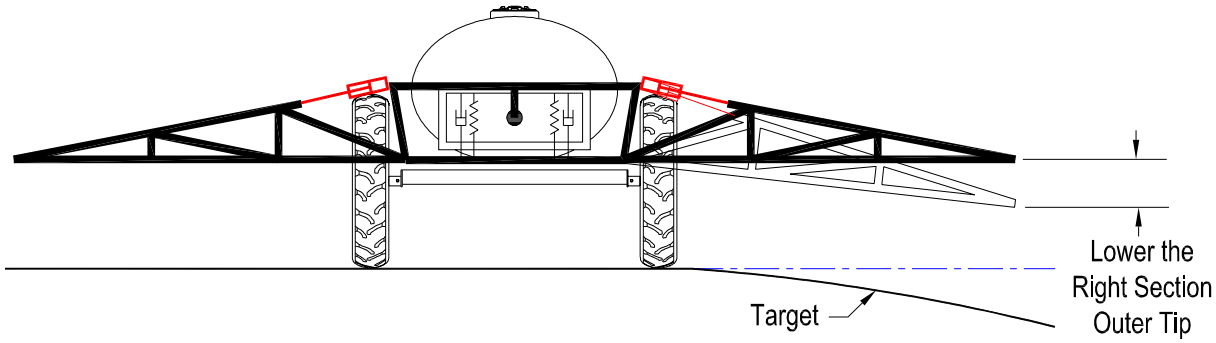

Figure 5.3: Suspended Sprayer Boom Orientation Change to Lower the Right Section's Outer Tip after Terrain Change

Typical suspended boom sprayers utilize on/off valve-driven actuators to reorient the boom wing sections independently of the center section. To 'raise'

a wing section to maintain the desired distance from the target, the actuator is retracted (Figure 5.2); to 'lower' a wing section, the actuator is extended (Figure 5.3).

The right and left sections' movements are coupled together because of the attachments between the booms and the center section and the attachment of the center section to the carrying frame via a passive suspension system. The effect of reorienting the right section on the distance from the target of the left section was to be quantified. To evaluate the boom's performance, four standard right section orientation changes were defined (with respect to the original horizontal position defined in Figures 5.2 & 5.3):

i. reorienting the right section such that the outer tip has raised 0.075 m,
ii. reorienting the right section such that the outer tip has lowered 0.075 m,
iii. reorienting the right section such that the outer tip has raised 0.25 m,
iv. reorienting the right section such that the outer tip has lowered 0.25 m,

It should be noted that the operation of reorienting the boom is open loop in that no mechanical or electronic feedback is present. However, in practice, there is always a visual feedback in which the changes to orientation are monitored by the operator. Thus, the operator observes the error and moves the boom in an attempt to correct for it. Ideally, it would be of benefit to simulate this visual feedback in the model; however, practically this is not feasible. Due to this, alternate approaches were considered to investigate the response of the boom system to various orientation change inputs.

One approach considered was to examine how the system responded to various types of inputs to the valves. This would be more of the traditional approach to evaluating the response of the boom system. A different (but

related) approach was to use a trial-and-error method to actuate the valve at various input voltage values until the right section's tip obtained the desired steady-state displacement value (those listed above). When the desired steady-state position was achieved, then an analysis was done on the relevant parameters and states to accommodate comparison studies. Thus, a form of visual feedback was employed to obtain the results for this study. In essence, studies evaluated how the left section moved with respect to a desired horizontal position for a known displacement of the right section. This is a very important point in setting up a parameter (to be introduced) in which to compare performance of the boom for various valve types.

Due to the geometry of the boom system (point of rotation of the passive suspension system being at the center of the machine), the position of the spray nozzle along the boom section's length amplifies the effect of boom oscillation. For this reason, only the outermost spray nozzle on each section was evaluated as it was considered the worst case. To evaluate the boom system performance, a value defined as set-point error (SPE) was calculated. This value is given for the outermost spray nozzle on each section by:

$$SPE = \int \left| \Delta h_{SP} \right| * dt \qquad [5.1]$$

where:

Δh_{SP} is the deviation of the outer tip from the desired distance to target (m)[3].

The magnitudes of orientation changes assumed in this study were based on the author's personal experience with machine operation. However, changes of any magnitude within the range of motion of the boom section (raise the outer tip 2.2 m or lower it 1.1 m (from horizontal)) would be plausible. Due to the associated high travel speeds and boom widths, it is difficult for an operator to notice and efficiently correct an error smaller than 0.075 meters. Larger changes (0.25 m) are typical when operating in hilly terrain.

[3] The equations derived in Chapter 2 define the orientation of the boom structures via angles. Due to this, conversion of the angular orientation values to an outer tip linear deviation value was necessary. The details of this portion of the model are explained in Appendix D.

The SPE begins to accumulate for both the left and right sections with the activation of the valve. This point in time was chosen as it is when the operator deems an error to be present in the system and makes the conscious decision to drive the actuator and raise/lower the right section. For all treatments the valve activation occurs at t=1 s as the model required a small period of time for all initial transients to 'die out' (due to inherent numerical properties of a dynamic model). SPE incorporates both the effects of the magnitude of the deviation from the desired distance to target and the duration over which the deviation lasts. As mentioned above, it is important to note that the changes to the right section were iteratively performed. That is, for all treatments the simulation was executed iteratively and the valve input modified until the desired orientation of the right section was achieved. Therefore, any steady-state influence the orientation change to the right section has on the left section would be visible as an increasing left section SPE value with time. As the right section was forced to the desired orientation, its SPE would always stop accumulating after the overall system oscillation was eliminated by the passive suspension system.

The nature of an on/off valve results in rapid acceleration and deceleration of the tilt actuator. For the examined changes, the duration of valve operation ranges from 0.044 s when lowering the right section 0.075 m, to 0.203 s when raising the right section 0.25 m. The results of lowering the right section 0.075 m are shown in Figure 5.4. Because the boom structure responds similarly to all magnitudes of changes evaluated, only a representative series of responses are shown. As the operator drives the actuator and lowers the right section (distance from the target is decreased), the force imbalance rotates the combined left and center sections counter clockwise. When the valve is deactivated the rapid deceleration of the right section reverses the force imbalance and with it the direction of rotation of the combined left and center sections (A in Figure 5.4). As the rotation has moved the relative position of the center of gravity of the combined left and center sections closer to the overall

boom point of rotation, the system is no longer in static balance. The system oscillates (B and C in Figure 5.4) until the passive suspension system can eliminate the motion (D in Figure 5.4). Also, a change in the static balance point orients the left section at a position slightly deviated from ideal (defined as the change in distance from the target of the left section); therefore its SPE continues to accumulate. For this reason SPE is calculated by integrating signals for 29 s, following the original activation of the valve for all cases.

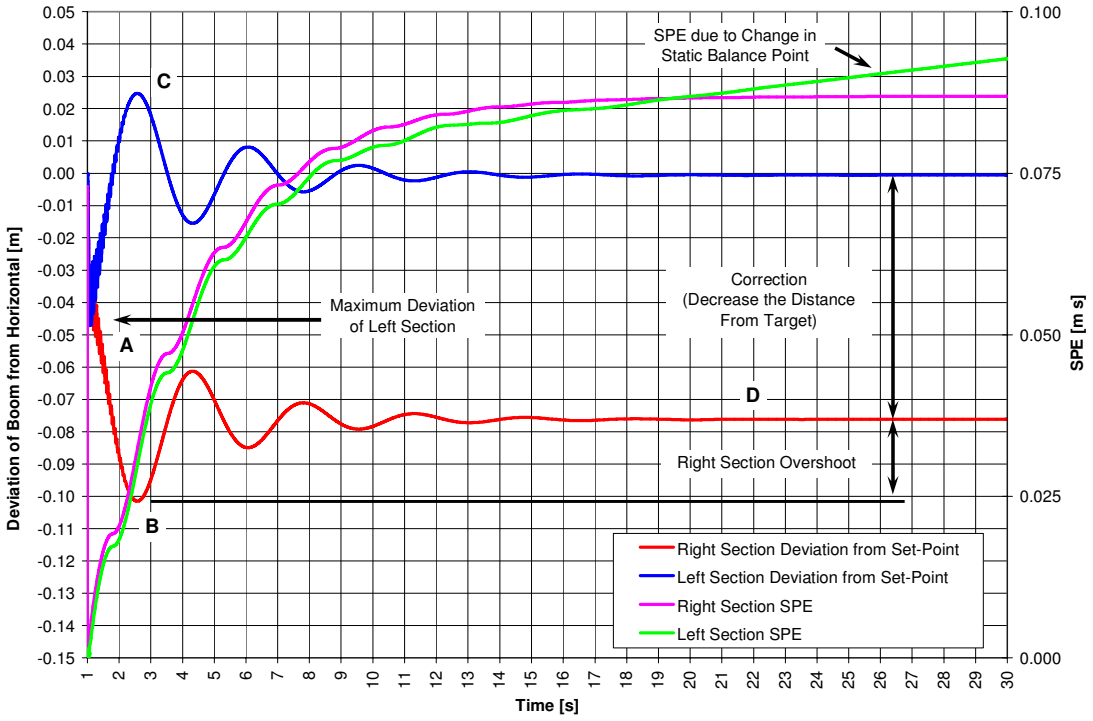

Figure 5.4: Definition of Terminology and Performance of Boom System when Lowering the Rt. Section 0.075 m using an On/Off Valve

Due to the coupling of the left and right sections through the center section, the SPE accumulated on the left section closely matches the right; that is an error of similar magnitude is created on the left section when attempting to reorient the right. For this scenario, the error accumulated due to only the change of terrain under the right section is insignificant when compared to the oscillation created. A summary of results for the four identified changes are

listed in Table 5.1. It is again noted that changes quoted in this and all subsequent tables are for the outermost spray nozzle on both the left and right sections with respect to an original horizontal orientation.

Table 5.1: Summary of Performance Results for Orientation Changes Driven by On/Off Valve

Orientation Change of Right Section Outer Tip [m]	Right Section Overshoot [m]	Maximum Deviation from Desired Distance to Target for Left Section [m]	Change in Distance from Target of Left Section due to Static Balance Point Change [m]	SPE of Right Section [m s]	SPE of Left Section [m s]
Raise 0.075	0.028	0.048	0.001	0.10	0.12
Lower 0.075	0.025	0.047	0.001	0.09	0.09
Raise 0.25	0.090	0.136	0.003	0.34	0.35
Lower 0.25	0.087	0.137	0.000	0.31	0.29

When raising the right section, the force imbalance rotates the combined left and center sections clockwise. Again, when the valve is deactivated the rapid deceleration of the right section reverses the force imbalance and with it the direction of rotation of the combined left and center sections (Figure 5.5). Both raising and lowering of the right section result in boom oscillation which continues for approximately 15 s. To put this in a practical context, for a typical operating speed of 25 kph, this sprayer would have its spray accuracy negatively affected for 104 m or 2800 m^2 (0.28 ha). The maximum deviation in distance from the target for the left section varies between 54% and 63% of the correction value. That is, when one section is raised or lowered a particular

magnitude, by making the change, a deviation of at least 54% of the change magnitude is induced in the non-actuated section.

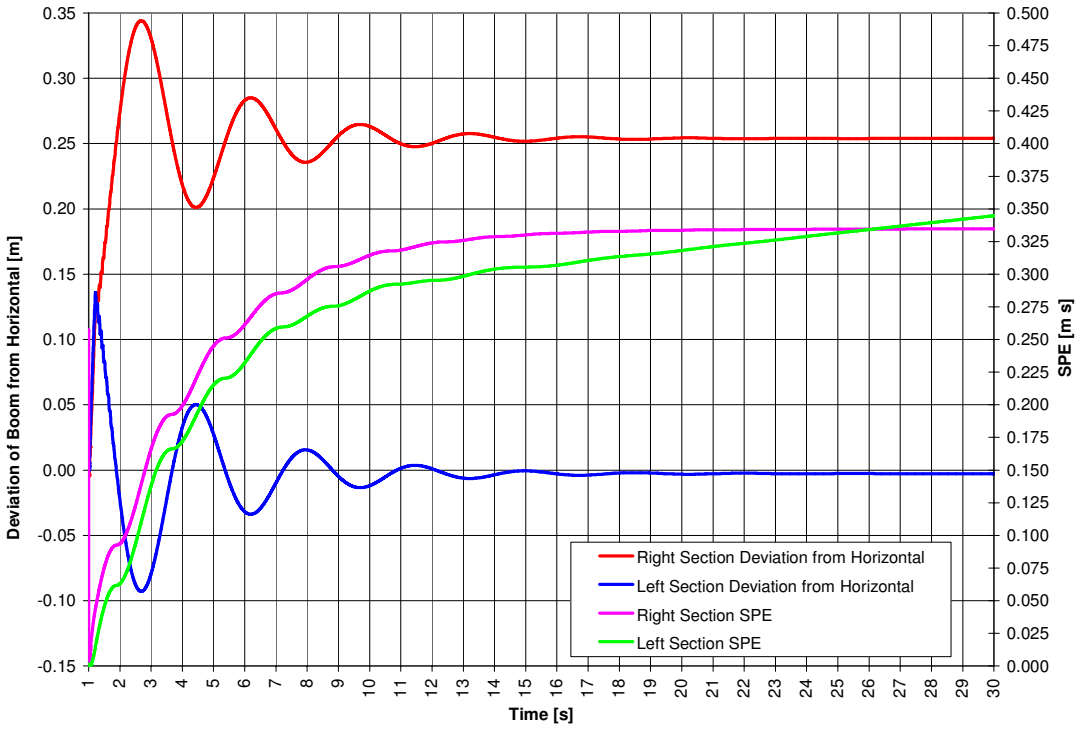

Figure 5.5: Performance of Boom System when Raising the Rt. Section 0.25 m using an On/Off Valve

The primary objective of this research was to focus on the orientation error of the boom structure, in particular the left section; however, the model facilitated other interesting simulation studies which warranted further investigations. Details of this are provided in the following section.

5.1.1 Other System Effects (On/Off Valve)

The sprayer under examination utilizes a double-acting actuator, where fluid flow and pressure can be supplied to both the rod and non-rod ends. The pressure on the rod end must be maintained as the geometry of the boom makes this system a run-away load. Figure 5.6 shows the simulated pressure in both ends of the actuator for a 0.25 m decrease. When the valve is opened, the pressure on the rod end of the actuator immediately begins to decrease as the

boom section's weight is driving the system (A in Figure 5.6). As the load on the actuator is defined by the weight of the right section, the non-rod end pressure builds as the orifice created by the valve begins to limit the amount of flow that escapes from the rod end (B in Figure 5.6). The right section is effectively being 'pushed'. The rapid closure of the valve decelerates the right section quickly which results in a substantial pressure spike in the actuator (C in Figure 5.6).

When the valve is closed, no flow passes through the valve. The large inertial effects of the boom compress the fluid in the rod end and the actuator continues to extend. Oscillation results as the fluid on both sides of the actuator acts as a spring (D in Figure 5.6). The resultant oscillation is eventually damped out by the actuator friction.

A problem can occur due to the rapid valve closure. When the valve is closed, there no longer is flow being provided to the non-rod end of the actuator. As the non-rod-end chamber expands with the continued motion of the actuator, the pressure decreases (E in Figure 5.6). This decrease in pressure results in a potentially damaging phenomenon called cavitation. Cavitation is a result of the formation of bubbles within the fluid as the pressure in the actuator drops below the vapor pressure of the fluid. These bubbles then implode when compressed, eroding material in these localized areas.

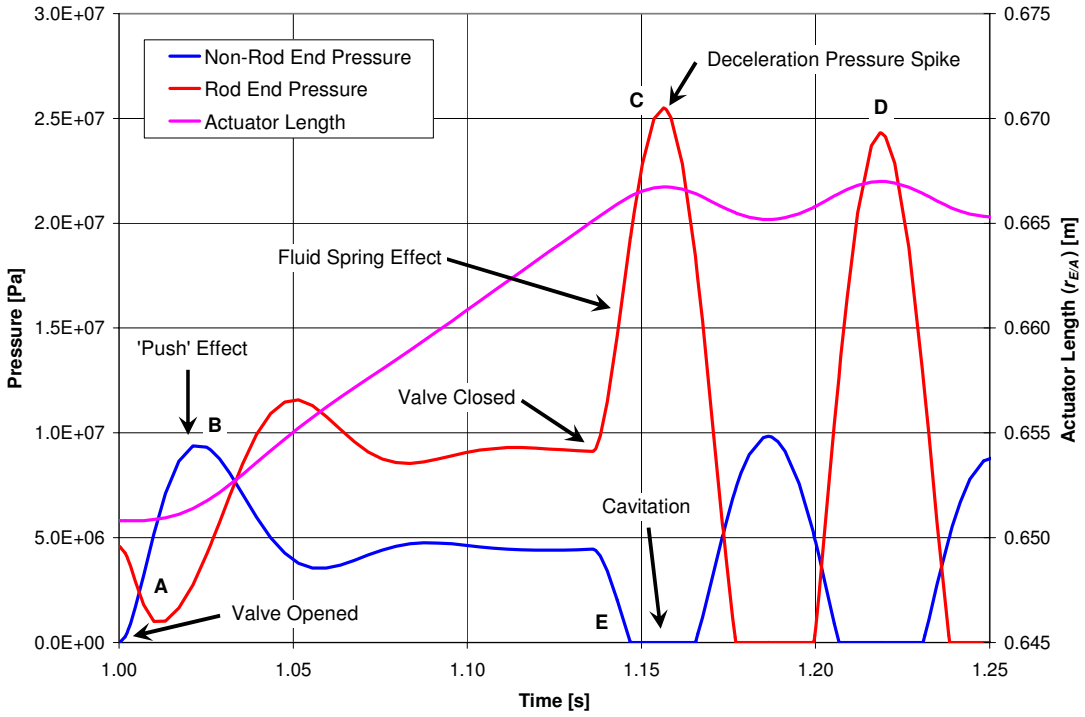

Figure 5.6: Actuator Effects when Lowering the Rt. Section 0.25 m using an On/Off Valve

When raising the right section outer tip 0.25 m, the system behaves differently. The weight of the system no longer helps to accelerate the actuator. The pressure spike required to decelerate the system is significantly less, with the highest pressure actually seen on the rod end due to compressibility effects (Figure 5.7). The system still oscillates; however no cavitation occurs.

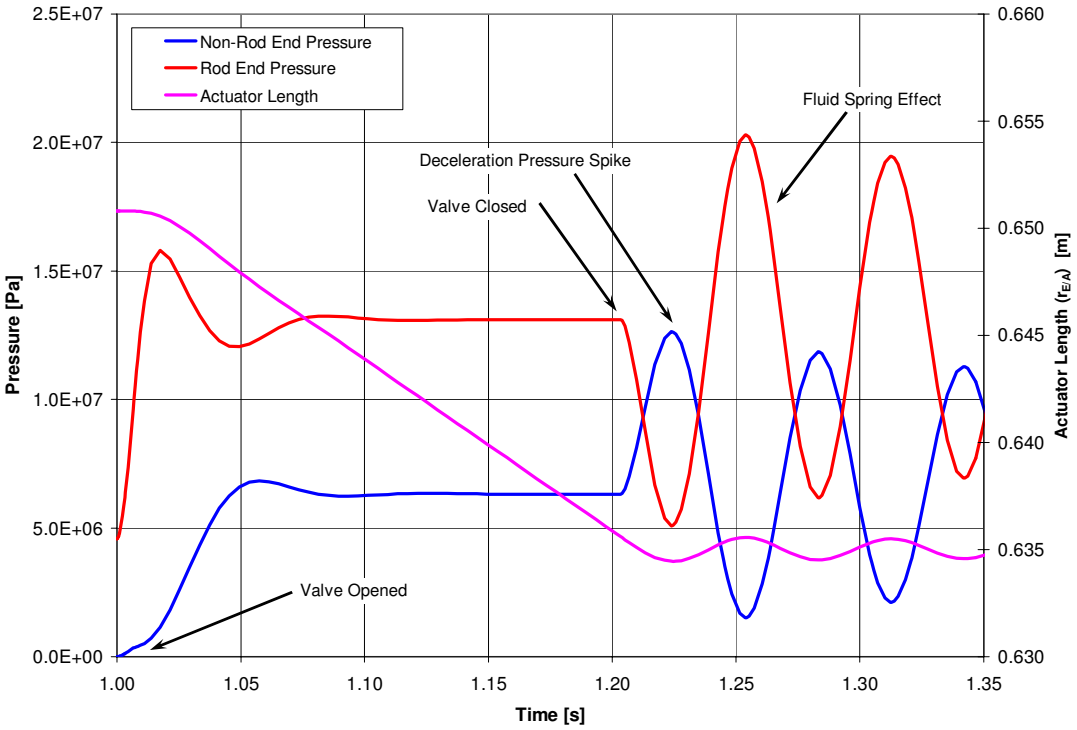

Figure 5.7: Actuator Effects when Raising the Rt. Section 0.25 m using an On/Off Valve

Sudden changes to the actuator flow due to an on/off motion of the valve spool can create unwanted movement of the opposing boom section or very large pressure spikes in the actuator which may induce cavitation conditions. A slower rate change in the position of the valve spool should reduce these effects. It was postulated that by employing a proportional valve to control the actuator acceleration rate, the overall system oscillation and pressure fluctuations within the actuator should be improved. Such an approach is considered in the next section.

5.2 Performance of Boom System Using Proportional Valve Technology

Proportional valve technology allows modulation of the flow rate being supplied to the actuator. As seen in the previous section, the actuator rod position with use of an on/off valve is the integral of the valve flow and results in

a ramp-shaped function in a plot of actuator position as a function of time. As acceleration is the second derivative of position, the sharp corners of the ramp position profile create impulses in the actuator acceleration. This rapid acceleration and deceleration create the pressure spikes and large force imbalance, which drive the boom system oscillation. The most appropriate profile for actuator position, which eliminates these sudden pressure changes, would be a sigmoidal ('S') shape. To create a simplified 'S' profile, it can be shown that the actuator velocity must be a ramp profile given by:

$$\dot{x}_C = \mathrm{m}_{\mathrm{SLOPE}} * t, \qquad [5.2]$$

where:

$\dot{x}_C$ is the velocity of the actuator (m/s), and

$\mathrm{m}_{\mathrm{SLOPE}}$ is constant rate of change of the actuator velocity, acceleration (m/s^2).

Neglecting compressibility, flow to the actuator is given by:

$$Q_1 = A_1 * \dot{x}_C. \qquad [5.3]$$

Substituting equations 5.2 and 5.3 into 3.11 and solving for valve position yields:

$$x_V = \left(\frac{A_1}{C_d * w * \sqrt{\frac{2}{\rho} * (\Delta P)}} \right) * \mathrm{m}_{\mathrm{SLOPE}} * t. \qquad [5.4]$$

Assuming a constant pressure drop across the valve orifice, the position of the valve spool must therefore also be a ramp function to yield the desired response for actuator velocity. A comparison between the actuator rod positions driven by an on/off valve and a ramp-driven proportional valve is shown in Figure 5.8. In this figure the actuator rod position follows an 'S' shape profile but reached steady state much slower than the on/off valve situation.

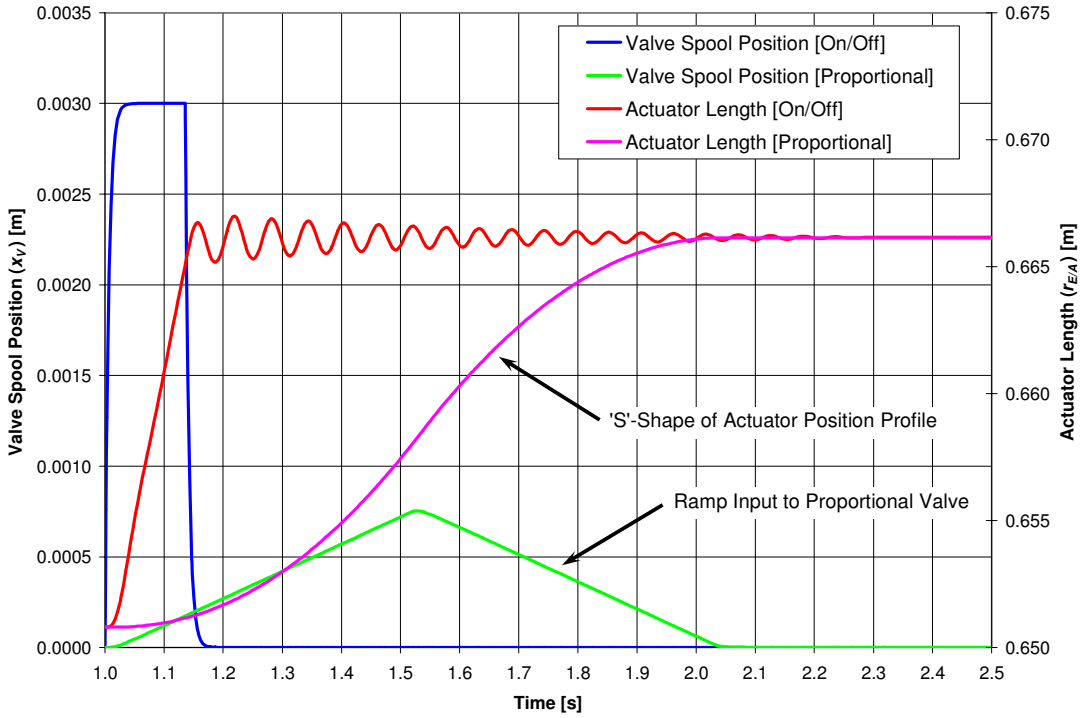

Figure 5.8: Comparison of Valve Spool and Actuator Positions between On/Off and Prop. Valves for Orientation Changes of Equal Magnitudes

Using this information, ramp functions at rates of 0.0003 m/s, 0.0015 m/s, 0.003 m/s, 0.006 m/s, and 0.015 m/s were evaluated. These rates were chosen by defining the maximum displacement of the valve in one second as the 100% (that is, 0.003 m/s) rate. The aforementioned ramp rates correspond to 10%, 50%, 100%, 200%, and 500% and were defined to encompass an acceptable range of rates and establish trends of this configuration. As the ramp profile can be segmented into a series of very small changes in spool position, the small change transfer function derived in Chapter 3 was used for all trials. Figure 5.9 shows the response of the boom system when lowering the outer tip on the right section 0.75 m using a 50% ramp function (all magnitudes of corrections follow similar profiles and therefore are not presented). An improvement in the maximum deviation of both the left and right sections from the desired distance to target was seen. Figure 5.10 shows the SPE comparison to the on/off valve

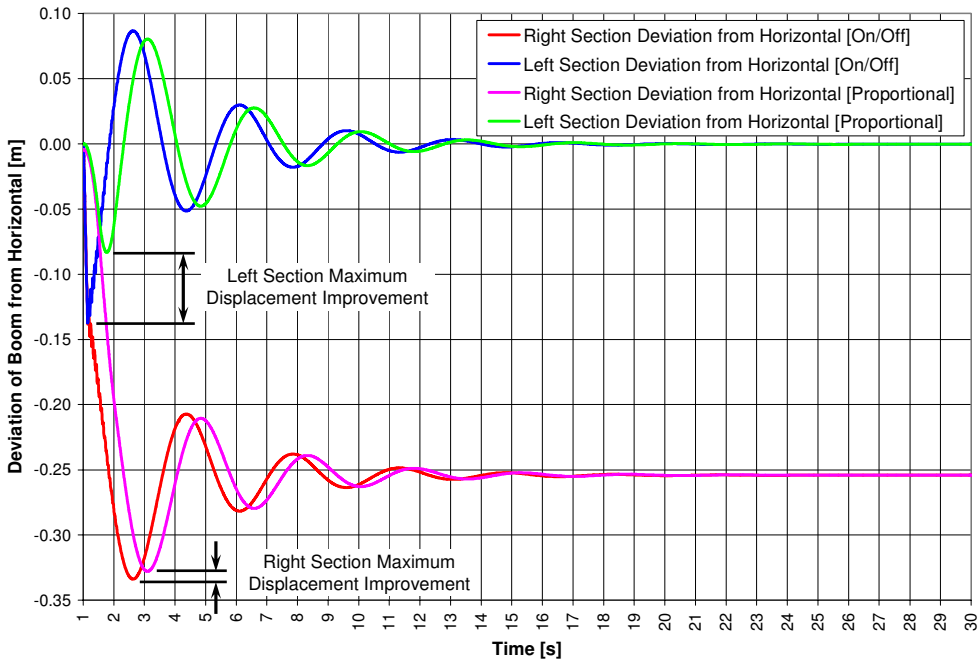

Figure 5.9: Comparison of Rt. and Lt. Section Deviations from Horizontal between On/Off and Prop. Valve Driven Orientation Changes of Equal Magnitudes

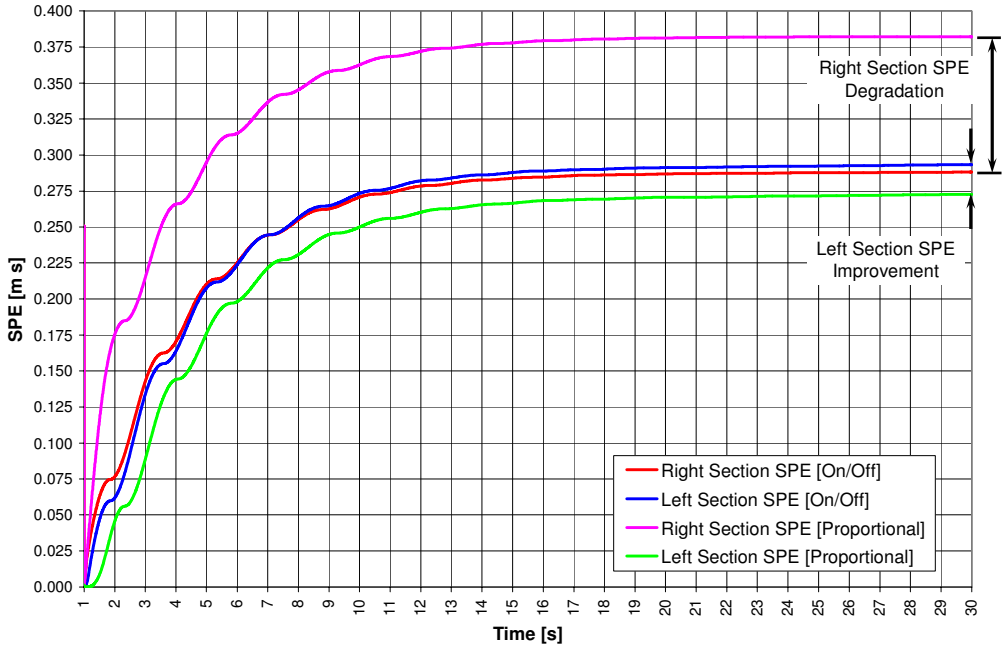

Figure 5.10: Comparison of Rt. and Lt. Section SPEs between On/Off and Prop. Valve Driven Orientation Changes of Equal Magnitudes

for the same magnitude orientation change. An improvement is noticed for the left section; however, the performance of the right section degrades. The degradation in right section SPE is due to the overall amount of increased time for the right section to lower 0.25 m; this increase outweighs the benefits of a reduction in oscillation amplitude. The amount of time to make the orientation change increases as the ramp input function does not allow the spool to reach the fully open position (maximum flow), thereby limiting the actuator velocity for changes of any of the evaluated magnitudes. The results of all trials are listed in Table 5.2 with Δ referring to the difference between the proportional valve trial and the on/off valve trial of equivalent orientation change magnitude reported in Table 5.1.

The SPE for the left section using a 500% valve input closely matches those using the on/off valve for all magnitudes of right section orientation changes. The 500% valve input was then deemed the 'cut-off' for spool position rate changes; any higher slopes would mimic the on/off valve and provide little benefit.

Table 5.2: Comparison of On/Off and Proportional Valve (Ramp Profile) Driven Boom Orientation Changes

Orientation Change of Right Section Outer Tip [m]	Proportional Valve Slope [mm/s] [% of Max Displacement]	Proportional Valve Spool Peak Displacement [mm]	Δ Max Distance to Target for Left Section [m]	Δ Max Distance to Target for Right Section [m]	Δ SPE of Left Section [m s]	Δ SPE of Right Section [m s]
Raise 0.075	0.3 [10%]	0.23	-0.027	-0.003	-0.01	+0.05
Lower 0.075	0.3 [10%]	0.18	-0.026	-0.004	-0.01	+0.03
Raise 0.25	0.3 [10%]	0.41	-0.104	-0.039	-0.13	+0.20
Lower 0.25	0.3 [10%]	0.34	-0.093	-0.027	-0.09	+0.18
Raise 0.075	1.5 [50%]	0.50	-0.015	0.000	0.00	+0.03
Lower 0.075	1.5 [50%]	0.40	-0.017	-0.002	-0.01	+0.01
Raise 0.25	1.5 [50%]	0.91	-0.061	-0.008	-0.03	+0.11
Lower 0.25	1.5 [50%]	0.75	-0.055	-0.007	-0.02	+0.09
Raise 0.075	3.0 [100%]	0.70	-0.011	0.000	0.00	+0.02
Lower 0.075	3.0 [100%]	0.56	-0.014	-0.002	-0.01	+0.01
Raise 0.25	3.0 [100%]	1.29	-0.043	-0.003	-0.01	+0.08
Lower 0.25	3.0 [100%]	1.05	-0.040	-0.004	-0.01	+0.06
Raise 0.075	6.0 [200%]	0.98	-0.008	0.000	0.00	+0.01
Lower 0.075	6.0 [200%]	0.77	-0.012	-0.002	0.00	+0.01
Raise 0.25	6.0 [200%]	1.81	-0.029	-0.001	-0.01	+0.05
Lower 0.25	6.0 [200%]	1.48	-0.028	-0.002	-0.01	+0.04
Raise 0.075	15.0 [500%]	1.50	-0.006	0.000	0.00	+0.01
Lower 0.075	15.0 [500%]	1.18	-0.010	0.001	0.00	+0.00
Raise 0.25	15.0 [500%]	2.83	-0.015	0.000	0.00	+0.03
Lower 0.25	15.0 [500%]	2.29	-0.016	-0.002	-0.01	+0.02

5.2.1 Other System Effects (Proportional Valve)

As expected, a distinct improvement was seen in the rod and non-rod end pressures when employing a ramp-driven proportional valve. This is illustrated in Figure 5.11 in which the smoothed pressure traces of the proportional valve are evident. By controlling the actuator's acceleration rate, pressure transients along with cavitation effects were eliminated.

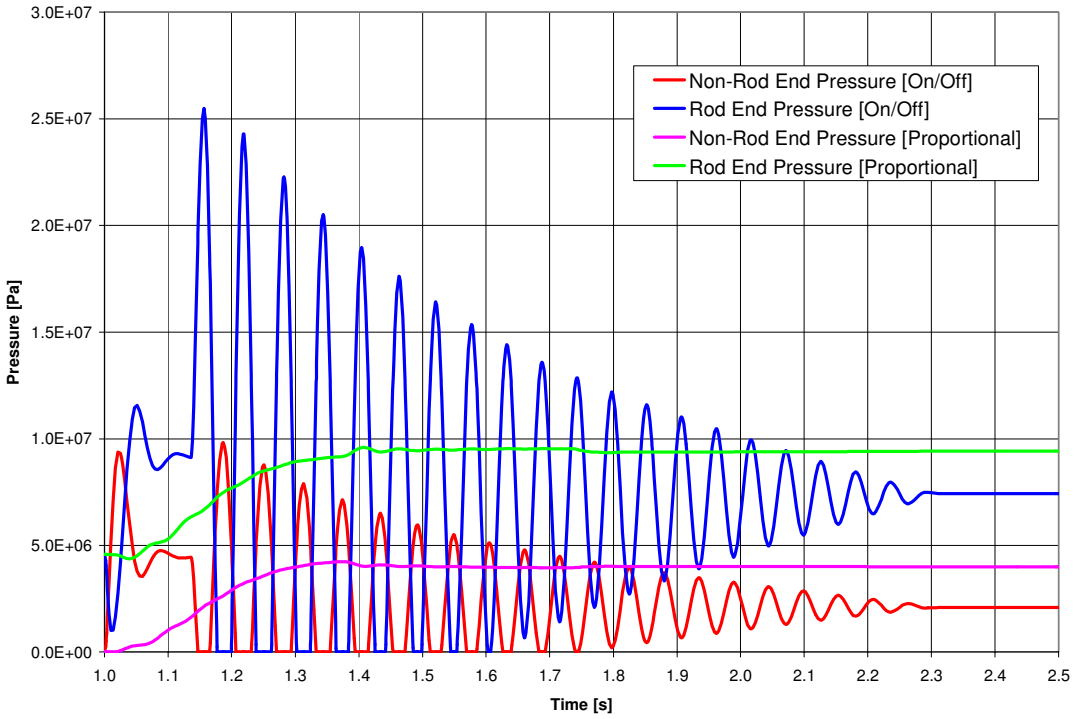

Figure 5.11: Comparison of Rod and Non-Rod End Actuator Pressures between On/Off and Prop. Valve Driven Orientation Changes of Equal Magnitudes

The results of the ramp trials showed that the performance of both sections of the boom did not benefit from the approach. Due to this, it was decided to investigate the effects of limiting the maximum overall velocity of the actuator. To accomplish this, different magnitudes of step inputs were used to drive the proportional valve and limit the displacement of the spool. Due to the nature of a step input, the large-change transfer function developed in Chapter 3 was used for all trials. Three valve positions were evaluated; 25%, 50%, and

75% of maximum spool displacement (MSD). As with the ramp trials, an improvement is seen in the SPE of the left section; however it is at a cost to the right section's SPE. The reduced maximum speed of the actuator also improves the maximum deviation of both sections, but increases the time required for the right section to reach its desired orientation (Figure 5.12). The results of all trials are shown in Table 5.3.

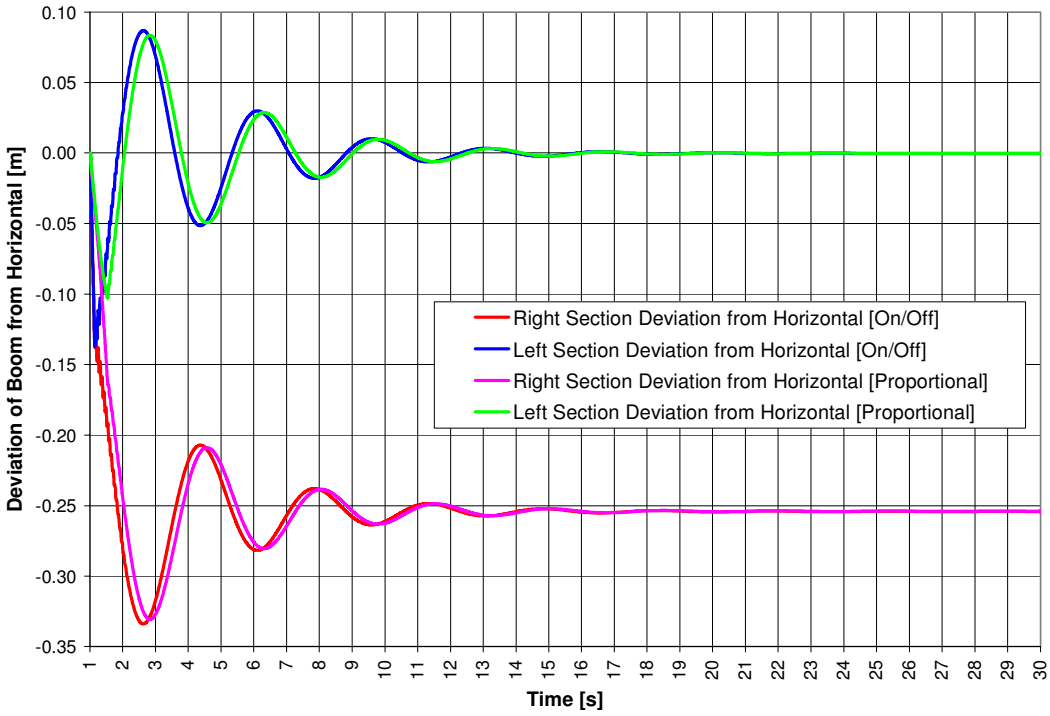

Figure 5.12: Comparison of Rt. and Lt. Sections Deviations from Horizontal between On/Off Valve and Prop. Valve Operated to 25% MSD (Rt. Section Lowered 0.25 m)

Table 5.3: Comparison of On/Off and Prop. Valve (Step Profile) Driven Boom Orientation Changes

Orientation Change of Right Section Outer Tip [m]	Proportional Valve Spool Displacement [mm] [% of MSD]	Δ Max Distance to Target for Left Section [m]	Δ Max Distance to Target for Right Section [m]	Δ SPE of Left Section [m s]	Δ SPE of Right Section [m s]
Raise 0.075	0.75 [25%]	-0.006	0.000	0.00	+0.01
Lower 0.075	0.75 [25%]	-0.007	0.000	0.00	0.00
Raise 0.25	0.75 [25%]	-0.055	-0.006	-0.02	+0.05
Lower 0.25	0.75 [25%]	-0.034	-0.004	-0.01	+0.04
Raise 0.075	1.50 [50%]	-0.002	0.000	0.00	+0.01
Lower 0.075	1.50 [50%]	-0.003	0.000	0.00	0.00
Raise 0.25	1.50 [50%]	-0.018	-0.002	0.00	+0.02
Lower 0.25	1.50 [50%]	-0.010	-0.001	0.00	+0.01
Raise 0.075	2.25 [75%]	0.000	0.000	0.00	0.00
Lower 0.075	2.25 [75%]	-0.004	0.000	0.00	0.00
Raise 0.25	2.25 [75%]	-0.005	0.000	0.00	+0.01
Lower 0.25	2.25 [75%]	-0.006	0.000	0.00	+0.01

By limiting the maximum velocity of the actuator the amplitude of the pressure spike seen by the actuator is reduced. The results for one condition are shown in Figure 5.13. As all other trials were similar in response, only one is presented. Table 5.4 lists the reduction in pressure amplitude for both the rod and non-rod ends of the actuator.

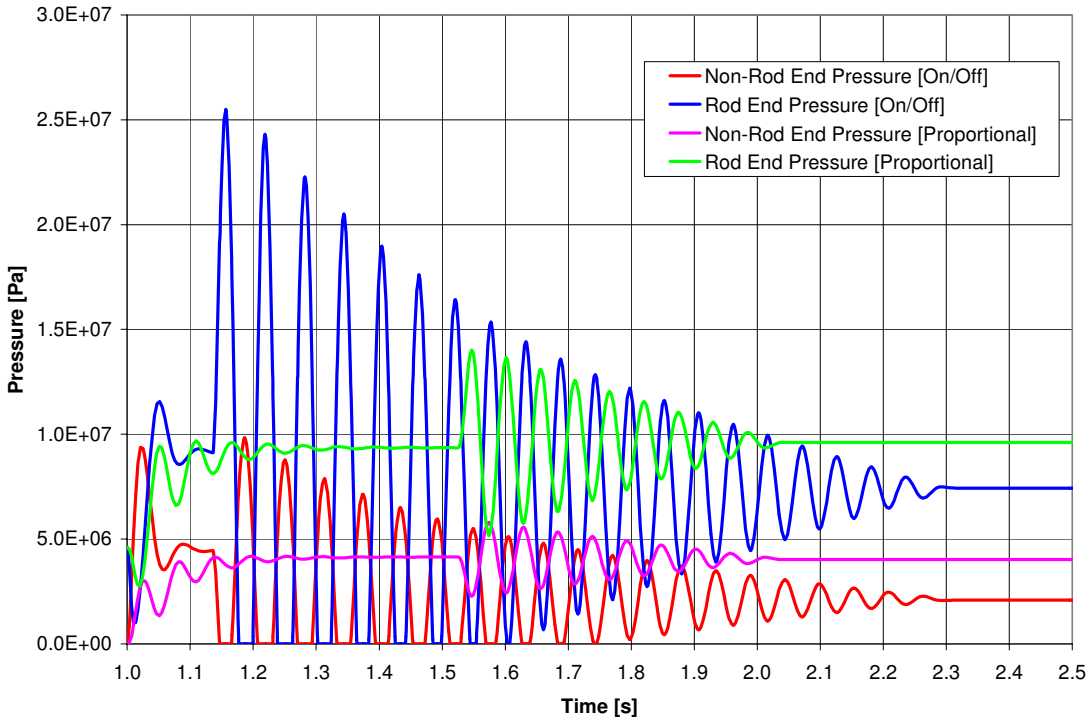

Figure 5.13: Comparison of Actuator Pressures between On/Off Valve and Prop. Valve Driven to 25% MSD (Rt. Section Lowered 0.25 m)

Table 5.4: Comparison of Actuator Pressures between On/Off and Prop. Valve (Step Profile) Driven Boom Orientation Changes

Orientation Change of Right Section Outer Tip [m]	Peak Rod End Pressure (On/Off Valve) [MPa]	Proportional Valve Spool Displacement [mm] [% of MSD]	Peak Rod End Pressure (Proportional Valve) [MPa]	Difference of Peak Pressure Between On/Off & Proportional Valves [%]
Raise 0.075	20.9	0.75 [25%]	15.0	-29
Lower 0.075	27.5	0.75 [25%]	13.4	-51
Raise 0.25	20.3	0.75 [25%]	14.9	-27
Lower 0.25	25.4	0.75 [25%]	14.0	-45
Raise 0.075		1.50 [50%]	17.6	-16
Lower 0.075		1.50 [50%]	18.4	-33
Raise 0.25		1.50 [50%]	17.3	-15
Lower 0.25		1.50 [50%]	18.6	-27
Raise 0.075		2.25 [75%]	20.3	-3
Lower 0.075		2.25 [75%]	21.1	-23
Raise 0.25		2.25 [75%]	19.6	-3
Lower 0.25		2.25 [75%]	23.1	-9

The overall SPE benefits of using a proportional valve were not as pronounced as had been anticipated prior to the simulation trials. It remained of interest to examine an alternative method of achieving a proportional valve effect using PWM techniques with an on/off valve; this is now considered.

5.3 Performance of Boom System Using Pulse Width Modulation Technology

Pulse width modulation is the rapid cycling of an on/off valve to create average flow rates which can be varied proportionally between minimum and maximum valve specified values. The rapid valve movement between the spool's on and off positions induces cyclic perturbations of the flow and pressure in the hydraulic system. However, the effects of these perturbations are minimized due to the inherent filtering effect of the boom system's low natural frequency and large associated inertias.

The step input to create 50% of the MSD analyzed in the previous section was used for comparison purposes. Drive frequencies of 50 and 200 Hz were chosen to provide insight into any improvements that may be had by increasing the drive frequency significantly (four times). Comparisons of the pulsations in flow between the PWM and proportional valves when lowering the right section 0.25 m are presented in Figures 5.14 and 5.15. The boom positional results are compared to the proportional valve trial for the same 50% spool displacement magnitude and are shown in Figures 5.16 and 5.17. The boom system acts as an adequate filter with the flow pulsations being essentially unnoticeable in the boom performance results for both drive frequencies evaluated (Figures 5.18 and 5.19). Due to the boom's filtration effect, there are no discernible differences between all of the boom performance traces which follow.

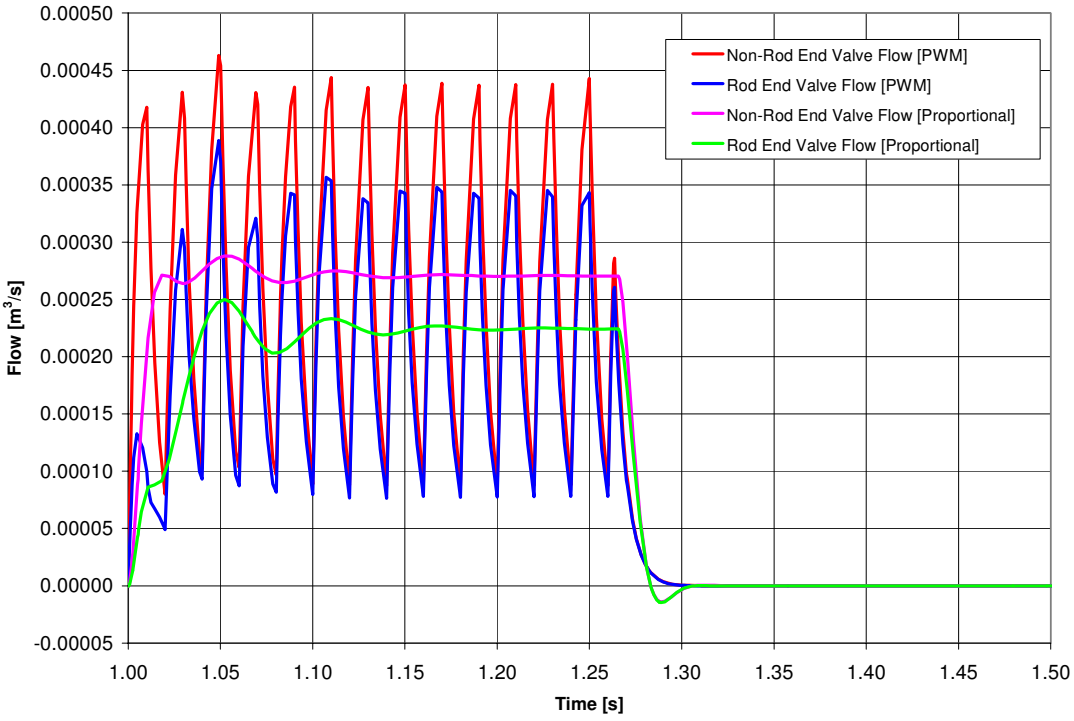

Figure 5.14: Comparison of Flow Through Prop. & PWM Valves (50 Hz) at 50% of MSD (Rt. Section Lowered 0.25 m)

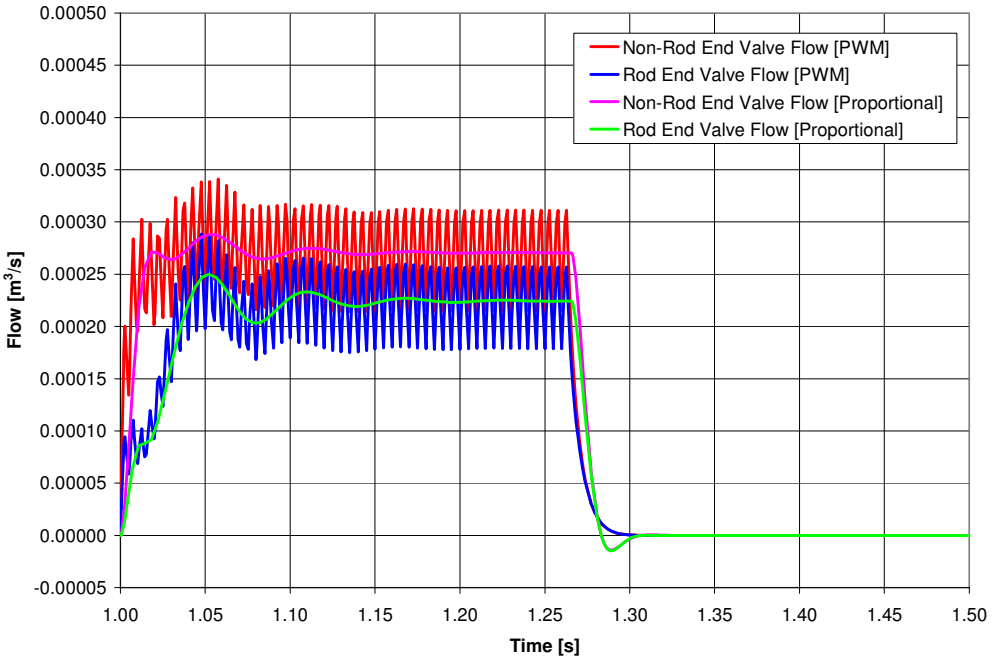

Figure 5.15: Comparison of Flow Through Prop. & PWM Valves (200 Hz) at 50% of MSD (Rt. Section Lowered 0.25 m)

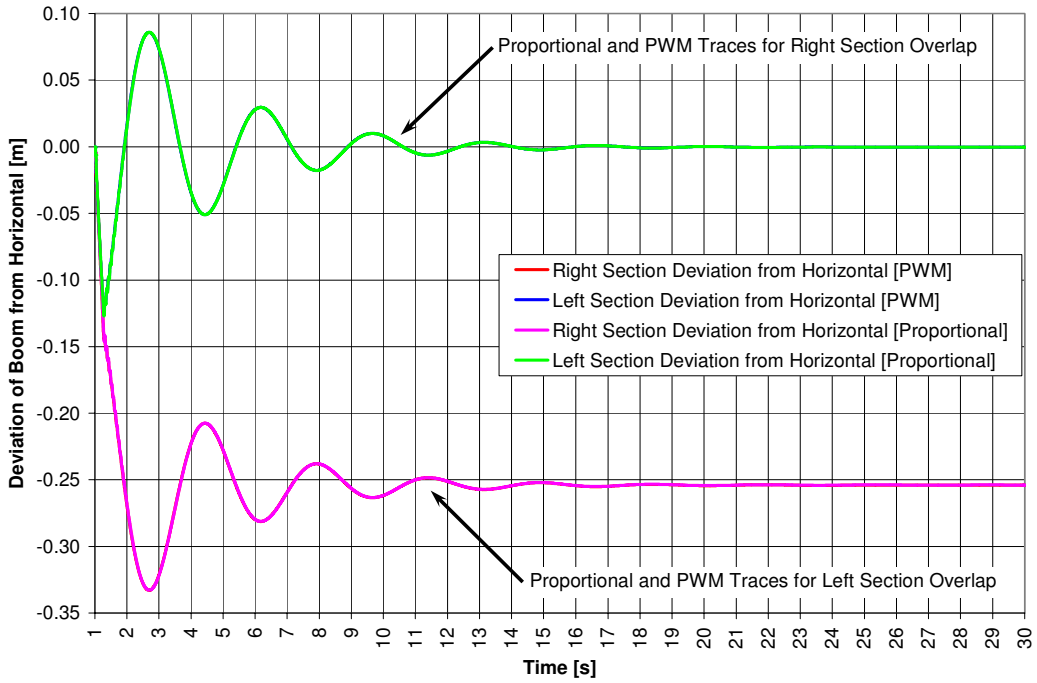

Figure 5.16: Comparison of Boom Deviation from Horizontal between Prop. & PWM Valves (50 Hz) at 50% of MSD (Rt. Section Lowered 0.25 m)

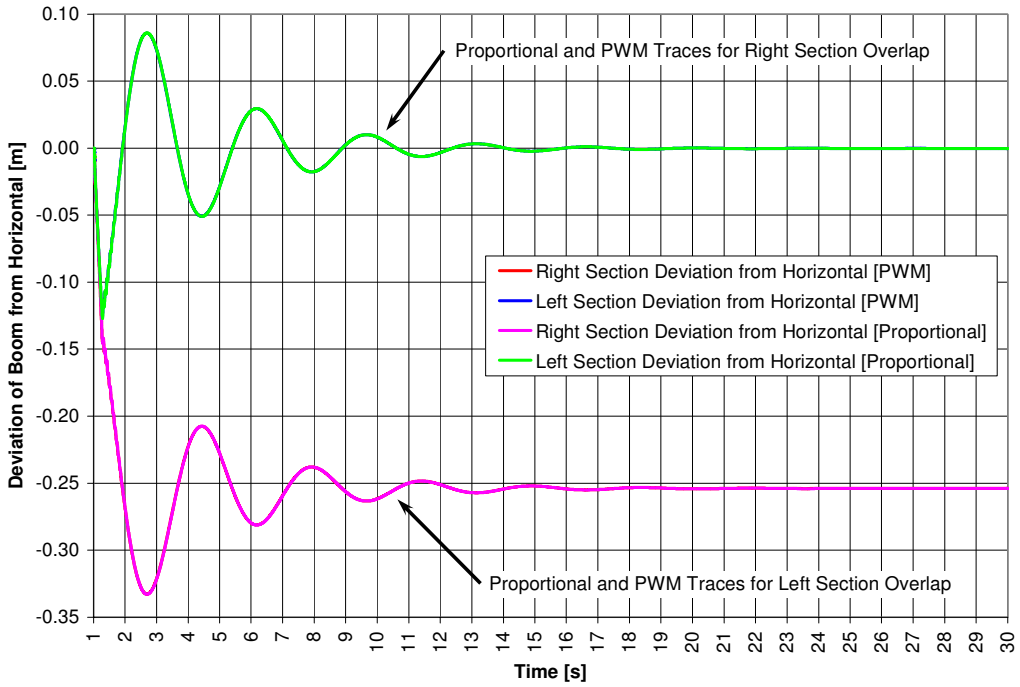

Figure 5.17: Comparison of Boom Deviation from Horizontal between Prop. & PWM Valves (200 Hz) at 50% of MSD (Rt. Section Lowered 0.25 m)

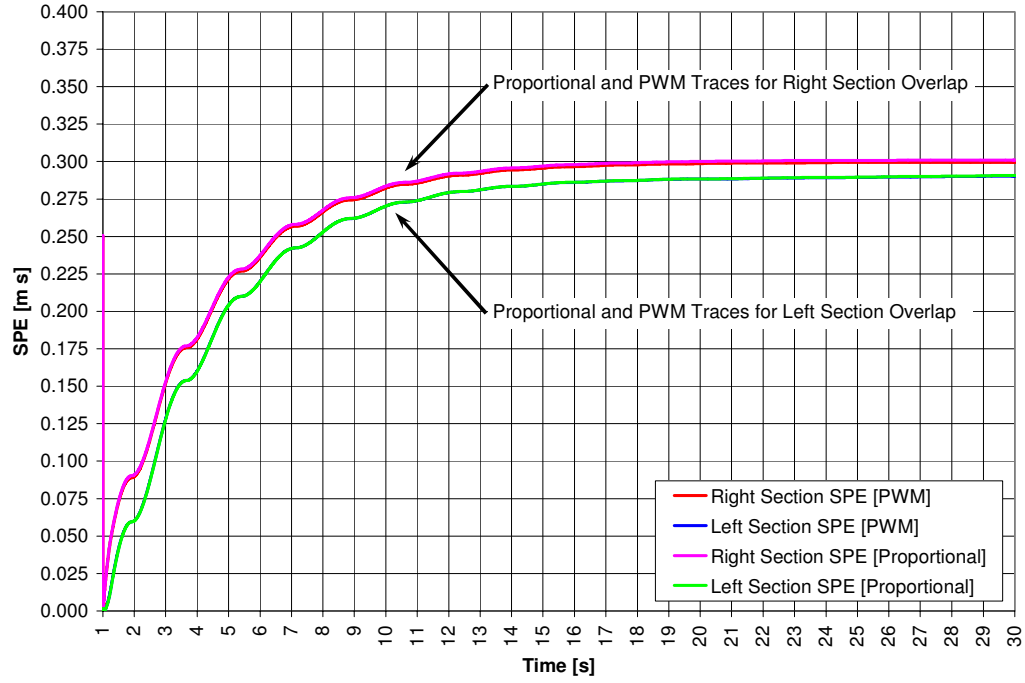

Figure 5.18: Comparison of Boom SPE between Prop. & PWM Valves (50 Hz) at 50% of MSD (Rt. Section Lowered 0.25 m)

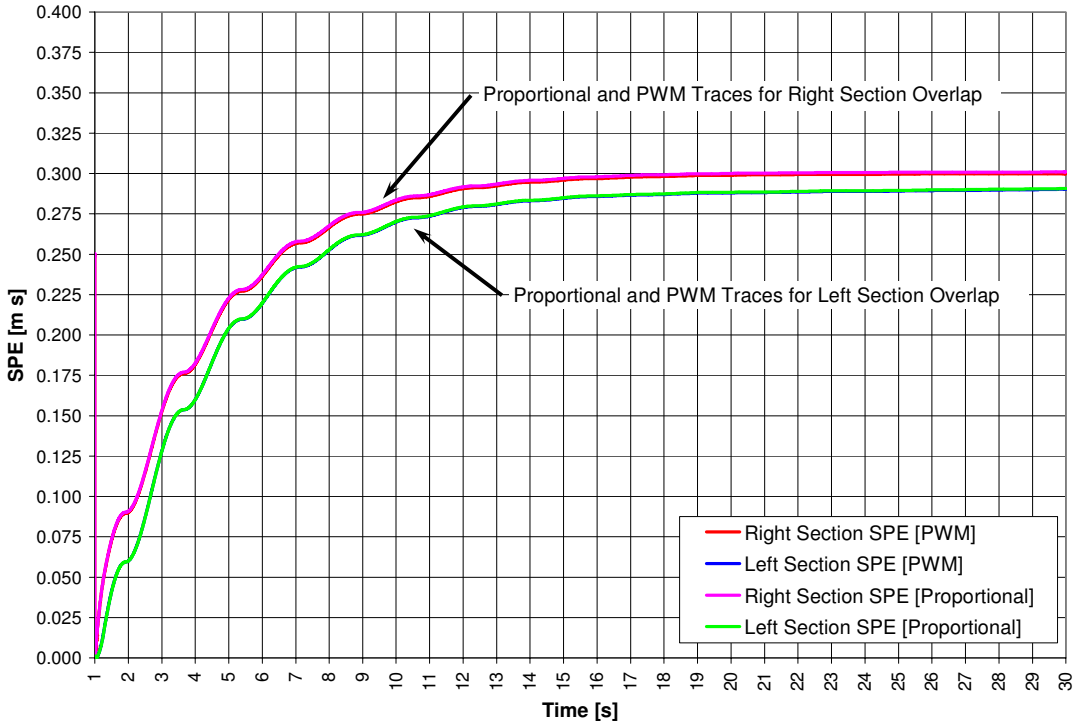

Figure 5.19: Comparison of Boom SPE between Prop. & PWM Valves (200 Hz) at 50% of MSD (Rt. Section Lowered 0.25 m)

In summary, the desired improvement in the SPE of the boom system using a proportional valve (both traditional proportional and PWM driven on/off valves) was only seen on the non-actuated boom section. This improvement on the non-actuated half of the structure was less than the degradation in performance of the actuated section regardless of valve input profile. However, PWM technology was shown to have no discernable negative effects on actuation of the boom system due to its large inertia and low natural frequency.

Chapter 6

Discussion, Conclusions and Future Considerations

In this Chapter, the problems investigated during the course of this research are reviewed and a discussion of the research results follows. The research objectives presented in Chapter 1 are then summarized. The conclusions resulting from this work and a discussion of potential future work to address remaining challenges associated with dynamic control of suspended sprayer boom orientation are also presented.

6.1 Discussion

6.1.1 Review of Problem

Suspended boom sprayers are used to apply chemical to agricultural crops. To accurately apply the desired rate across the width of the machine the distance from the spray nozzles (boom) to the target must be maintained. A review of published literature showed much work has been done to optimize passive suspension system designs thereby limiting boom motion induced through the carrying frame; other work has been undertaken to actively control the orientation of the boom structure as a whole. As the boom is typically divided into three sections, both wing sections may be oriented independently by hydraulic actuators. Generally, operators adjust the orientation of each of the boom sections separately to maintain the best overall distance from the target

across the entire boom width. Due to both wing sections being attached to the center section, motion of one section adversely affects the orientation of the opposing section through the coupling created by the passive suspension system. The effect of orientation changes to one section on the opposing section was defined as the problem requiring investigation.

6.1.2 Review of Research Objectives

To allow evaluation of the problem within a lab environment, a computer simulation model of the boom structure, passive suspension system, and tilt actuator was required. This task was defined as the first research objective. Through the use of kinetic, kinematic, trigonometric, and fluid power relations, a model of a specific sprayer was constructed within a software simulation environment (Mathworks, 2001). As only the boom structure, passive suspension system, and tilt actuator were modeled, the model and experimental data were not well correlated due to other system effects (carrying tires and frame member torsion) that could not be isolated during data acquisition. However, the model was deemed sufficient for this study as it predicted performance trends comparable to those demonstrated in the actual boom system.

The second research objective was to quantify the scale of the problem, that is, to determine the effects orientation changes to one boom section have on the opposing section. Through use of the model, the dynamic orientations of both the left and right sections were evaluated for different magnitudes and directions of orientation changes to the right section made through use of an on/off valve-driven actuator (typical system components). An accumulation error term, SPE, was defined that included both magnitude and duration of distance to target deviation. These simulation trials quantified the problem and represented a baseline to which potential improvements were compared.

The third research objective involved evaluating proportional and PWM valves as means to overcome negative effects quantified in the second research objective.

6.1.3 Summary of Results

Typical operation for a suspended boom structure involves use of on/off valve-driven actuators to adjust either the left or right section's distance to target. As the boom is attached to the carrying frame via a passive suspension system, by making an orientation change to one wing section, the operator induces a detrimental deviation from the desired orientation in the opposing wing section. This coupling effect between the actuated and non-actuated sections creates an oscillatory response across the boom width. The oscillation further propagates orientation errors for both the actuated and non-actuated sections. The SPE induced in the non-actuated section was determined to be similar in magnitude to the actuated section. That is, the contribution of the original orientation error on the actuated section's SPE is minimal, with the oscillatory response dominating both sections' SPEs. The maximum deviation induced in the non-actuated section was shown to be at least 54% of the magnitude of change desired to the actuated section.

The use of an on/off valve-driven actuator to make the required orientation changes results in large pressure spikes within the hydraulic system; these pressure spikes are due to the boom sections' large masses and the on/off valves inability to modulate flow to limit acceleration rates. Cavitation within the actuator may result unless the maximum velocity of the actuator is limited by some external means to reduce boom acceleration effects.

Proportional valves may be used in place of the typical on/off valves to eliminate pressure spikes in the tilt actuator. Proportional valves also reduce the SPE of the non-actuated section during a correction as coupling effects through the center section are limited. However, the SPE associated to the

actuated section increases more significantly regardless of the chosen valve positional profile. The increase in the actuated section's SPE is due to the extended period of time required to reorient the boom section at a reduced actuator velocity. That is, the contribution of the original orientation error on the actuated section's SPE begins to contribute significantly.

Although use of the proportional valve did not provide the desired improvements in reducing the entire boom's SPE for orientation changes of this type, a PWM valve was shown to be an effective alternative to a true proportional valve. The pulsations in flow and pressure created through use of a PWM-driven on/off valve are filtered effectively by the boom system's large inertia and low natural frequency.

6.2 Conclusions

Based on the accomplishment of the research objectives, the following conclusions are forwarded:

i. The computer models of the boom structure, hydraulic actuator, and alternative valve types developed were sufficient to provide results for the trend type study undertaken.

ii. The configuration of the boom structure results in a runaway load scenario. If the maximum velocity of the tilt actuator is not limited, cavitation within the actuator will occur due to the boom sections' large inertias.

iii. A proportional valve may be used to modulate flow and define distinct tilt actuator velocity profiles. Both step and ramp spool positional profiles were shown to reduce the accumulated SPE in the non-actuated section and prevent cavitation. However, the SPE of the actuated section increases to a greater extent; to reduce movement due to coupling in the non-actuated section, the velocity of the actuator driving the orientation change must be reduced. This velocity reduction changes the

dominance from the error due to oscillation to that of the deviation from the desired distance of the boom section from the target.

iv. PWM technology allows modulation of flow by rapidly cycling an on/off valve to create an average flow rate. This technology may be used effectively in the suspended boom system modeled as the sections' large inertias and boom structure low natural frequency act to filter the flow pulsations created. No adverse effects from these pulsations were noticeable in the orientation of the boom; the boom position using the PWM valve closely matches that of a true proportional valve through a wide range of drive frequencies.

6.3 Future Considerations

Many alternative passive suspension systems along with rigid boom structures exist in the marketplace. These alternative designs warrant evaluation to quantify current performance versus that which may be had with proportional or PWM valves; similar to the assessment performed for the specific suspension and boom design in this thesis.

The model may be further developed to include other system effects, such as those introduced by the carrying frame tires, connecting member torsion, and boom frame member flexure; improvements to the hydraulic system portion may also be investigated with the addition of actuator leakage. The addition of the left section actuator would also be beneficial. This extended model would then provide a more accurate picture of the level of the problem and potential improvements that may be had.

If an extended model was developed, a second avenue for exploration would involve simultaneous control of the opposing tilt actuator during a correction to one section. Two avenues may be explored:

i. active control of the orientation of the opposing section to only compensate for the error being induced by the actuated section, and

ii. active control of both sections tilt actuators to reduce the overall SPE across the entire width of the boom.

The scenarios investigated during this research may be classified as open-loop control, as the desired output of the system (boom sections' orientations) were not 'fed back' to drive the input to the system (valve spool position). A logical next step would be to investigate possible improvements via feedback. The potential for improving boom-system performance by feeding back the orientation of both sections to a valve control algorithm exists.

Experimental work to fully quantify the problem under field conditions would also add greatly to the academic knowledge base.

Overall, further work is necessary to improve the performance of agricultural sprayer booms under the dynamic conditions identified in this thesis.

References

Anthonis, J., J. Audenaert, and H. Ramon. 2005. "Design Optimisation for the Vertical Suspension of a Crop Sprayer Boom." *Biosystems Engineering*, V90 (2): pg. 153-160.

Bosch Rexroth AG. 2002. *4/3-, 4/2- and 3/2-Way Directional Valves with Wet Pin DC Solenoids; Type WE6 ../.S.* St. Neots, Cambs, U.K.: Bosch Rexroth Ltd., 6 pp.

Chinniah, Y. 2004. "Fault Detection in the Electrohydraulic Actuator using Extended Kalman Filter." M. Sc. Thesis, University of Saskatchewan. Saskatoon, Saskatchewan, Canada: Unpublished, 251 pp.

CNH Canada Ltd. 2003. 67*.A, 67XL.A, and 67XLT.A Field Sprayer Parts Catalog*. Saskatoon, Saskatchewan, Canada: CNH Canada Ltd., 572 pp.

Deprez, K., J. Anthonis, and H. Ramon. 2003. "System for Vertical Boom Corrections on Hilly Fields." *Journal of Sound and Vibration*, V266: pg. 613-624.

Herbst, A., and P. Wolf. 2001. "Spray Deposit Distribution from Agricultural Boom Sprayers in Dynamic Conditions." ASAE Paper No. 01-1054. St. Joseph, Michigan, U.S.A.: ASAE, 12 pp.

Hibbeler, R. C. 1992. Engineering Mechanics: Statics and Dynamics. 6th edition. Toronto, Ontario, Canada: Maxwell Macmillan Canada, 588 pp.

Hindman, J. J.. 2002. "Condition Monitoring of Valves and Actuators in a Mobile Hydraulic System using an Artificial Neural Network and Expert Data." M. Sc. Thesis, University of Saskatchewan. Saskatoon, Saskatchewan, Canada: Unpublished, 132 pp.

Jeon, H. Y., A. R. Womac, and J. Gunn. 2004. "Sprayer Boom Dynamic Effects on Application Uniformity." *Transactions of the American Society of Agricultural Engineers*, V47: pg. 647-659.

Langenakens, J. J., L. Clijmans, H. Ramon, and J. De Baerdemaeker. 1999. "The Effects of Vertical Sprayer Boom Movements on the Uniformity of Spray Distribution." *Journal of Agricultural Engineering Research*, V74: pg. 281-291.

MathWorks, Inc. 2001. *MatLAB® Version 6.1.0.450 Release 12.1.* Computer software. Natick, Massachusetts, U.S.A.: MathWorks, Inc.

Merritt, H. E. 1967. Hydraulic Control Systems. New York, New York, U.S.A.: John Wiley and Sons, 358 pp.

Microsoft Corporation. 2001. *Microsoft Excel 2002 Version 10.4302.6735*. Computer software. Redmond, Washington, U.S.A.: Microsoft Corporation.

Monroe Automotive Equipment Company. 2001. *Shock Absorber 0E10081.* Chicago, Illinois, U.S.A.: Monroe Automotive Equipment Company, 1 pp.

Olsson, H., K. J. Astrom, C. C. De Wit, M. Gafvert, and P. Lischinsky. 1998. "Friction Models and Friction Compensation." *European Journal of Control*, V4 (3): pg. 176-195.

Parametric Technology Corporation, 2001. *Pro/ENGINEER® Release 2001*. Computer Software. Needham, Massachusetts, U.S.A.: Parametric Technology Corporation.

Phillips, C. L., and R. D. Harbor. 1996. Feedback Control Systems. 3rd edition. Englewood Cliffs, New Jersey, U.S.A.: Prentice Hall, 683 pp.

Ramon, H., B. Missotten, and J. De Baerdemaeker. 1997. "Spray Boom Motions and Spray Distribution: Part 2, Experimental Validation of the Mathematical Relation and Simulation Results." *Journal of Agricultural Engineering Research*, V66: pg. 31-39.

Rexroth Hydraulics Division. 1998. *4/2-, 4/3-Way Proportional Directional Control Valve; Direct Operated, Model 4 WRA(E)B (Series 1X).* Bethlehem, Pennsylvania, U.S.A.: Mannesmann Rexroth Corporation, 6 pp.

Statistics Canada. 2002. "2001 Census of Agriculture." http:// www.statcan.ca/english/agcensus2001/. Accessed March 24, 2005. Ottawa, Ontario, Canada: Government of Canada.

Stewart, J. 1999. Single Variable Calculus. 4th edition. Scarborough, Ontario, Canada: Brooks/Cole Publishing Company, 781 pp.

Wolfram Research. 2000. *Mathematica® Version 4.1.0.0.* Computer software. Champaign, Illinois, U.S.A.: Wolfram Research.

Appendix A

Differential Equations Required for Simulation Model

As the differentiation process may result in discontinuities, it is beneficial when using a computer simulation model to implement the highest-order differential equation for each required variable. Integration may then be used to calculate dependent quantities (i.e. implement the equation for acceleration and integrate once to calculate velocity and again to calculate position). For this reason the trigonometric equations developed for the angle of orientation of the right section due to length changes of the actuator (θ_W) needed to be differentiated to provide its angular acceleration (α_W). Equation 2.73 may be written as follows:

$$2 * r_{E/B} * r_{E/A} * \sin(Z - \theta_{E/A} + \theta_W) = {r_{E/B}}^2 - {r_{B/A}}^2 + {r_{E/A}}^2, \qquad [A.1]$$

where:

Z is a constant representing $\tau_{B/A} - \pi/2 + \phi_{B/A} - \phi_{E/B} + \phi_{E/A}$ (rad).

Employing the product and chain rules to differentiate equation A.1 with respect to time yields:

$$\begin{pmatrix} 2 * r_{E/B} * \frac{dr_{E/A}}{dt} * \sin(Z - \theta_{E/A} + \theta_W) + \\ 2 * r_{E/B} * r_{E/A} * \cos(Z - \theta_{E/A} + \theta_W) * \left(- \frac{d\theta_{E/A}}{dt} + \frac{d\theta_W}{dt} \right) \end{pmatrix} = 2 * r_{E/A} * \frac{dr_{E/A}}{dt}. \qquad [A.2]$$

Differentiating equation A.2 with respect to time gives:

$$\begin{pmatrix} 2*r_{E/B}*\dfrac{d^2 r_{E/A}}{dt^2}*\sin(Z-\theta_{E/A}+\theta_W)+ \\ \left(4*r_{E/B}*\dfrac{dr_{E/A}}{dt}*\cos(Z-\theta_{E/A}+\theta_W)*\right. \\ \left.\left(-\dfrac{d\theta_{E/A}}{dt}+\dfrac{d\theta_W}{dt}\right)\right)- \\ \left(2*r_{E/B}*r_{E/A}*\sin(Z-\theta_{E/A}+\theta_W)*\right. \\ \left.\left(-\dfrac{d\theta_{E/A}}{dt}+\dfrac{d\theta_W}{dt}\right)^2\right)+ \\ \left(2*r_{E/B}*r_{E/A}*\cos(Z-\theta_{E/A}+\theta_W)*\right. \\ \left.\left(-\dfrac{d^2\theta_{E/A}}{dt^2}+\dfrac{d^2\theta_W}{dt^2}\right)\right) \end{pmatrix} = \begin{pmatrix} 2*\left(\dfrac{dr_{E/A}}{dt}\right)^2+ \\ 2*r_{E/A}*\dfrac{d^2 r_{E/A}}{dt^2} \end{pmatrix}. \quad [A.3]$$

Solving for $\frac{d^2\theta_W}{dt^2}$, or α_W, yields:

$$\alpha_W = \frac{\begin{pmatrix} 2*\left(\dfrac{dr_{E/A}}{dt}\right)^2+2*r_{E/A}*\dfrac{d^2 r_{E/A}}{dt^2}- \\ 2*r_{E/B}*\dfrac{d^2 r_{E/A}}{dt^2}*\sin(Z-\theta_{E/A}+\theta_W)- \\ 4*r_{E/B}*\dfrac{dr_{E/A}}{dt}*\cos(Z-\theta_{E/A}+\theta_W)*\left(-\dfrac{d\theta_{E/A}}{dt}+\dfrac{d\theta_W}{dt}\right)+ \\ 2*r_{E/B}*r_{E/A}*\sin(Z-\theta_{E/A}+\theta_W)*\left(-\dfrac{d\theta_{E/A}}{dt}+\dfrac{d\theta_W}{dt}\right)^2 \end{pmatrix}}{2*r_{E/B}*r_{E/A}*\cos(Z-\theta_{E/A}+\theta_W)}+\frac{d^2\theta_{E/A}}{dt^2}. \quad [A.4]$$

Through the differentiation process above the second derivative of the angular orientation of the actuator due to changes in its length is required. Equation 2.72 may be written as:

$$2*r_{B/A}*r_{E/A}*\sin(\phi_{B/A}+\phi_{E/A}-\theta_{E/A})=r_{B/A}{}^2-r_{E/B}{}^2+r_{E/A}{}^2. \quad [A.5]$$

Again, by employing the product and chain rules to differentiate equation A.5 with respect to time:

$$\begin{pmatrix} 2*r_{B/A}*\dfrac{dr_{E/A}}{dt}*\cos(\phi_{B/A}+\phi_{E/A}-\theta_{E/A})+ \\ 2*r_{B/A}*r_{E/A}*\sin(\phi_{B/A}+\phi_{E/A}-\theta_{E/A})*\dfrac{d\theta_{E/A}}{dt} \end{pmatrix} = 2\cdot r_{E/A}*\frac{dr_{E/A}}{dt}. \quad [A.6]$$

Differentiating equation A.6 with respect to time gives:

$$\begin{pmatrix} 2*r_{B/A}*\dfrac{d^2r_{E/A}}{dt^2}*\cos(\phi_{B/A}+\phi_{E/A}-\theta_{E/A})+ \\ 4*r_{B/A}*\dfrac{dr_{E/A}}{dt}*\sin(\phi_{B/A}+\phi_{E/A}-\theta_{E/A})*\dfrac{d\theta_{E/A}}{dt}- \\ 2*r_{B/A}*r_{E/A}*\cos(\phi_{B/A}+\phi_{E/A}-\theta_{E/A})*\left(\dfrac{d\theta_{E/A}}{dt}\right)^2+ \\ 2*r_{B/A}*r_{E/A}*\sin(\phi_{B/A}+\phi_{E/A}-\theta_{E/A})*\dfrac{d^2\theta_{E/A}}{dt^2} \end{pmatrix} = \begin{pmatrix} 2*\left(\dfrac{dr_{E/A}}{dt}\right)^2+ \\ 2*r_{E/A}*\dfrac{d^2r_{E/A}}{dt^2} \end{pmatrix}. \quad [A.7]$$

Solving for $\frac{d^2\theta_{E/A}}{dt^2}$ gives:

$$\frac{d^2\theta_{E/A}}{dt^2} = \frac{\begin{pmatrix} 2*\left(\dfrac{dr_{E/A}}{dt}\right)^2+2*r_{E/A}*\dfrac{d^2r_{E/A}}{dt^2}- \\ 2*r_{B/A}*\dfrac{d^2r_{E/A}}{dt^2}*\cos(\phi_{B/A}+\phi_{E/A}-\theta_{E/A})- \\ 4*r_{B/A}*\dfrac{dr_{E/A}}{dt}*\sin(\phi_{B/A}+\phi_{E/A}-\theta_{E/A})*\dfrac{d\theta_{E/A}}{dt}+ \\ 2*r_{B/A}*r_{E/A}*\cos(\phi_{B/A}+\phi_{E/A}-\theta_{E/A})*\left(\dfrac{d\theta_{E/A}}{dt}\right)^2 \end{pmatrix}}{2*r_{B/A}*r_{E/A}*\sin(\phi_{B/A}+\phi_{E/A}-\theta_{E/A})}. \quad [A.8]$$

Appendix B

Constant Values Required for Simulation Model

Many constants were required within the equations developed in Chapters 2 and 3. The values of the constants defined in those chapters are listed in Table B1.

Table B1: Constant Values used in Simulation Model

Symbol	Definition	Value	Units
m_R	Mass of right boom section.	324.1	kg
W_R	Weight of right boom section.	3179.3	N
$\phi_{E/A}$	Initial angle between the y-axis and a vector between points A and E.	0.782	rad
I_R	Right boom section mass moment of inertia about the z-axis.	3.66E3	$kg \cdot m^2$
$r_{B/R}$	Magnitude of vector between points R and B.	4.631	m
$\phi_{B/R}$	Initial angle between the y-axis and a vector between points R and B.	0.820	rad
m_Q	Mass of combined center and left boom sections.	587.8	kg
W_Q	Weight of combined center and left boom sections.	5766.5	N

Symbol	Definition	Value	Units
I_Q	Combined center and left boom sections mass moment of inertia about the z-axis.	8.43E3	$kg \cdot m^2$
$r_{Q/A}$	Magnitude of vector between points A and Q.	3.670	m
$\phi_{Q/A}$	Initial angle between the y-axis and a vector between points A and Q.	0.621	rad
$r_{Q/B}$	Magnitude of vector between points B and Q.	4.138	m
$\phi_{Q/B}$	Initial angle between the y-axis and a vector between points B and Q.	0.827	rad
$r_{Q/C}$	Magnitude of vector between points C and Q.	2.998	m
$\phi_{Q/C}$	Initial angle between the y-axis and a vector between points C and Q.	0.695	rad
$r_{Q/M1}$	Magnitude of vector between points M1 and Q.	3.444	m
$\phi_{Q/M1}$	Initial angle between the y-axis and a vector between points M1 and Q.	0.779	rad
$r_{Q/M2}$	Magnitude of vector between points M2 and Q.	3.548	m
$\phi_{Q/M2}$	Initial angle between the y-axis and a vector between points M2 and Q.	0.797	rad
$r_{Q/M3}$	Magnitude of vector between points M3 and Q.	2.527	m
$\phi_{Q/M3}$	Initial angle between the y-axis and a vector between points M3 and Q.	0.777	rad
$r_{Q/M4}$	Magnitude of vector between points M4 and Q.	2.423	m
$\phi_{Q/M4}$	Initial angle between the y-axis and a vector between points M4 and Q.	0.796	rad

Symbol	Definition	Value	Units
$r_{B/C}$	Magnitude of vector between points C and B.	1.232	m
$\tau_{B/C}$	Initial angle between the y-axis and a vector between points C and B.	0.416	rad
k	Spring constant for all struts.	52617	N/m
ℓ_o	Spring free length for all struts.	0.314	m
β_S	Damping ratio for all struts.	10000	kg/s
$r_{C/N1}$	Magnitude of vector between points N1 and C.	0.599	m
$\phi_{C/N1}$	Initial angle between the y-axis and a vector between points N1 and C.	0.860	rad
$r_{C/N2}$	Magnitude of vector between points N2 and C.	0.701	m
$\phi_{C/N2}$	Initial angle between the y-axis and a vector between points N2 and C.	0.780	rad
$r_{C/N3}$	Magnitude of vector between points N3 and C.	0.599	m
$\phi_{C/N3}$	Initial angle between the y-axis and a vector between points N3 and C.	0.860	rad
$r_{C/N4}$	Magnitude of vector between points N4 and C.	0.701	m
$\phi_{C/N4}$	Initial angle between the y-axis and a vector between points N4 and C.	0.780	rad
$\lambda_{M1/C}$	Initial angle between the y-axis and a vector between points C and M1.	0.287	rad
$\lambda_{M2/C}$	Initial angle between the y-axis and a vector between points C and M2.	0.298	rad
$\lambda_{M3/C}$	Initial angle between the y-axis and a vector between points C and M3.	0.287	rad

Symbol	Definition	Value	Units
$\lambda_{M4/C}$	Initial angle between the y-axis and a vector between points C and M4.	0.298	rad
$r_{B/A}$	Magnitude of vector between points A and B.	0.930	m
$r_{E/B}$	Magnitude of vector between points B and E.	0.785	m
$\phi_{B/A}$	Initial angle between the y-axis and a vector between points A and B.	0.199	rad
$\tau_{B/A}$	Initial angle between the x-axis and a vector between points A and B.	1.371	rad
$\phi_{B/C}$	Initial angle between horizontal and a vector between points C and B.	0.369	rad
$\phi_{E/B}$	Initial angle between the x-axis and a vector between points B and E.	0.611	rad
m_C	Mass of right boom section tilt actuator.	5	kg
A_1	Area of the tilt actuator piston.	0.0046	m^2
A_2	Area of the tilt actuator piston less the area of the rod.	0.0038	m^2
w	Area gradient of the valves.	0.0017	m^2/m
P_S	Hydraulic system supply pressure.	17.2E6	Pa
P_T	Hydraulic system return pressure.	0.3E6	Pa
β_E	Hydraulic fluid effective bulk modulus.	1.26E9	Pa
ρ	Hydraulic fluid density.	830.1	kg/m^3
C_d	Valve discharge coefficient.	0.60	
ω_{NL}	Natural frequency of proportional valve transfer function for large positional changes (50%±40%).	188	rad/s

Symbol	Definition	Value	Units
ζ_{NL}	Damping ratio of proportional valve transfer function for large positional changes (50%±40%).	0.7	
ω_1	First cut-off frequency of proportional valve transfer function for small positional changes (50%±10%).	63	rad/s
ω_2	Second cut-off frequency of proportional valve transfer function for small positional changes (50%±10%).	113	rad/s
ω_{NS}	Natural frequency of proportional valve transfer function for small positional changes (50%±10%).	220	rad/s
ζ_{NS}	Damping ratio of proportional valve transfer function for small positional changes (50%±10%).	0.7	

Appendix C

Simulation Model

The dynamic simulation model was created using the software package MatLAB Simulink ®. The model in its entirety is presented in this Appendix.

The software follows a 'tree' structure with systems and sub-systems. The format of the explanation uses the following numbering system to identify each block:

1.4.2 – meaning system 1, sub-system 4, sub-sub-system 2.

Numerical operators employing standard mathematical symbols were used to form the equations. When an equation became too long making it impractical to enter 'piece by piece', a function block was employed which allowed direct entry of the equation. Any variables that were dynamically changing within the simulation were routed into the function block via an operator which assigned variable names used within. These variable names were assigned using the format u[3] (meaning the third variable) and are identified as such within each figure in this Appendix.

Due to limitations within the software for identifying different constants and variables, much of the nomenclature was represented in an alternative way. A cross-reference table is provided for clarity (Table C1).

Table C1: Variable Name to MatLAB ® Representation Cross-Reference

Symbol	Definition	MatLAB
m_R	Mass of right boom section.	mR
W_R	Weight of right boom section.	WR
$\phi_{E/A}$	Initial angle between the y-axis and a vector between points A and E.	phiEA
I_R	Right boom section mass moment of inertia about the z-axis.	IR
$r_{B/R}$	Magnitude of vector between points R and B.	dW
$\phi_{B/R}$	Initial angle between the y-axis and a vector between points R and B.	phiW
m_Q	Mass of combined center and left boom sections.	mQ
W_Q	Weight of combined center and left boom sections.	WQ
I_Q	Combined center and left boom sections mass moment of inertia about the z-axis.	IQ
$r_{Q/A}$	Magnitude of vector between points A and Q.	dA
$\phi_{Q/A}$	Initial angle between the y-axis and a vector between points A and Q.	phiA
$r_{Q/B}$	Magnitude of vector between points B and Q.	dB
$\phi_{Q/B}$	Initial angle between the y-axis and a vector between points B and Q.	phiB
$r_{Q/C}$	Magnitude of vector between points C and Q.	dC
$\phi_{Q/C}$	Initial angle between the y-axis and a vector between points C and Q.	phiC

Symbol	Definition	MatLAB
$r_{Q/M1}$	Magnitude of vector between points M1 and Q.	rM1Q
$\phi_{Q/M1}$	Initial angle between the y-axis and a vector between points M1 and Q.	phiM1
$r_{Q/M2}$	Magnitude of vector between points M2 and Q.	rM2Q
$\phi_{Q/M2}$	Initial angle between the y-axis and a vector between points M2 and Q.	phiM2
$r_{Q/M3}$	Magnitude of vector between points M3 and Q.	rM3Q
$\phi_{Q/M3}$	Initial angle between the y-axis and a vector between points M3 and Q.	phiM3
$r_{Q/M4}$	Magnitude of vector between points M4 and Q.	rM4Q
$\phi_{Q/M4}$	Initial angle between the y-axis and a vector between points M4 and Q.	phiM4
$r_{B/C}$	Magnitude of vector between points C and B.	rBC
$\phi_{B/C}$	Initial angle between horizontal and a vector between points C and B.	phiBC
$\tau_{B/C}$	Initial angle between the y-axis and a vector between points C and B.	tauC
k	Spring constant for all struts.	k
ℓ_o	Spring free length for all struts.	lo
β_S	Damping ratio for all struts.	betaS
$r_{C/N1}$	Magnitude of vector between points N1 and C.	rCN1
$\phi_{C/N1}$	Initial angle between the y-axis and a vector between points N1 and C.	phiN1

Symbol	Definition	MatLAB
$r_{C/N2}$	Magnitude of vector between points N2 and C.	rCN2
$\phi_{C/N2}$	Initial angle between the y-axis and a vector between points N2 and C.	phiN2
$r_{C/N3}$	Magnitude of vector between points N3 and C.	rCN3
$\phi_{C/N3}$	Initial angle between the y-axis and a vector between points N3 and C.	phiN3
$r_{C/N4}$	Magnitude of vector between points N4 and C.	rCN4
$\phi_{C/N4}$	Initial angle between the y-axis and a vector between points N4 and C.	phiN4
$\lambda_{M1/C}$	Initial angle between the y-axis and a vector between points C and M1.	lamdaM1
$\lambda_{M2/C}$	Initial angle between the y-axis and a vector between points C and M2.	lamdaM2
$\lambda_{M3/C}$	Initial angle between the y-axis and a vector between points C and M3.	lamdaM3
$\lambda_{M4/C}$	Initial angle between the y-axis and a vector between points C and M4.	lamdaM4
$r_{B/A}$	Magnitude of vector between points A and B.	rBA
$r_{E/B}$	Magnitude of vector between points B and E.	rEB
$\phi_{B/A}$	Initial angle between the y-axis and a vector between points A and B.	phiAB

Symbol	Definition	MatLAB
$\tau_{B/A}$	Initial angle between the x-axis and a vector between points A and B.	tauAB
$\phi_{E/B}$	Initial angle between the x-axis and a vector between points B and E.	phiBE
m_C	Mass of right boom section tilt actuator.	mC
A_1	Area of the tilt actuator piston.	A1
A_2	Area of the tilt actuator piston less the area of the rod.	A2
w	Area gradient of the valves.	w
P_S	Hydraulic system supply pressure.	Ps
P_T	Hydraulic system return pressure.	Pt
β_E	Hydraulic fluid effective bulk modulus.	Be
ρ	Hydraulic fluid density.	row
C_d	Valve discharge coefficient.	Cd
ω_{NL}	Natural frequency of proportional valve transfer function for large positional changes (50%±40%).	wL
ζ_{NL}	Damping ratio of proportional valve transfer function for large positional changes (50%±40%).	zL
ω_1	First cut-off frequency of proportional valve transfer function for small positional changes (50%±10%).	k1
ω_2	Second cut-off frequency of proportional valve transfer function for small positional changes (50%±10%).	k2

Symbol	Definition	MatLAB
ω_{NS}	Natural frequency of proportional valve transfer function for small positional changes (50%±10%).	wS
ζ_{NS}	Damping ratio of proportional valve transfer function for small positional changes (50%±10%).	zS
RS_F	An additive series of terms that all involved $F_{E/A}$ (right side of equation).	RSF
LS_F	An additive series of terms that all involved $F_{E/A}$ (left side of equation).	LSF
RS_x	An additive series of terms that all involved $\ddot{x}_C$ (right side of equation).	RSx
LS_x	An additive series of terms that all involved $\ddot{x}_C$ (left side of equation).	LSx
RS	An additive series of terms that did not involve either $F_{E/A}$ or $\ddot{x}_C$ (right side of equation).	RS
LS	An additive series of terms that did not involve either $F_{E/A}$ or $\ddot{x}_C$ (left side of equation).	LS
LS_α	An additive series of terms that all involved α_Q (left side of equation).	LSalpha
RS_Q	An additive series of terms that did not involve α_Q (right side of equation).	RSQ
LS_Q	An additive series of terms that did not involve α_Q (left side of equation).	LSQ
x_C	Actuator length.	rAE

Symbol	Definition	MatLAB
$\dot{x}_C$	Actuator velocity.	rAEp
$\ddot{x}_C$	Actuator acceleration.	rAEpp
numL(s)	Numerator of the large signal change transfer function (proportional valve).	numL
denL(s)	Denominator of the large signal change transfer function (proportional valve).	denL
numS(s)	Numerator of the small signal change transfer function (proportional valve).	numS
denS(s)	Denominator of the small signal change transfer function (proportional valve).	denS

Referencing Figure C1 it is shown the model was developed in four main blocks:

1. the actuator sub-system,
2. the boom sub-system,
3. the SPE sub-system, and
4. the valve transfer function sub-system.

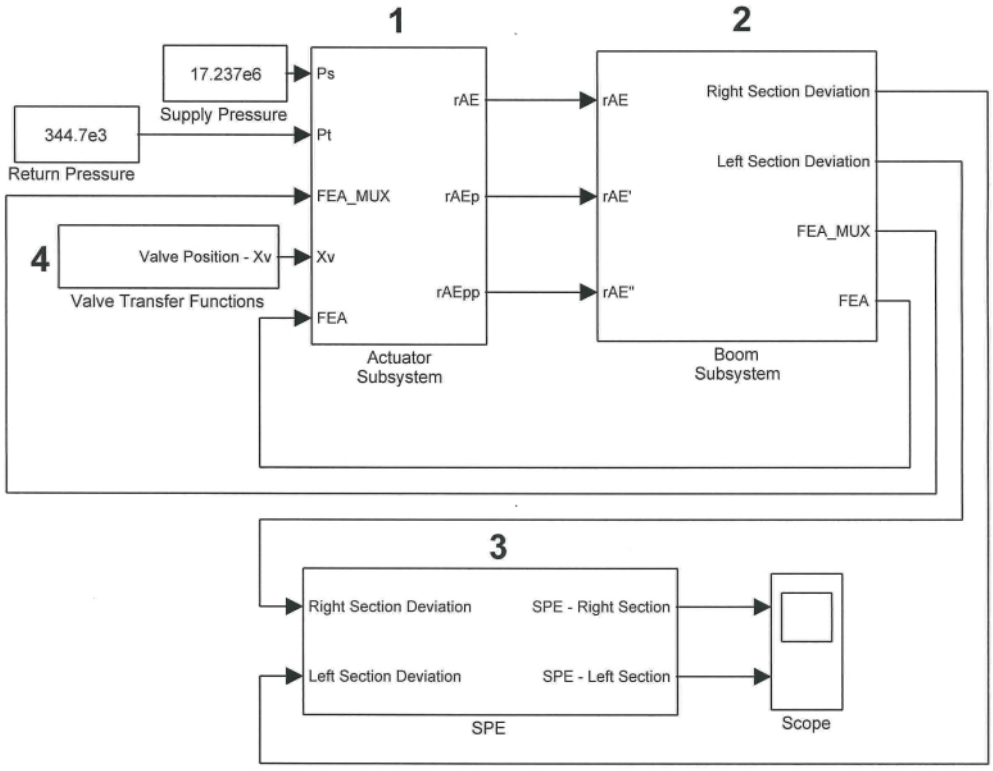

Figure C1: Model Main System

C1 Actuator Sub-System

The actuator sub-system is divided into nine sub-systems (Figure C2). Sub-system 1.1 is shown in Figure C3 and represents the equation of motion for the actuator (equation 3.1). This block uses equation 3.3 rearranged into the following form, allowing forces to be used as the input to solve for the acceleration of the actuator:

$$\ddot{x}_C = \frac{F_1 - F_2 + F_{E/A} - F_f}{m_C} \qquad [C.1]$$

The force of the actuator is a variable which when evaluated is a function of the actuator's acceleration; therefore, when attempting to model all equations which represent equation C.1 separately, an algebraic loop is created. Although there is functionality and methodology within the software to iteratively solve a series of equations containing an algebraic loop, the process is both a drain on computing power and creates the potential for numerical instability. By solving

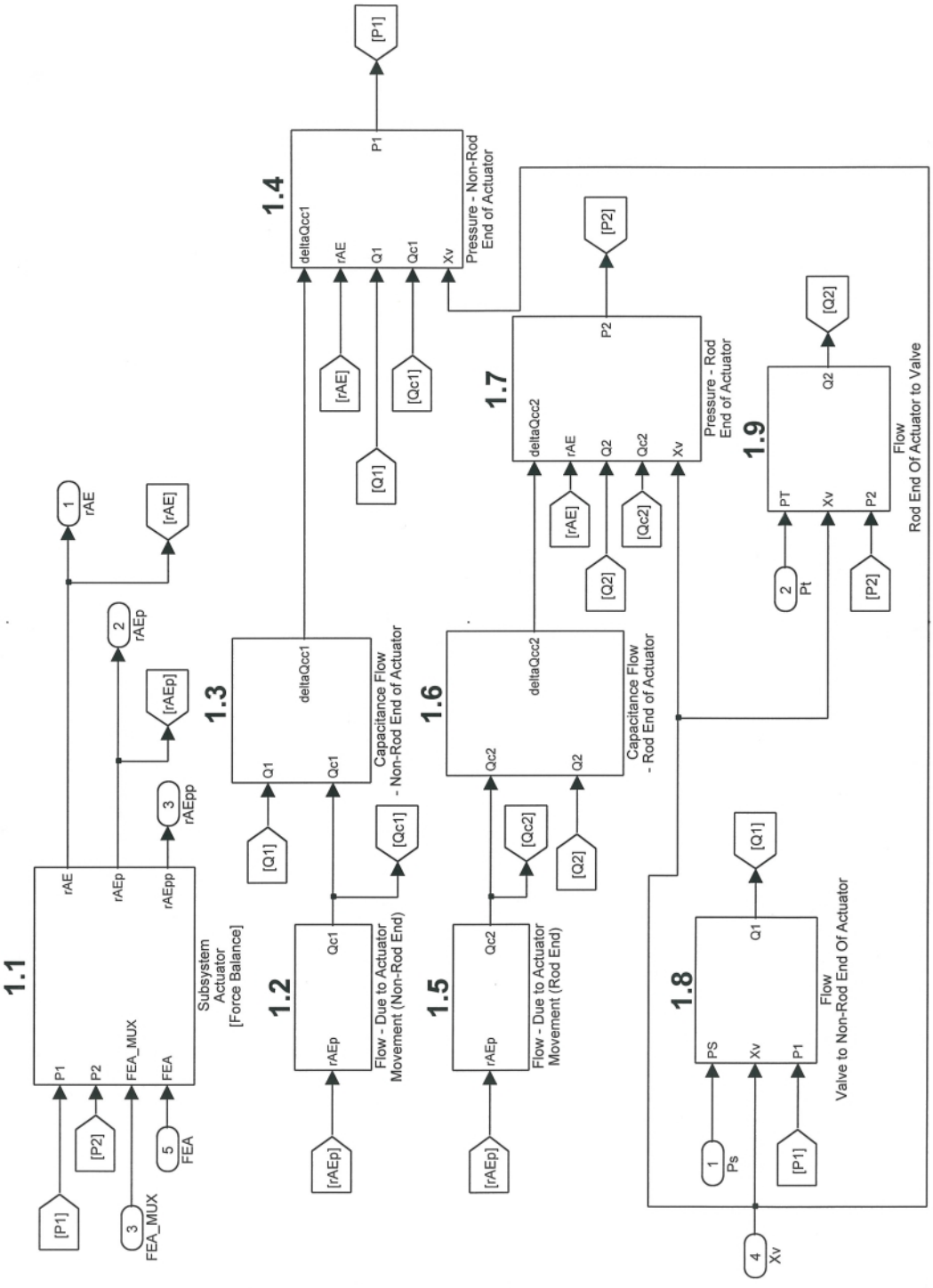

Figure C2: Actuator Sub-System 1

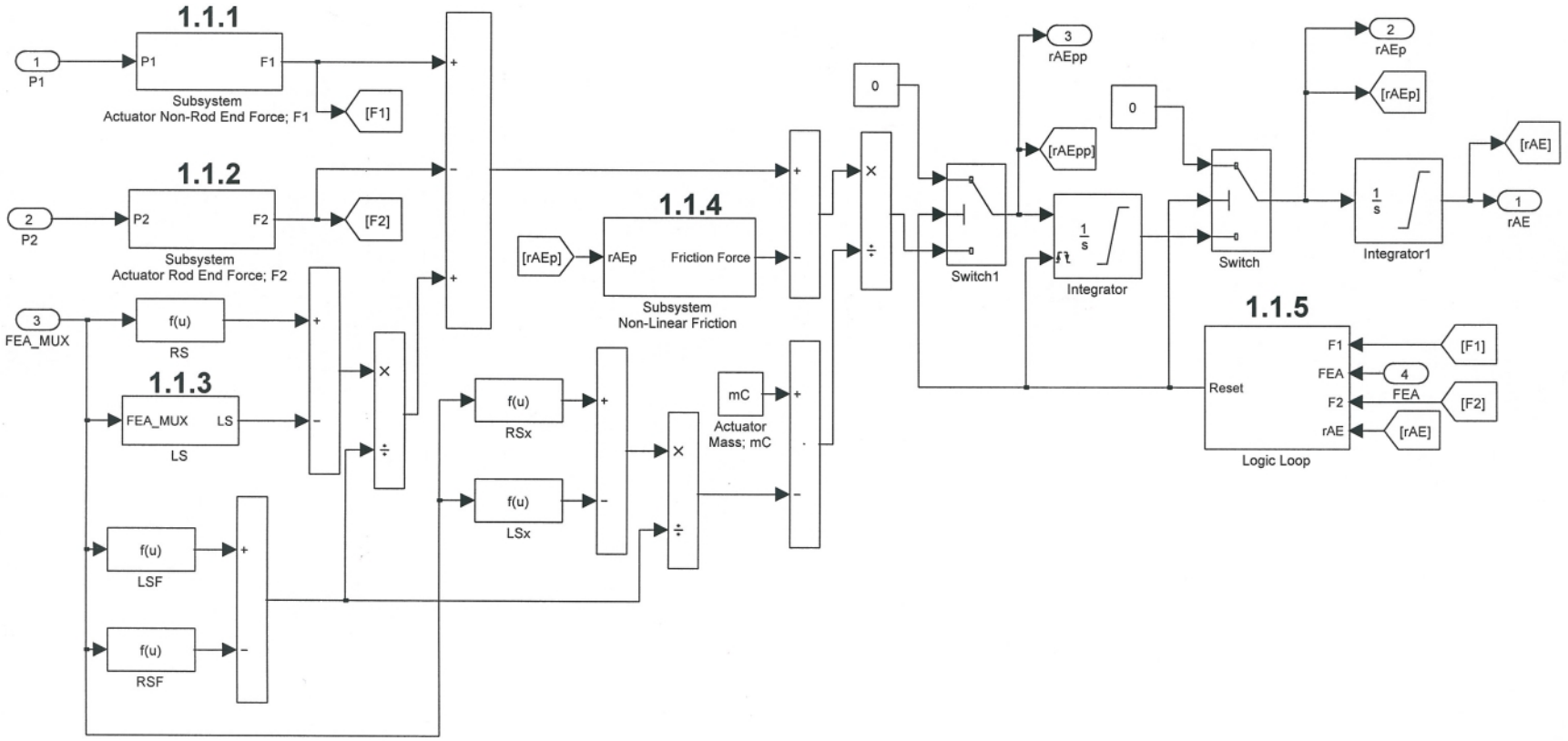

Figure C3: Actuator Sub-System 1.1

the equations simultaneously in variable form, the algebraic loop may be avoided. Thus creating a more efficient and robust model. In this case, equations 2.4, 2.7, 2.10, 2.14, 2.17, 2.20, 2.26, 2.27, 2.39, 2.40, 2.41, and 2.42 were solved simultaneously in a numerical software package (Wolfram Research, 2000) and an equation for $F_{E/A}$ as a function of $\ddot{x}_C$ created. The equation created was of the form:

$$F_{E/A} * (LS_F) + \ddot{x}_C * (LS_x) + LS = F_{E/A} * (RS_F) + \ddot{x}_C * (RS_x) + RS, \qquad [C.2]$$

where:

LS_F is an additive series of terms that all involved $F_{E/A}$ on the left side of the generated equation,

LS_x is an additive series of terms that all involved $\ddot{x}_C$ on the left side of the generated equation,

LS is an additive series of terms that did not involve either $F_{E/A}$ or $\ddot{x}_C$ on the left side of the generated equation,

RS_F is an additive series of terms that all involved $F_{E/A}$ on the right side of the generated equation,

RS_x is an additive series of terms that all involved $\ddot{x}_C$ on the right side of the generated equation, and

RS is an additive series of terms that did not involve either $F_{E/A}$ or $\ddot{x}_C$ on the right side of the generated equation,

Solving equation C.2 for $F_{E/A}$ yields:

$$F_{E/A} = \frac{\ddot{x}_C * (RS_x - LS_x) + (RS - LS)}{LS_F - RS_F}. \qquad [C.3]$$

Substituting equation C.3 into C.1 and solving for $\ddot{x}_C$ yields:

$$\ddot{x}_C = \frac{F_1 - F_2 + \left(\frac{RS - LS}{LS_F - RS_F}\right) - F_f}{m_C - \left(\frac{RS_x - LS_x}{LS_F - RS_F}\right)}, \qquad [C.4]$$

which is the form represented by sub-system 1.1. The resultant of this equation is extremely lengthy and therefore is not included here. A copy of the model is included with the thesis, allowing the full form of the equation to be extracted by the reader if required.

Sub-system 1.1.1 represents equation 3.4 and relates actuator rod end pressure to a force (Figure C4). Similarly, sub-system 1.1.2 represents equation 3.5 and relates actuator non-rod end pressure to a force (Figure C5).

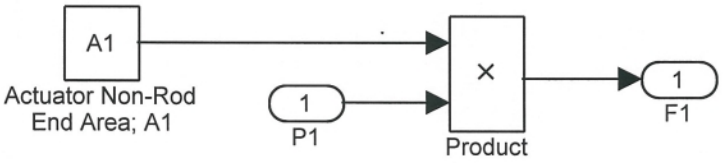

Figure C4: Actuator Sub-System 1.1.1

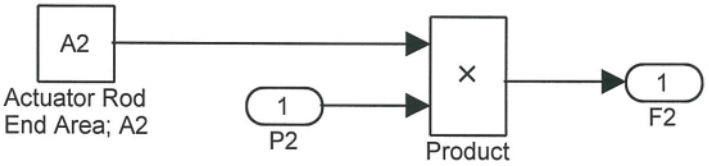

Figure C5: Actuator Sub-System 1.1.2

Sub-system 1.1.3 sums two portions of the lengthy series of left side additive terms that did not involve either $F_{E/A}$ or $\ddot{x}_C$ (Figure C6). This was required due to MatLAB limiting function blocks to less than 32,500 characters.

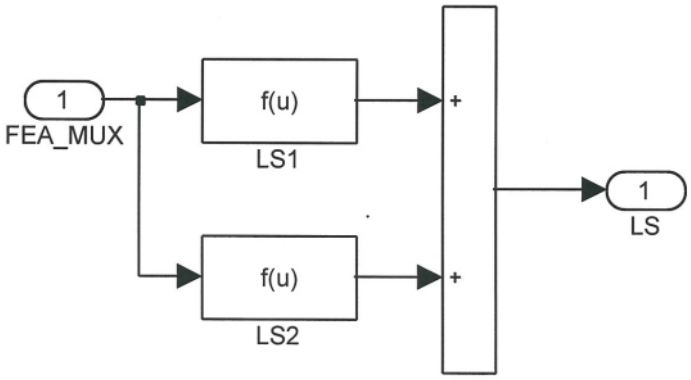

Figure C6: Actuator Sub-System 1.1.3

Sub-system 1.1.4 uses the experimental data determined in Chapter 4 (section 4.2) to produce the resultant actuator friction force for a given actuator velocity (Figure C7).

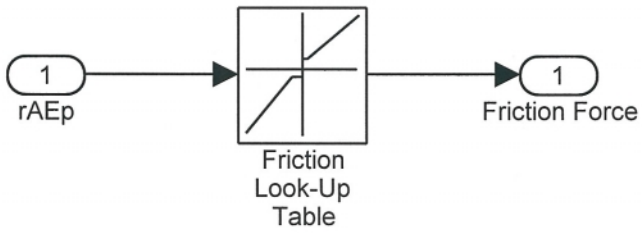

Figure C7: Actuator Sub-System 1.1.4

A logic loop is also presented (sub-system 1.1.5) which will restart the actuator acceleration integrator if the actuator reaches the physical extents of its stroke (Figure C8). The logic loop is necessary as the extents are non-linearities in the system. Based on the resultant force being applied to the actuator the logic loop, the actuator will either remain stationary against the physical extent or begin moving in the opposing direction.

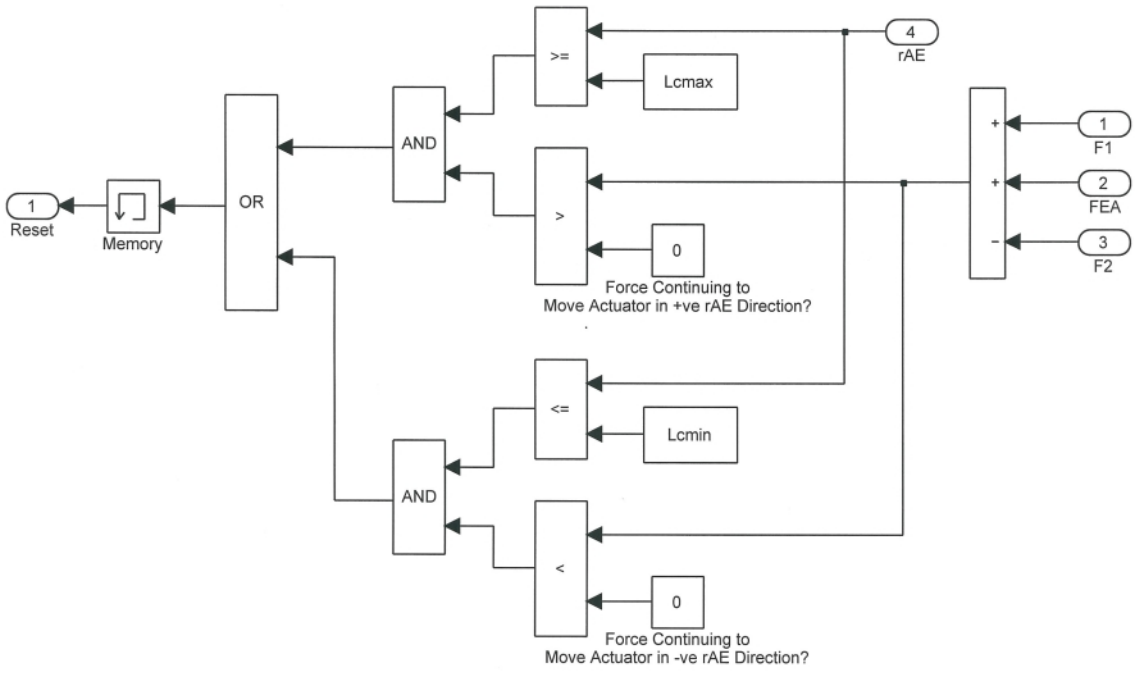

Figure C8: Actuator Sub-System 1.1.5

Sub-system 1.2 represents equation 3.8 which is the change in the actuator non-rod end control volume due to actuator movement (Figure C9). Similarly, sub-system 1.5 represents the change in the rod-end control volume (Figure C10).

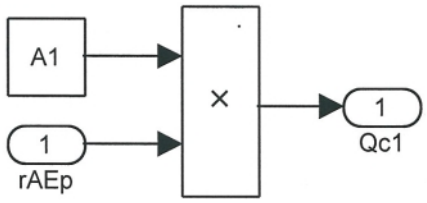

Figure C9: Actuator Sub-System 1.2

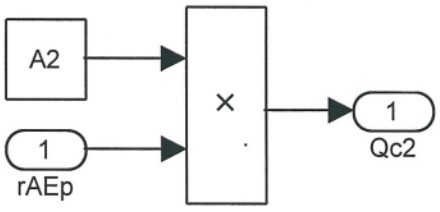

Figure C10: Actuator Sub-System 1.5

Sub-system 1.3 sums the change in actuator non-rod end control volume and the flow through the valve; this represents the term to be integrated in equation 3.9 (Figure C11). Similarly, sub-system 1.6 sums the change in actuator rod end control volume and the flow through the valve to represent the integral term in equation 3.10 (Figure C12).

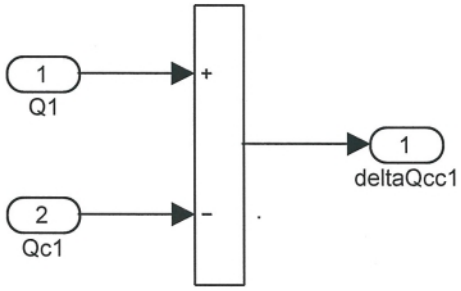

Figure C11: Actuator Sub-System 1.3

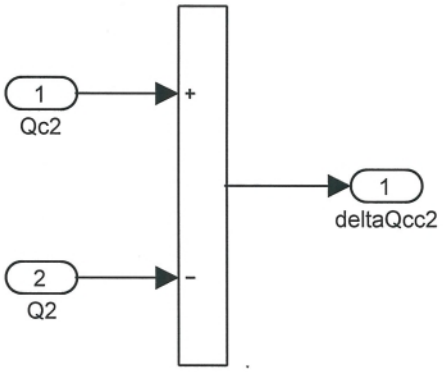

Figure C12: Actuator Sub-System 1.6

Sub-system 1.8 represents the flow through the valve attached to the non-rod side of the actuator presented in equation 3.13 (Figure C13). The sign of the resultant of the pressure differential term is taken to determine flow direction. Similarly, sub-system 1.9 represents the flow through the valve attached to the rod-end side of the actuator presented in equation 3.14 (Figure C14).

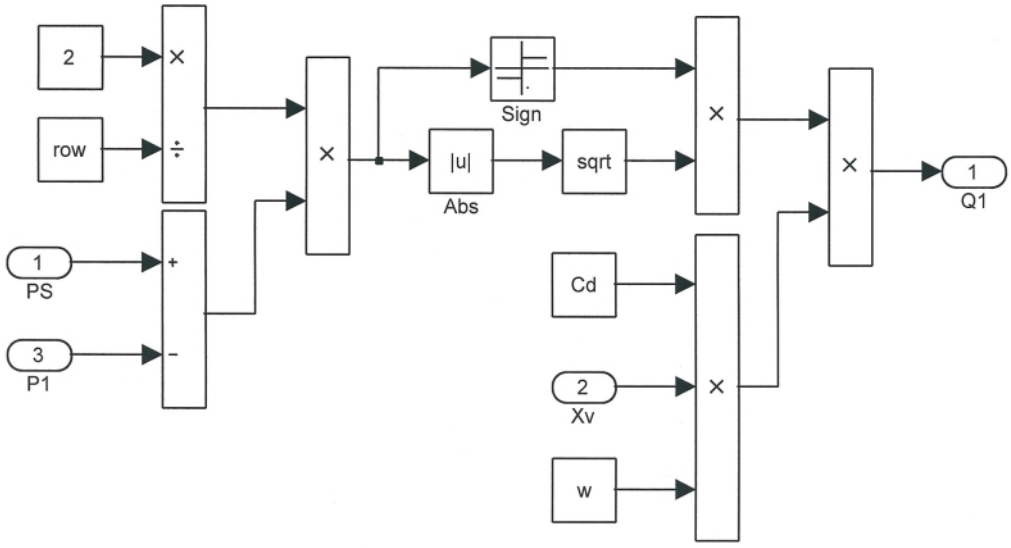

Figure C13: Actuator Sub-System 1.8

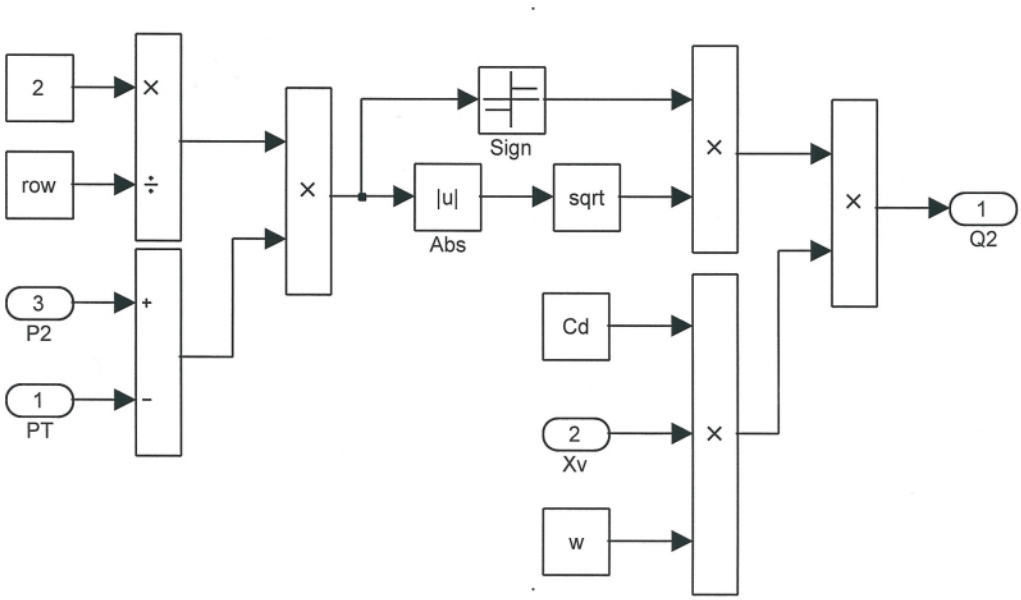

Figure C14: Actuator Sub-System 1.9

The final two actuator sub-systems calculate the actuator non-rod end pressure (sub-system 1.4) and the rod end pressure (sub-system 1.7). Sub-system 1.4 represents equation 3.9 and is shown in Figure C15. Sub-system 1.7 represents equation 3.10 and is shown in Figure C16. Both blocks have a logic loop to reset the integrator based on the effects of cavitation discussed in Chapter 5. If the actuator continues to move in one direction and cavitation

occurs, a ‘void’ is created. As the void does not contain fluid, the pressure on that side of the actuator cannot build until the actuator returns to the position where cavitation began. The logic loops monitor cavitation to ensure accurate calculation of the pressures in the actuator.

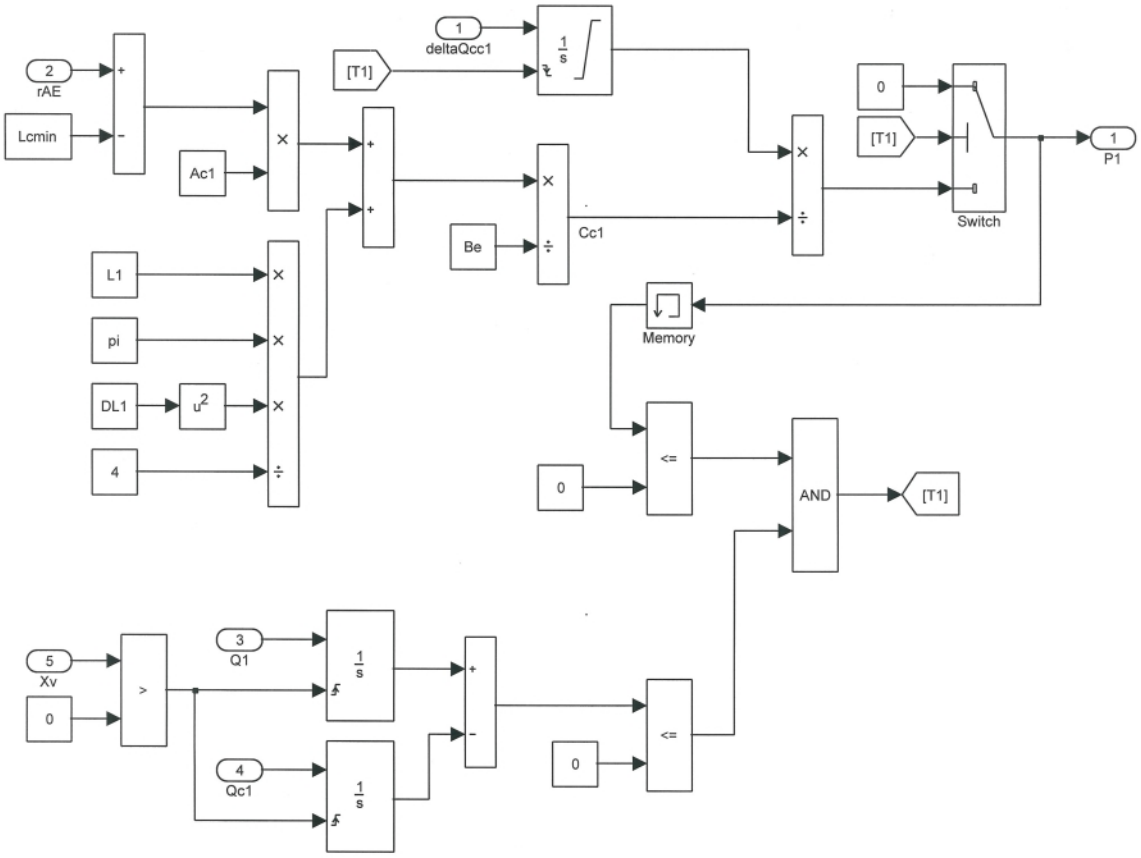

Figure C15: Actuator Sub-System 1.4

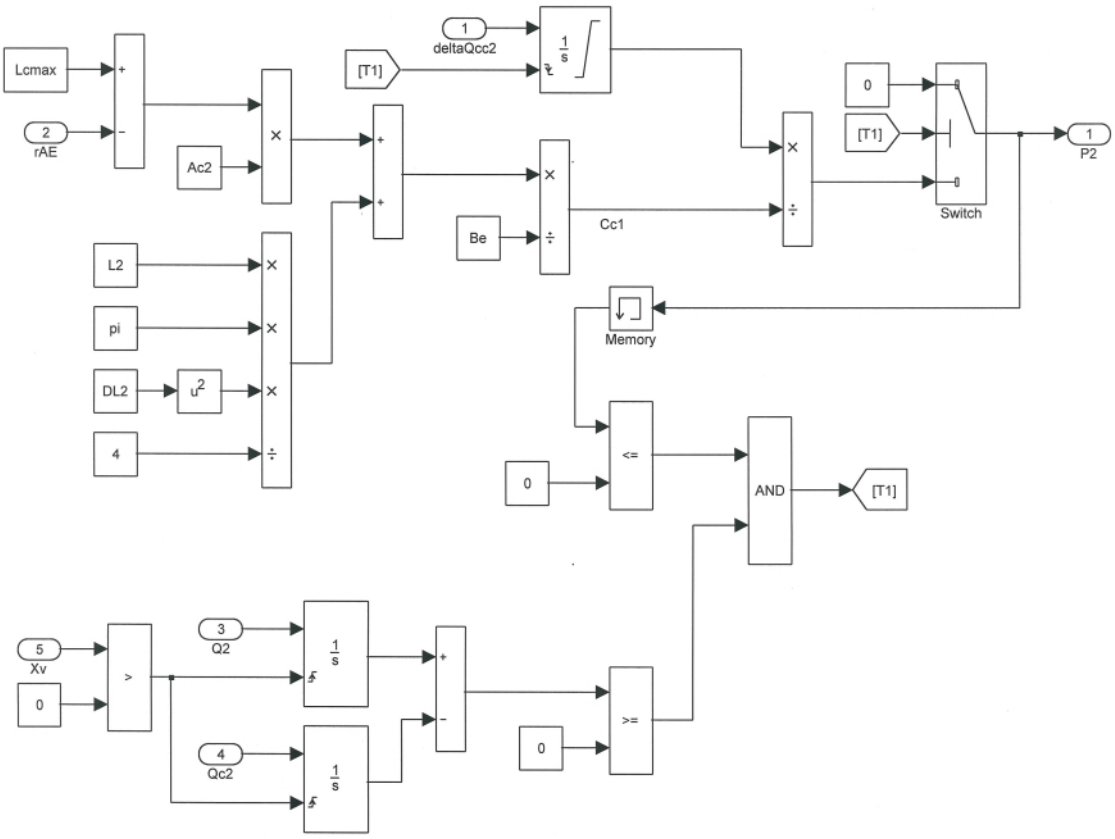

Figure C16: Actuator Sub-System 1.7

C2 Boom Sub-System

The boom sub-system is divided into eight sub-systems (Figure C17). Sub-system 2.1 is shown in Figure C18 and represents equation A.8 which is the second derivative of equation 2.67. Sub-system 2.4 represents equation A.4 which is the second derivative of equation 2.68 (Figure C19).

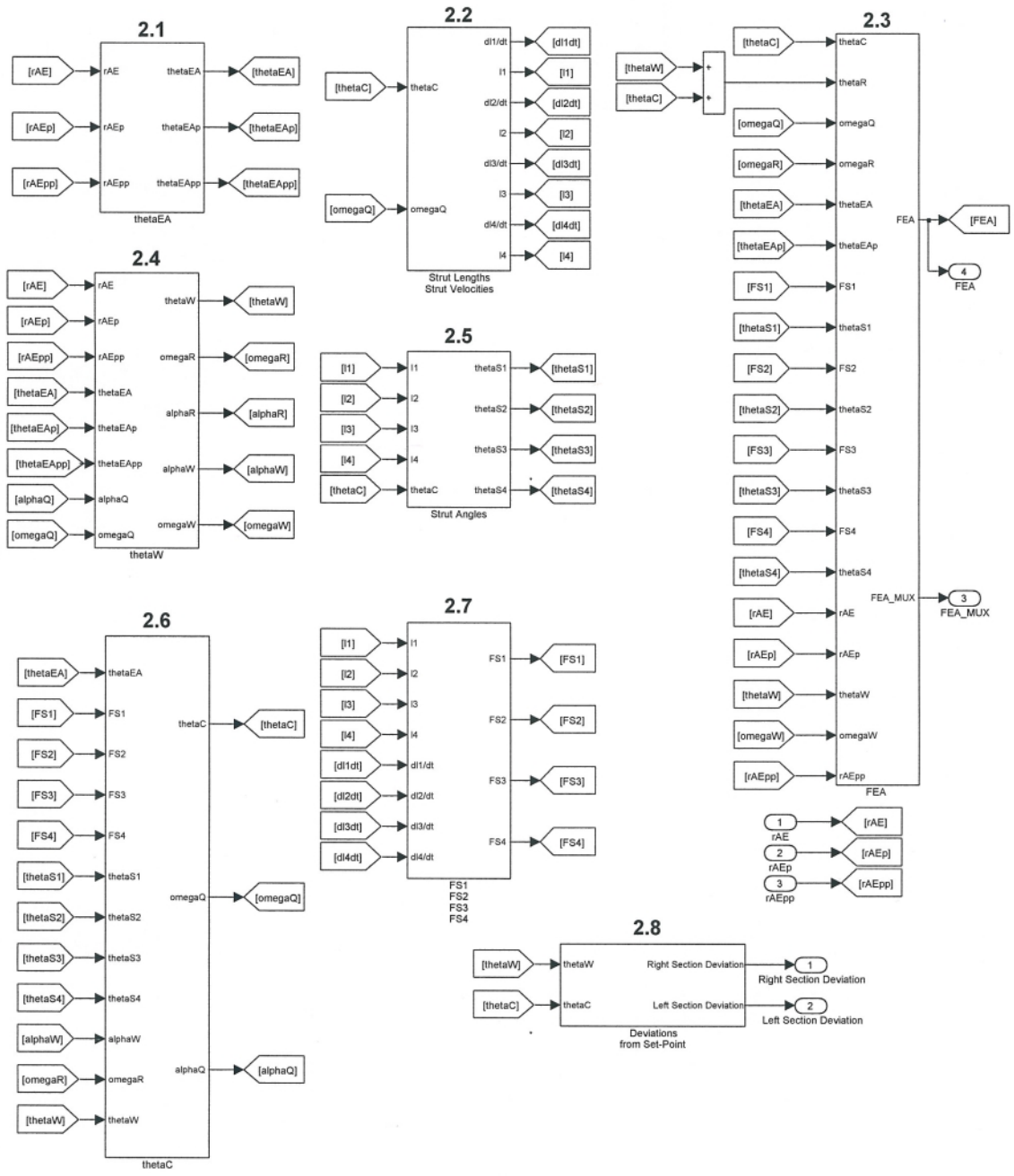

Figure C17: Boom Sub-System 2

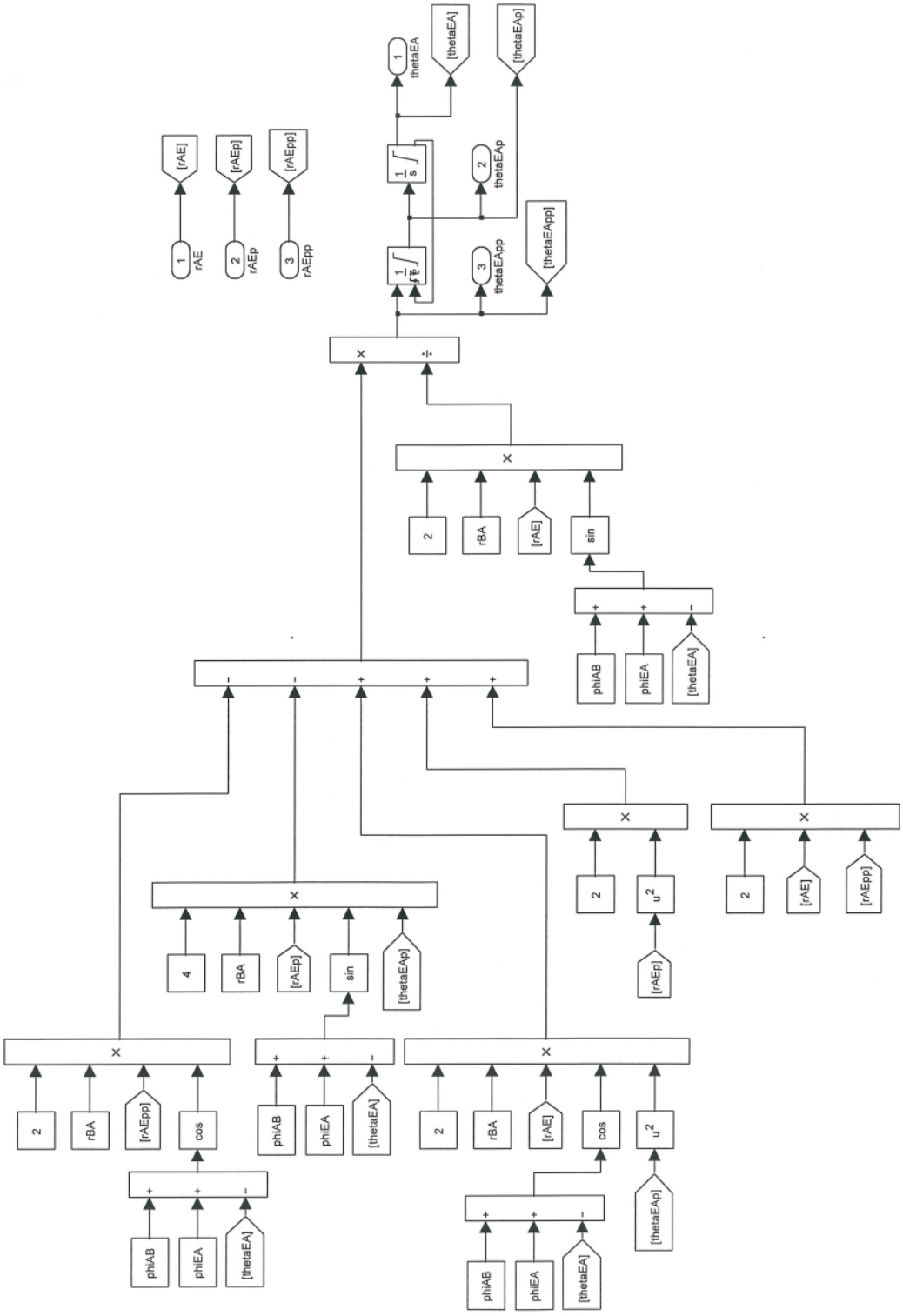

Figure C18: Boom Sub-System 2.1

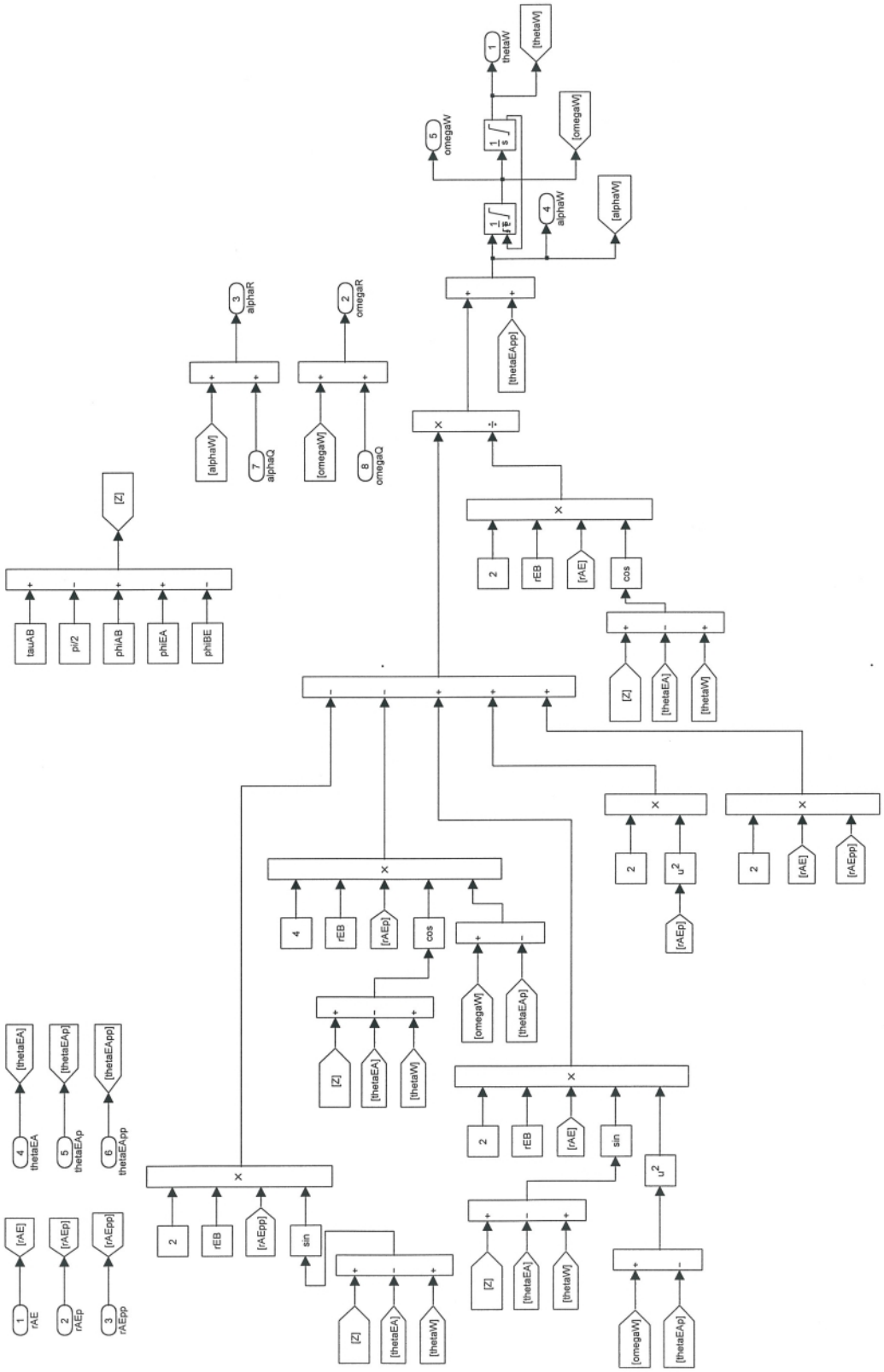

Figure C19: Boom Sub-System 2.4

Figure C20 shows sub-system 2.2; this block has four sub-systems (2.2.1, 2.2.2, 2.2.3, and 2.2.4) to represent each of the four struts attached between the carrying frame and the center section. These blocks are shown in Figures C21 through C24 and represent equations 2.51 through 2.58 which calculate the length and rate of length change of each strut.

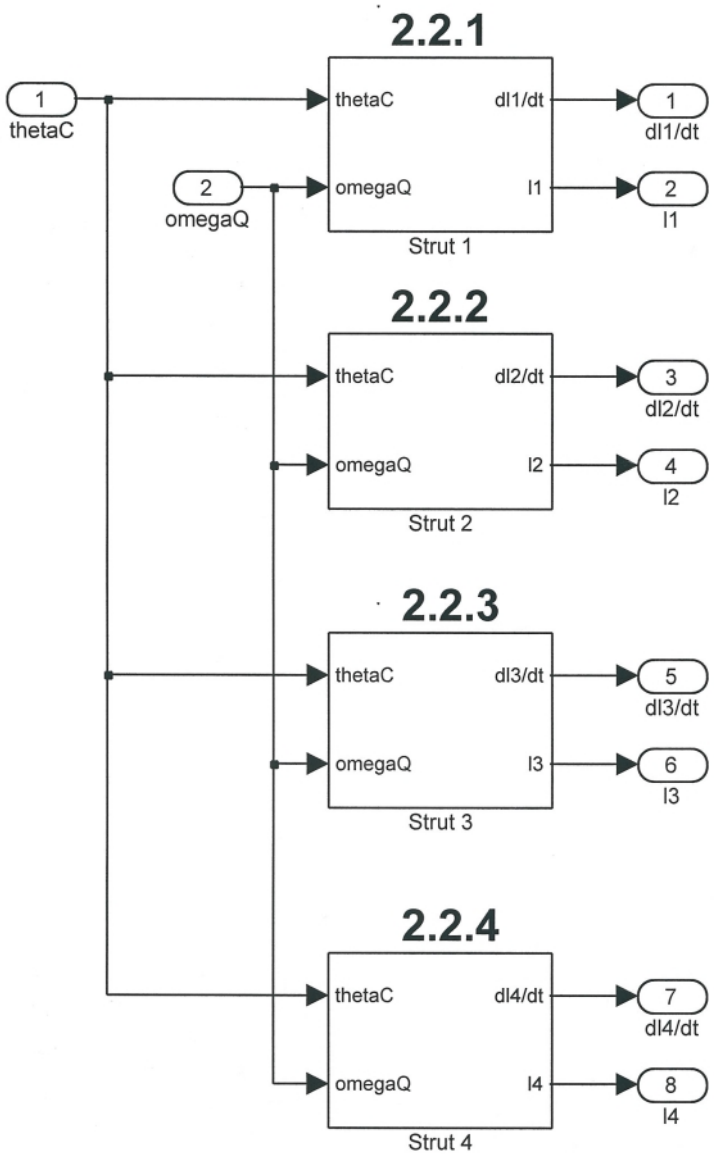

Figure C20: Boom Sub-System 2.2

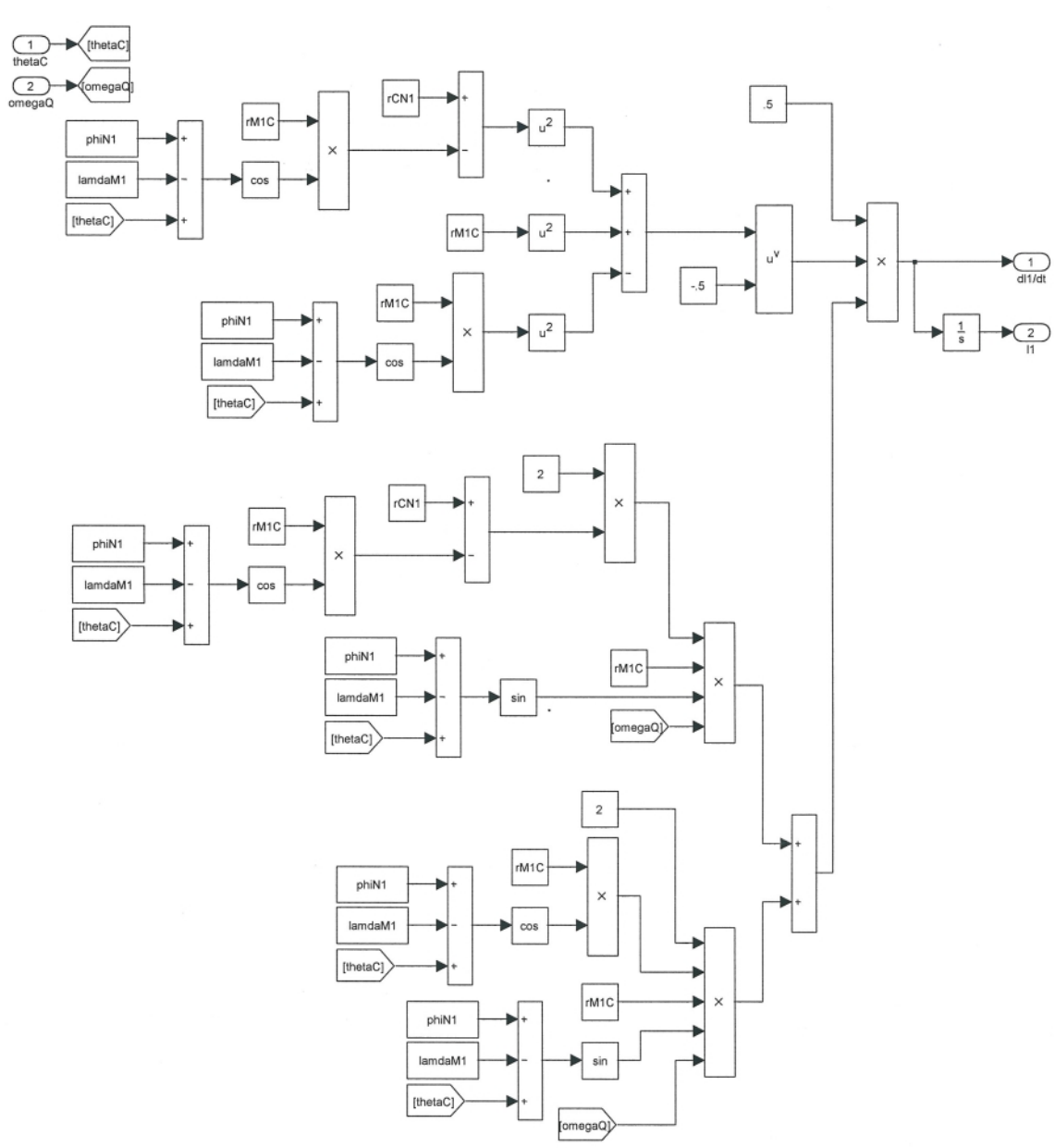

Figure C21: Boom Sub-System 2.2.1

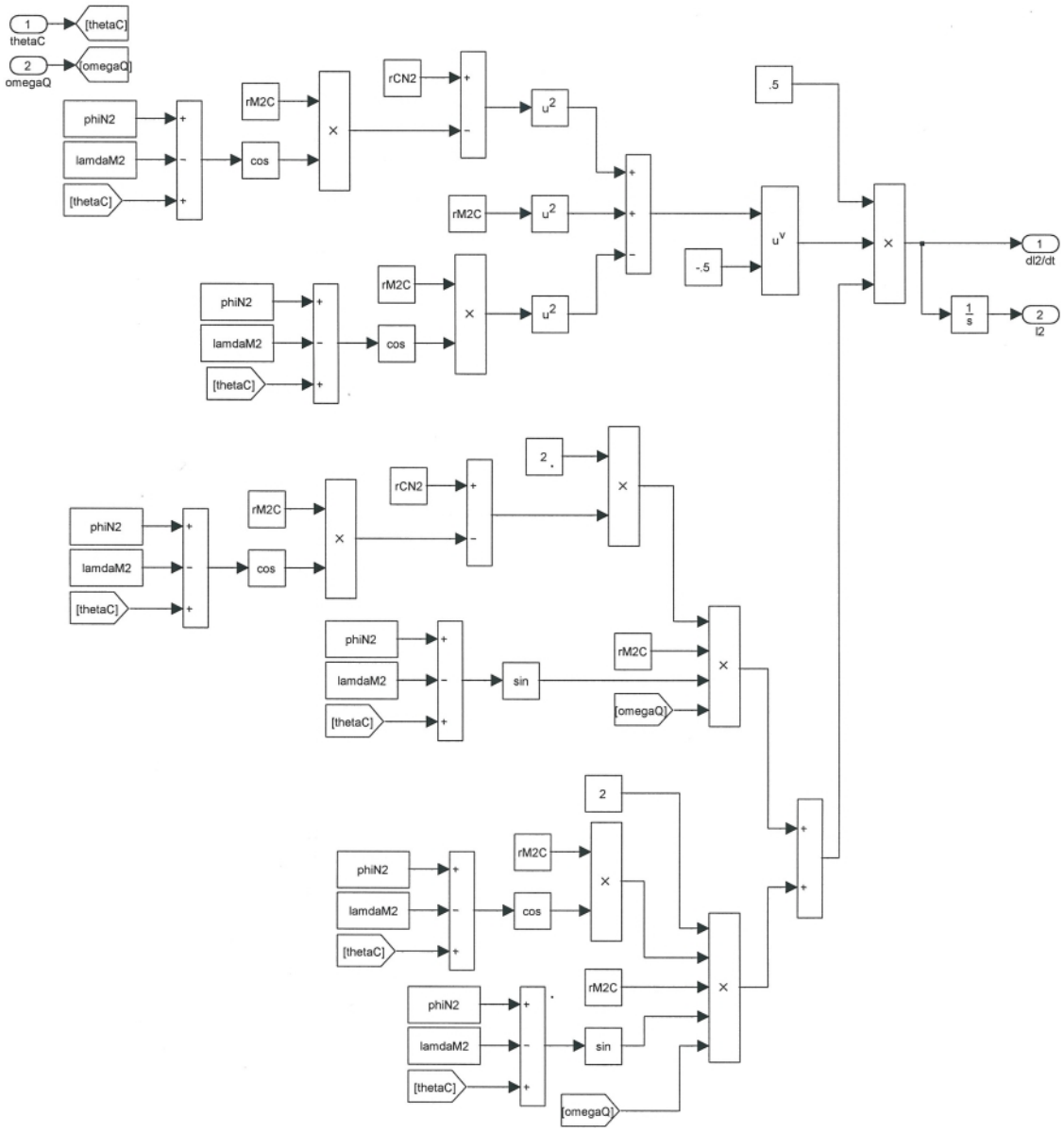

Figure C22: Boom Sub-System 2.2.2

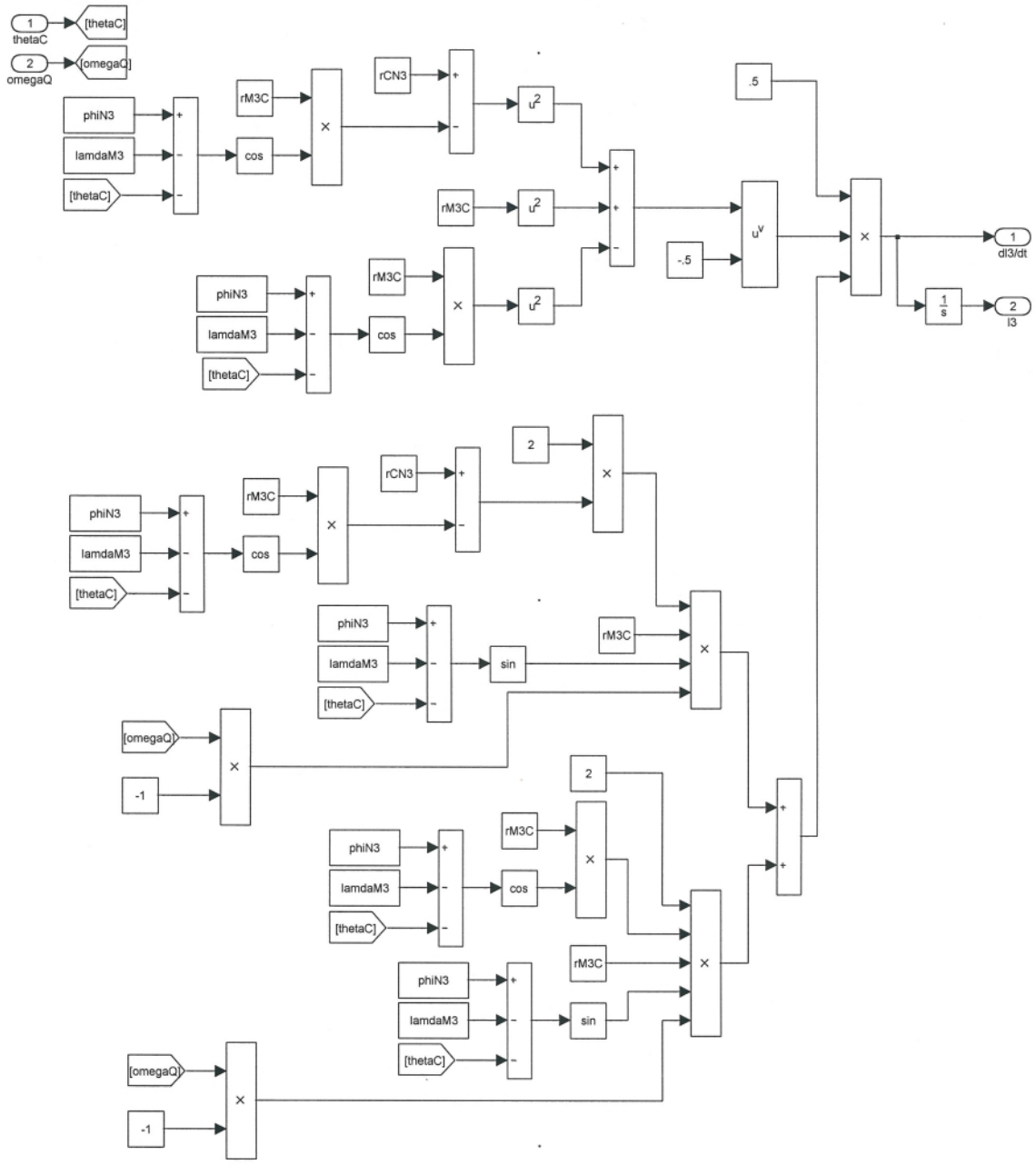

Figure C23: Boom Sub-System 2.2.3

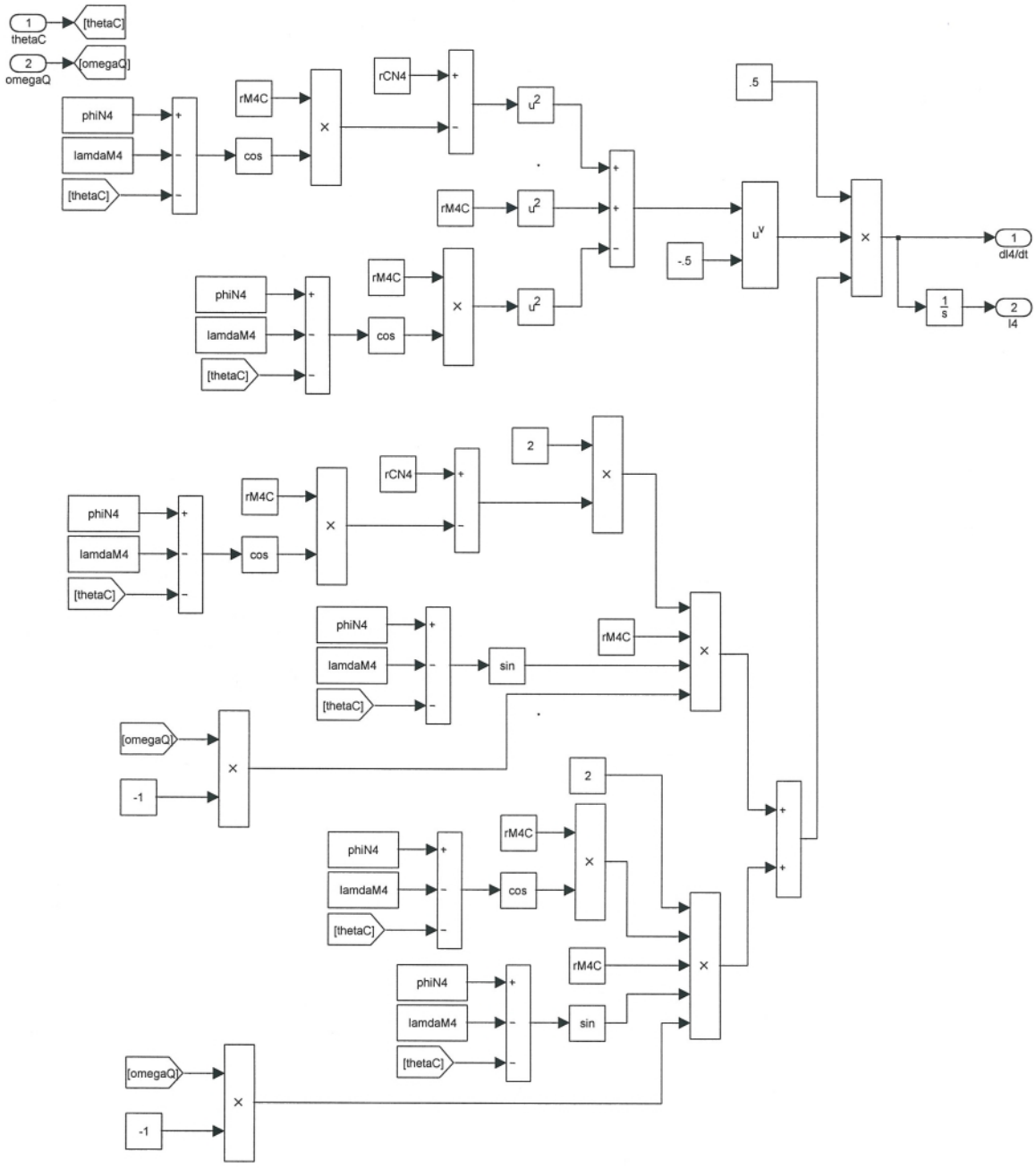

Figure C24: Boom Sub-System 2.2.4

Sub-system 2.3 uses equation C.3 defined earlier in this chapter to calculate the resultant actuator force (Figure C25).

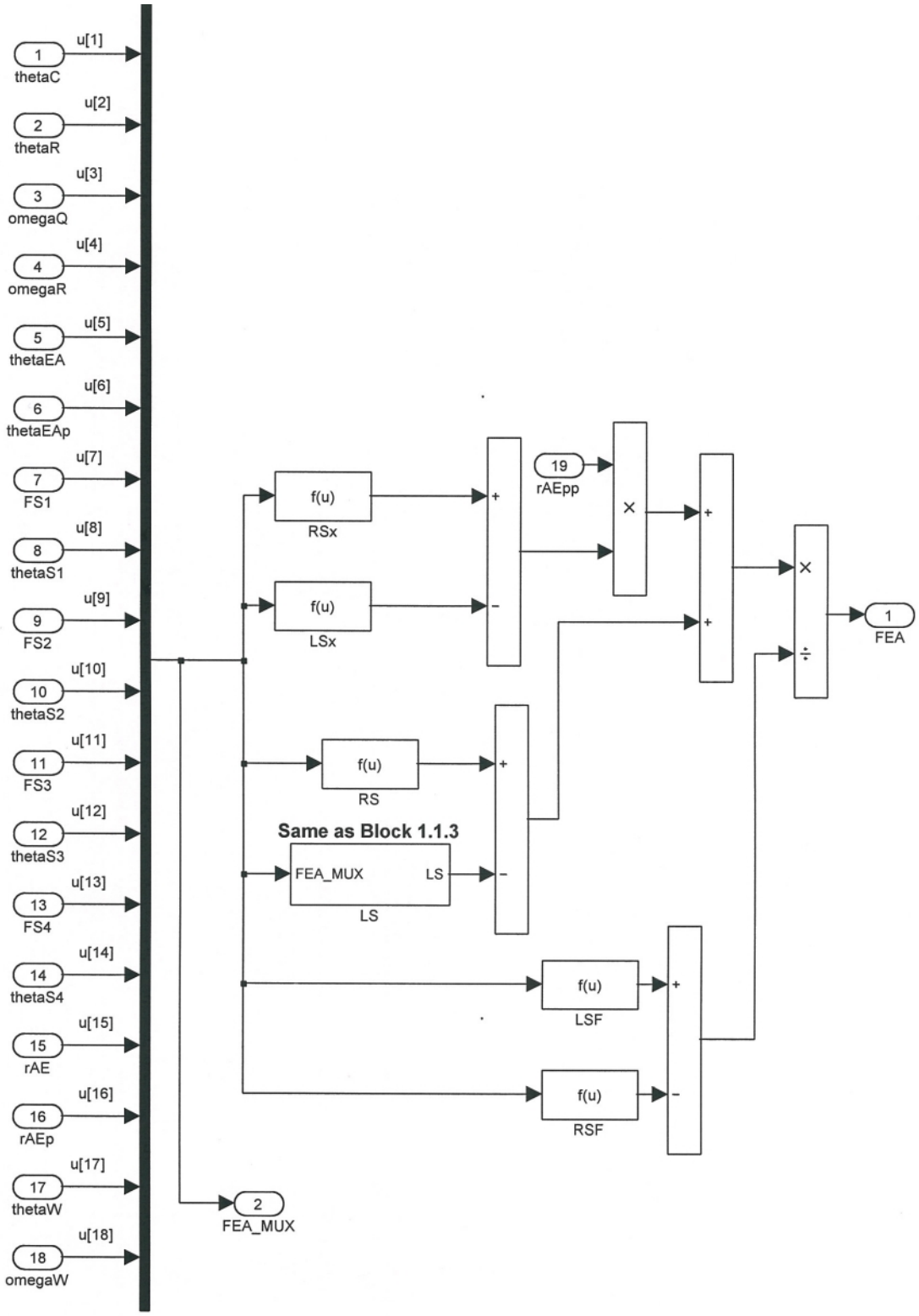

Figure C25: Boom Sub-System 2.3

Sub-system 2.5 represents equations 2.60 through 2.63 to define the angular orientation of each strut (Figure C26).

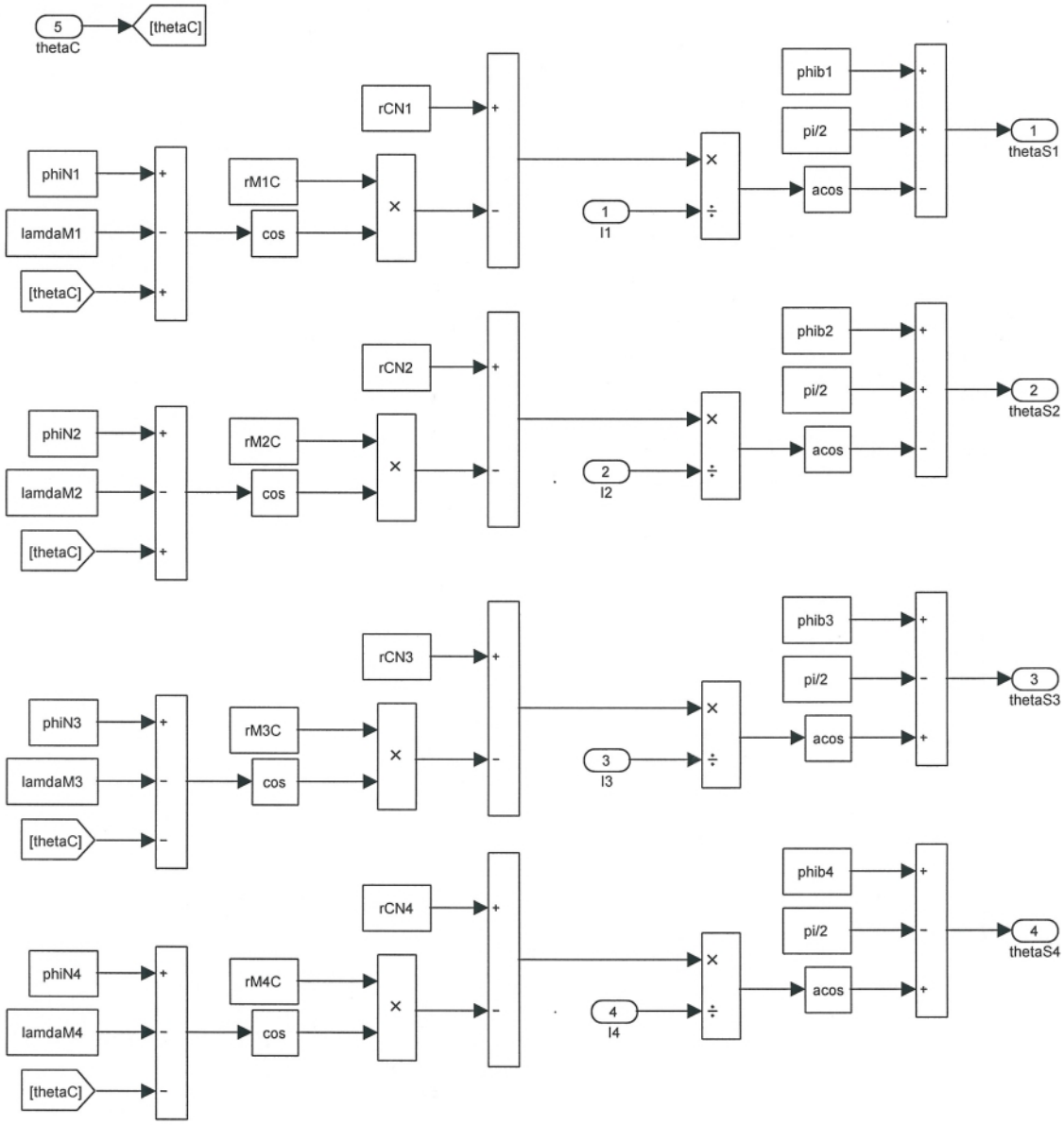

Figure C26: Boom Sub-System 2.5

To avoid algebraic loops, equations 2.4, 2.7, 2.10, 2.13, 2.16, 2.25, 2.26, 2.38, 2.39, 2.40, and 2.41 were solved simultaneously for α_Q. Again, the resultant equation is extremely long and is not presented here. The equation is of the form:

$$\alpha_Q = \frac{(RS_Q - LS_Q)}{LS_\alpha}, \qquad [C.5]$$

where:

RS_Q is an additive series of terms that do not involve α_Q on the right side of the generated equation,

LS_Q is an additive series of terms that do not involve α_Q on the leftt side of the generated equation, and

LS_α is an additive series of terms that involved α_Q on the right side of the generated equation.

The form of the equation is shown in Figure C27.

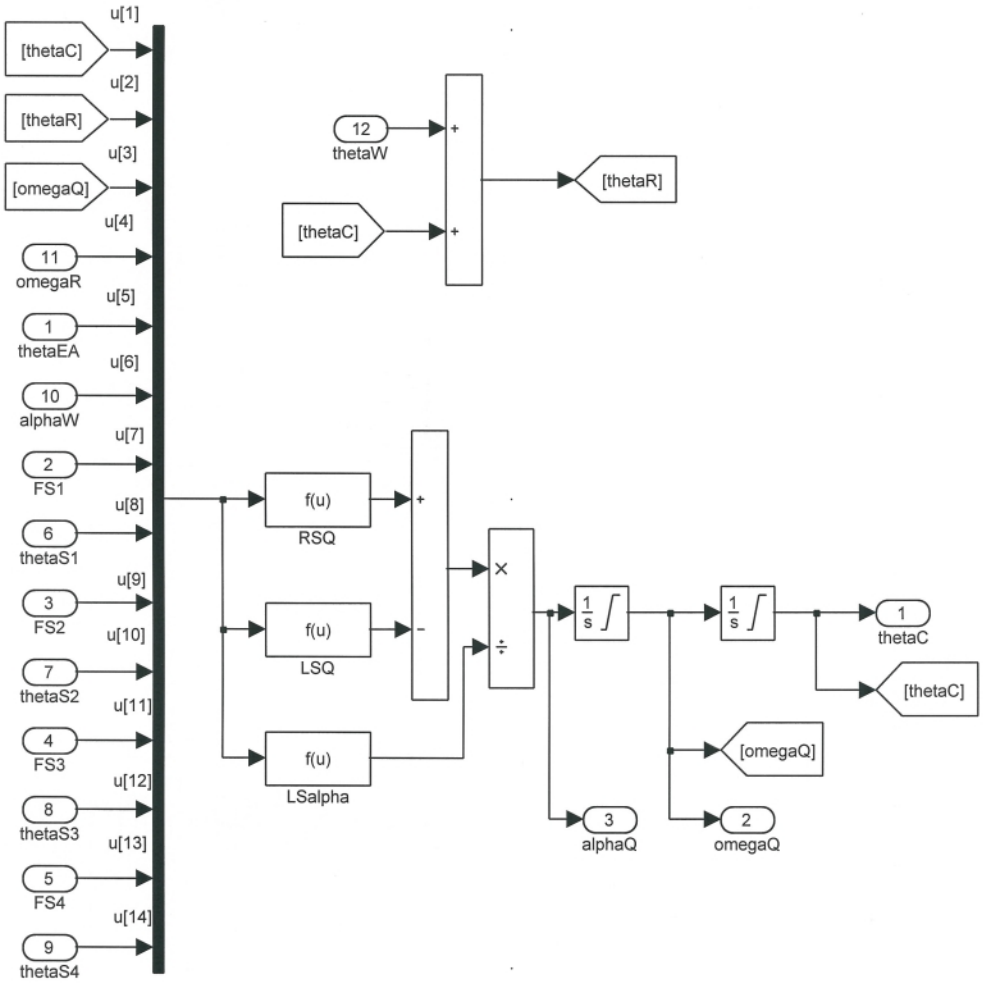

Figure C27: Boom Sub-System 2.6

Figure C28 shows sub-system 2.7 which represents the forces applied by each strut as presented in equations 2.43 through 2.46.

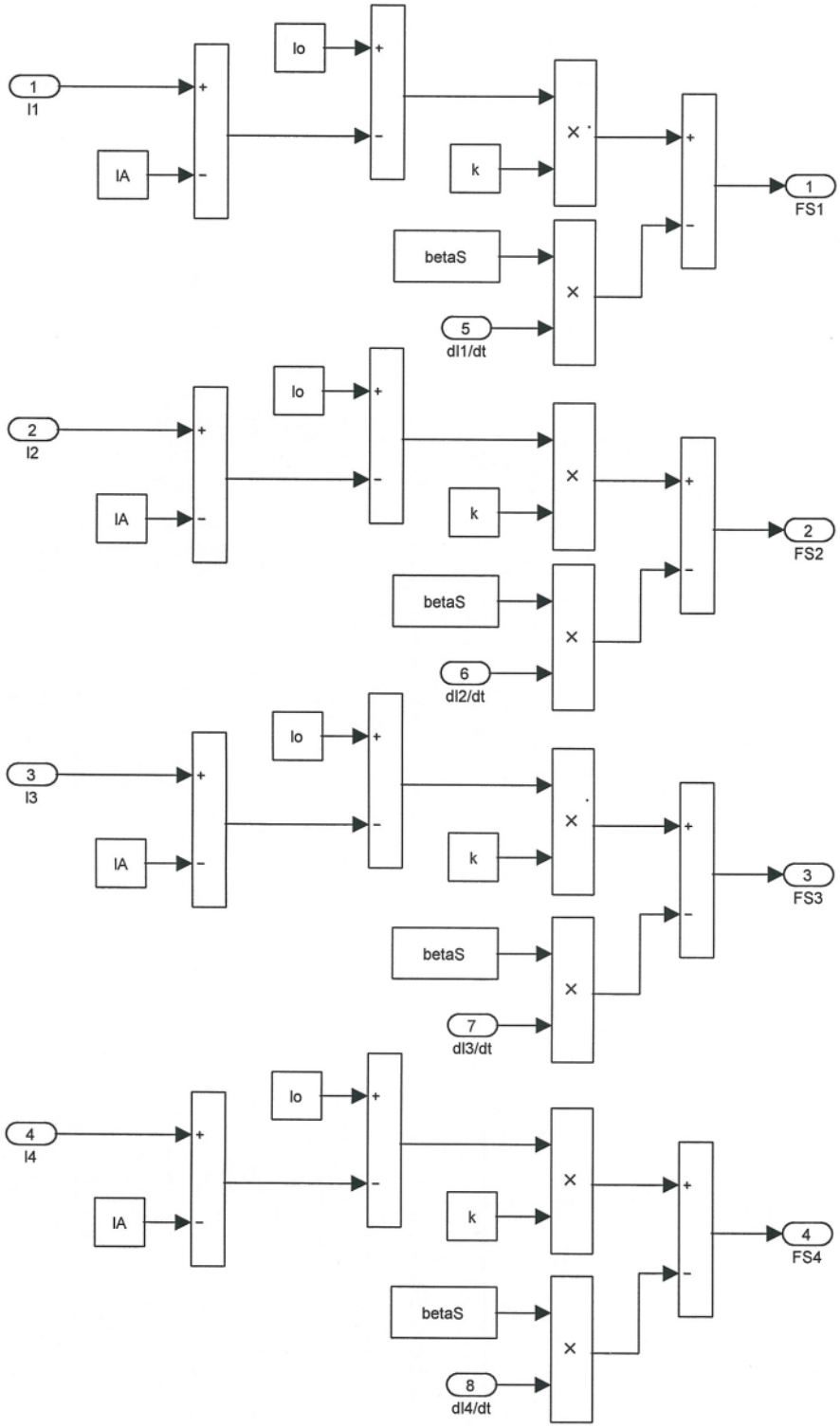

Figure C28: Boom Sub-System 2.7

Sub-system 2.8 represents equations D.1 and D.2 which define the deviations from horizontal of the right and left sections (Figure C29).

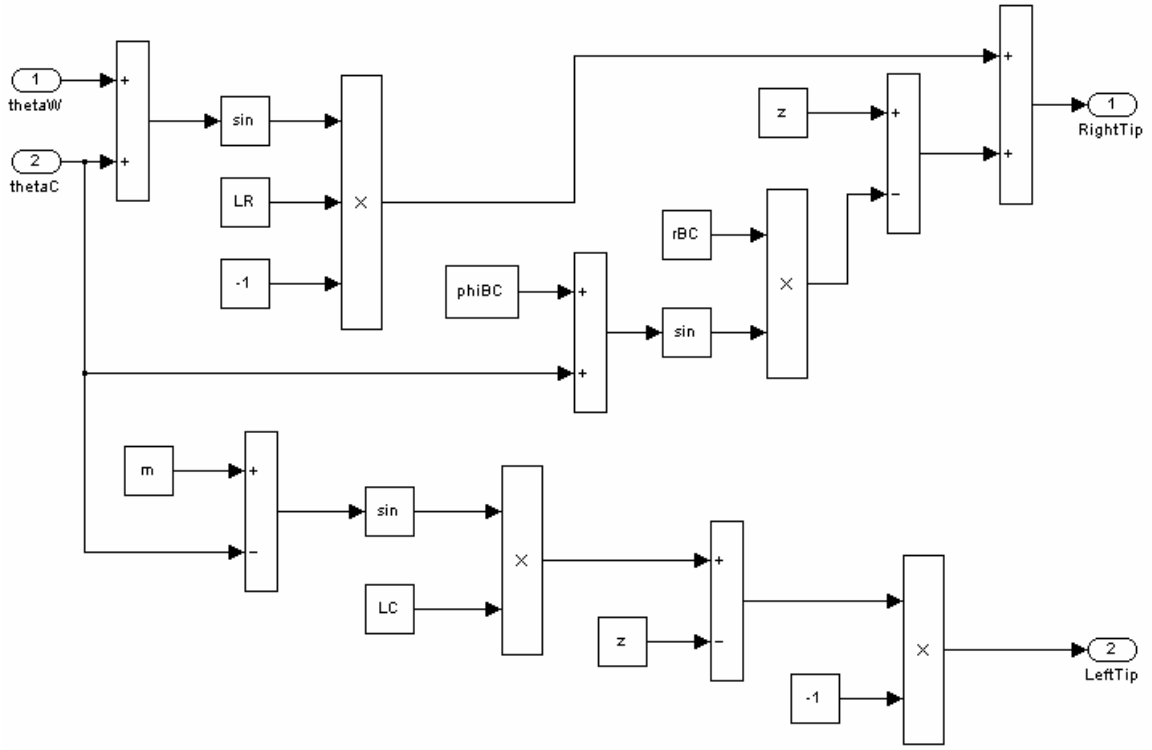

Figure C29: Boom Sub-System 2.8

C3 Set-Point Error Sub-System

Sub-system 3 calculates the SPE's of the right and left sections that results from corrections to the right section's orientation (Figure C30) (equation 5.1).

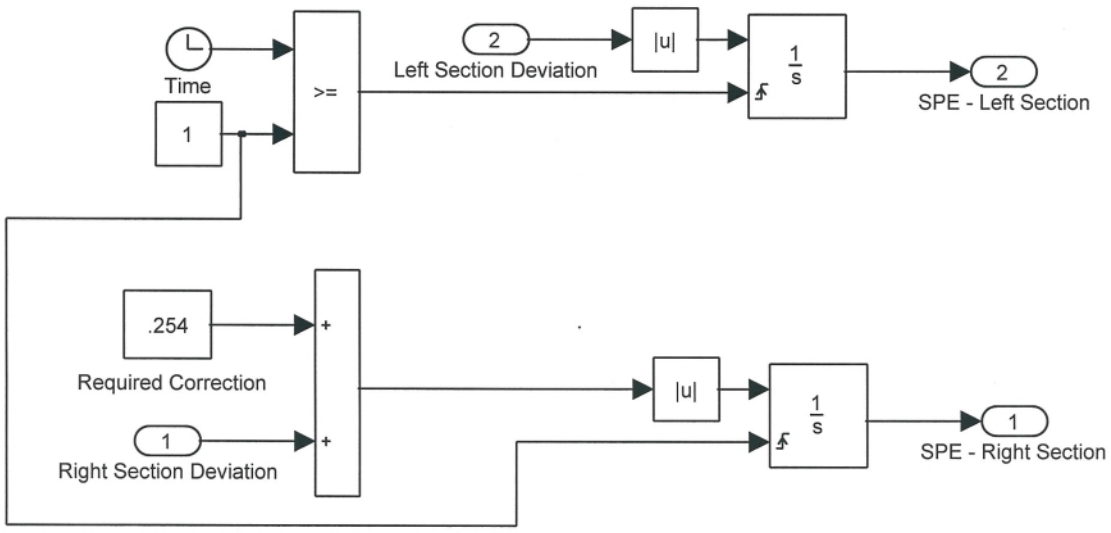

Figure C30: SPE Sub-System 3

C4 Valve Sub-System

Sub-system 4 drives the other sub-systems of the model (Figure C31). This block utilizes the transfer functions developed in Chapter 3 (section 5). Equations 3.16, 3.17, and 3.18 are used with various input functions representing voltage (steps and ramps). The transfer functions then convert the input voltage to valve spool position.

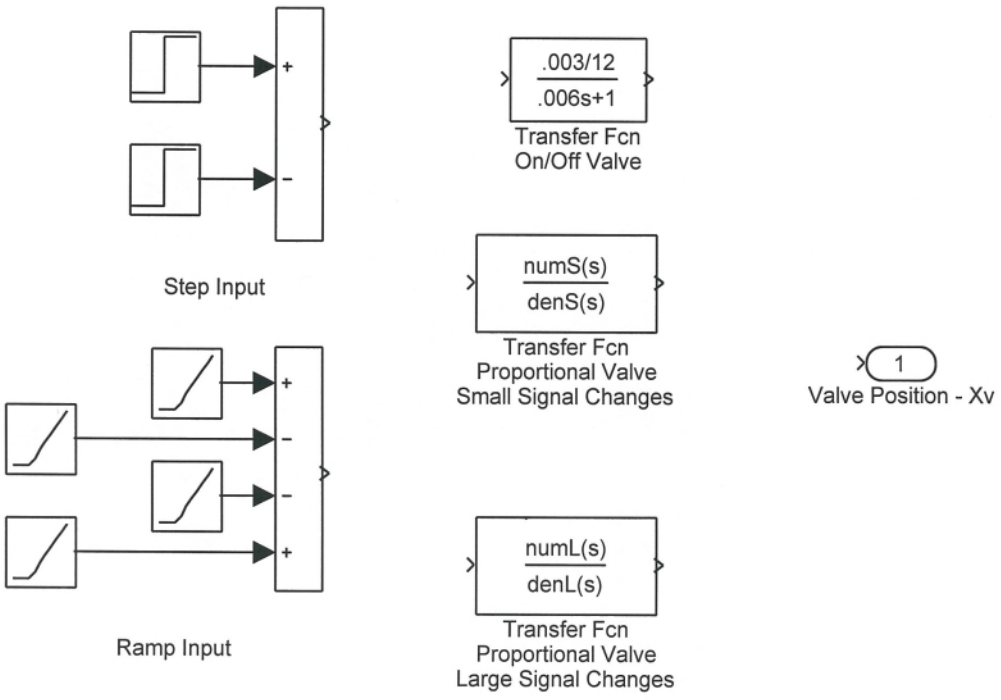

Figure C31: Valve Transfer Function Sub-System 4

Referencing equation 3.17, the large signal change transfer function for the proportional valve was defined as follows:

$$numL(s) = {\omega_{NL}}^2 / V_l \text{, and} \qquad [C.6]$$

$$denL(s) = s^2 + 2 * \zeta_L * \omega_{NL} + {\omega_{NL}}^2, \qquad [C.7]$$

where:

numL(s) is the numerator of the large signal change transfer function, and *denL(s)* is the denominator of the large signal change transfer function.

Similarly, for the small signal change transfer function (equation 3.18):

$$numS(s) = \left(\frac{1}{\omega_1} * s + 1\right) * {\omega_{NS}}^4 / V_l \text{, and} \qquad [C.8]$$

$$denS(s) = \left(\frac{1}{\omega_2} * s + 1\right) * \left(s^2 + 2 * \zeta_S * \omega_{NS} + {\omega_{NS}}^2\right) * \left(s^2 + 2 * \zeta_S * \omega_{NS} + {\omega_{NS}}^2\right), \qquad [C.9]$$

where:

numS(s) is the numerator of the small signal change transfer function, and

denS(s) is the denominator of the small signal change transfer function.

Appendix D

Conversion of Angular Section Orientation to Linear Deviation at Tip

As the orientation of both the right section and combined center and left sections were defined in Chapter 2 via angles, conversion formulae were necessary to allow discussion in linear terms. The necessary conversion equations are discussed in this appendix.

The locations of the outermost spray tips on both the right and left sections are the points of interest. Referencing Figure D1 it can be shown for the right section that:

$$\textit{Right Section Tip Deviation} = -\left(\sin\left(\theta_W + \theta_C\right) * L_R\right) + \left(z - r_{B/C} * \sin\left(\phi_{B/C} + \theta_C\right)\right), \quad [D.1]$$

where:

L_R is the length from point B to the outermost tip on the right section (m), and

$\phi_{B/C}$ is the initial angle between horizontal and a vector between points C and B (rad),

Referencing Figure D2 it can be shown for the left section that:

$$\textit{Left Section Tip Deviation} = -\left(\sin\left(\phi_{CTIP} - \theta_C\right) * L_C - z\right), \quad [D.2]$$

where:

ϕ_{CTIP} is the initial angle between horizontal and a vector between the outermost spray tip and point C (rad),

L_C is the length from point C to the outermost tip on the left section (m), and
z is the vertical distance between the initial position of the outermost spray tip on the left section and point C (m).

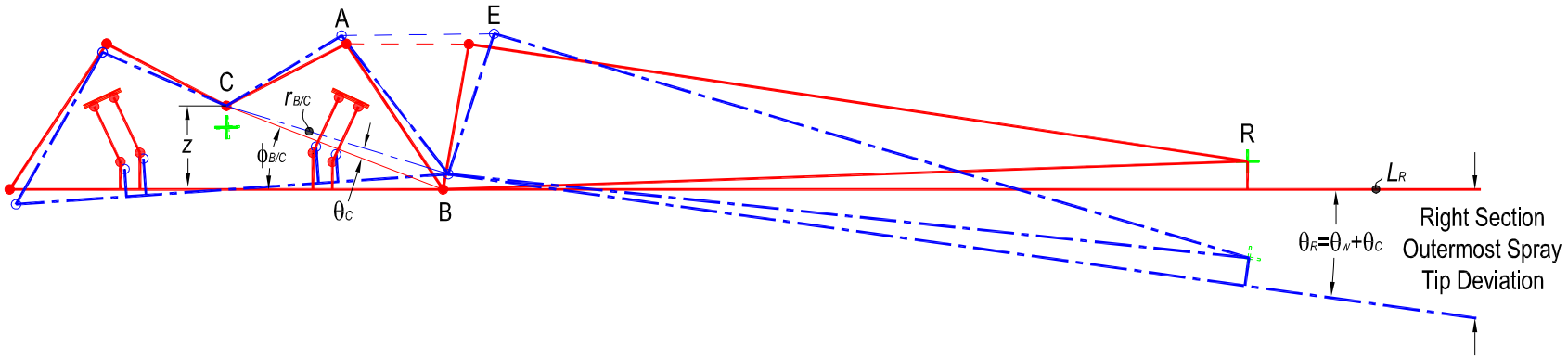

Figure D1: Right Section Outermost Spray Tip Deviation

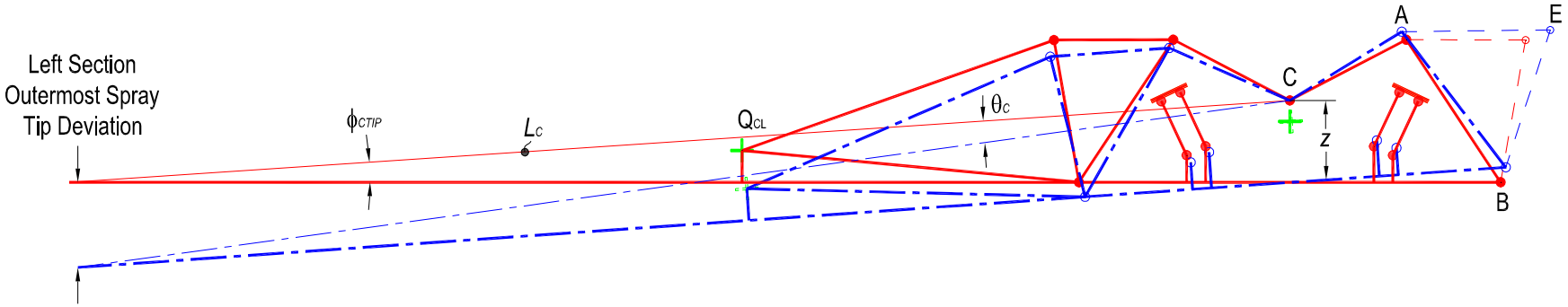

Figure D2: Left Section Outermost Spray Tip Deviation